Harmonic state space modelling of voltage source converters

James Ernest Ormrod

A thesis submitted in partial fulfilment
of the requirements for the degree of
Master of Engineering
in
Electrical and Computer Engineering
at the
University of Canterbury,
Christchurch, New Zealand.

April 2013

ABSTRACT

The thesis describes the development of a model of the three-phase Voltage Source Converter (VSC) in the Harmonic State Space (HSS) domain, a Linear Time Periodic (LTP) extension to the Linear Time Invariant (LTI) state space. The HSS model of the VSC directly captures harmonic coupling effects using harmonic domain modelling concepts, generalised to dynamically varying signals. Constructing the model using a reduced-order three-phase harmonic signal representation achieves conceptual simplification, reduced computational load, and direct integration with a synchronous frame vector control scheme.

The numerical switching model of the VSC is linearised to gain a small-signal controlled model, which is validated against time-domain PSCAD/EMTDC simulations. The controlled model is evaluated as a STATCOM-type system, exercising closed-loop control over the reactive power flow and dc-side capacitor voltage using a simple linear control scheme. The resulting state-space model is analysed using conventional LTI techniques, giving pole-zero and root-locus analyses which predict the dynamic behaviour of the converter system. Through the ability to independently vary the highest simulated harmonic order, the dependence on the closed-loop response to dynamic harmonic coupling is demonstrated, distinguishing the HSS model from fundamental-only Dynamic Phasor models by its ability to accurately model these dynamics.

ACKNOWLEDGEMENTS

Firstly, I would like to extend my thanks to my supervisor Dr Alan Wood, who has been a pleasure to work with and a font of patience and encouragement.

I would also like to thank the great teachers I have had at the University of Canterbury. Along with Dr Wood and others, Dr Hamish Laird, Dr Bill Heffernan, and the late Associate Professor Richard Duke all contributed their insight and fostered my enthusiasm for the field.

My family and friends have made this journey through academic pressures and seismic activity much more bearable, I thank you all.

This work was made possible by the financial support of the EPECentre and the University of Canterbury, for which I am grateful.

CONTENTS

LIST OF FIGURES

LIST OF TABLES

GLOSSARY

The following glossary contains a list of the commonly used nomenclature and abbreviations found in this thesis.

NOMENCLATURE

$\vec{M}$	switching modulation vector
m_f	carrier frequency multiple
$\Im$	imaginary component
$\Re$	real component
$\mathbb{C}$	set of complex numbers
$\mathbb{R}$	set of real numbers
$\mathbb{Z}$	set of integers
M_d	direct-axis component of modulation vector
M_q	quadrature-axis component of modulation vector
$x(t)$	time-domain signal
$x_\psi(t)$	generalised phase time-domain signal
$\mathbf{\Gamma}(t)$	vector of harmonic exponentials
$\boldsymbol{X}$	vector of harmonic coefficients
$\boldsymbol{X}_\psi$	generalised phase ac harmonic vector
$\bar{\boldsymbol{X}}$	harmonic state space matrix
$\boldsymbol{\Psi}$	phase-dependent shift matrix
$\mathcal{D}\{\cdot\}$	diagonal matrix operator
$\mathcal{T}\{\cdot\}$	Toeplitz matrix operator
ω_0	fundamental angular frequency

ABBREVIATIONS

EHD	Extended Harmonic Domain
EMP	Exponentially Modulated Periodic
FACTS	Flexible AC Transmission System

FFT	Fast Fourier Transform
FTM	Frequency Transfer Matrix
HSS	Harmonic State Space
HVDC	High Voltage Direct Current
LTI	Linear Time Invariant
LTISS	LTI State Space
LTP	Linear Time Periodic
PLL	Phase-Locked Loop
PWM	Pulse-Width Modulation
STATCOM	Static Synchronous Compensator
TCR	Thyristor-Controlled Reactor
UPS	Uninterruptible Power Supply
VSC	Voltage-Source Converter

Chapter 1

INTRODUCTION

This thesis is concerned with the modeling of the three-phase Voltage-Source Converter (VSC) using a framework developed in the Harmonic State Space (HSS) domain. This chapter summarizes the motivating factors behind this work.

1.1 RELEVANCE OF THE VOLTAGE-SOURCE CONVERTER

The three-phase VSC can be regarded as the fundamental building block of many grid-connected power electronic systems. Its ability to produce voltage waveforms comprised of arbitrary magnitudes, frequencies, and phases allows it to be used in many different applications including Flexible AC Transmission System (FACTS) devices, on-line Uninterruptible Power Supply (UPS) installations, high-efficiency switching controlled rectifiers, and VSC-HVDC transmission systems.

Continuing development in power semiconductor devices have increased device ratings, lowered cost, and improved efficiency, in turn enabling an expanding scope of applications. The significant and growing importance of the VSC in electric power systems is a major motivation for this research. Increased penetration of VSC-based systems is occurring at all levels and scales of the power system, from converters interfacing renewable generation sources, to FACTS devices supporting the efficient use of transmission resources, to high-efficiency controlled loads. The combined effect of increasing power levels and system penetration is a wider scope for interaction between converter systems, and thus the demand for models capable of describing these interactions, as highlighted in [Arrillaga and Watson 2008].

1.2 MOTIVATIONS FOR ALTERNATIVE MODELS

Time-domain simulation techniques for power electronic systems are technologically mature, with Electromagnetic Transient programs employing Dommel's technique in combination with inter-

polation algorithms and other subroutines to provide a fully general simulation framework for a wide class of power systems, including those incorporating switching elements [Dommel 1969].

Although able to compute solutions for arbitrary networks, the resulting time-domain output is of limited use for the purposes of control analysis, or the study of converter interactions, as the underlying dynamics are not revealed. As will be discussed in Chapter 5, linearised state-space control models exist for these converters, but they necessarily do not capture higher-order dynamics such as harmonic coupling effects. As discussed in Chapter 2, a wide variety of harmonic domain models exist for specific applications such as harmonic penetration studies. The legacy of these models is a large body of harmonic domain modelling and analysis techniques, some of which can be generalised to the dynamic HSS.

Modeling techniques using the HSS domain hold the promise of unifying harmonic and control analyses, while providing accurate transient simulated output. Simple controlled HSS models have proven their ability to produce closed-loop stability results [Möllerstedt and Bernhardsson 2000] for systems where harmonic interaction affects the control response, and to provide insight into control design in the presence of system resonances [Orillaza 2011].

1.3 RESEARCH OBJECTIVES

The principle objective of this research is to develop a general-purpose harmonic state space model of the controlled two-level three-phase voltage source converter, which provides a unified electrical and control model. In developing the modelling framework for this converter model, the secondary goal is to advance the state of the art of HSS modelling of FACTS devices, by articulating a coherent interpretation of HSS signals which allows for the unification of electrical and control models. Another area for investigation is the application of LTI system analysis techniques to these HSS models, in order to better characterise closed-loop system performance.

1.4 THESIS OUTLINE

Chapter 2 introduces the harmonic domain as the natural domain for modelling non-linear and modulating elements in power systems, and defines general concepts and procedures for mapping time-domain relations in linear time periodic systems to harmonic-domain operations using the construct of the Frequency Transfer Matrix.

Chapter 3 derives the Harmonic State Space as a periodic extension of the LTI State Space (LTISS). The properties of LTISS systems are identified, and it is demonstrated that the HSS formulation retains analogous properties. General procedures for the mapping of LTP systems

to self-contained HSS models are developed, and applied to passive LTI networks that will be later used as elements of an HSS power system model.

Chapter 4 details the operation and control of grid-connected Voltage Source Converters, so as to inform the development of a suitable HSS modelling framework. The HSS model of the VSC is developed as a set of reduced-order FTMs, described by a numerical switching model. These transfers are verified against an equivalent PSCAD/EMTDC model in isolation and as part of a STATCOM-type system.

Chapter 5 extends the VSC model to include linearised transfers from a synchronous vector control scheme, giving a dynamic small-signal model. Using the reduced-order three-phase harmonic domain modelling framework of Chapter 4, measurement concepts for dynamic HSS signals are developed to link the electrical and control elements. Closed-loop performance of the dynamic model is evaluated, and LTI analysis techniques are applied to generate discrete root-loci for control parameters.

Chapter 6 closes the thesis with a review of benefits and limitations of the modelling framework developed here, and suggests a domain of applicability. Potential research directions and applications are identified.

Chapter 2

HARMONIC DOMAIN MODELLING

2.1 INTRODUCTION

This chapter introduces the techniques of harmonic domain modelling, and how they map to time-domain operations within generalised Linear Time Periodic (LTP) systems. This will form the basis for the extension of these techniques to dynamically varying harmonic signals in Chapter 3.

Harmonic domain modelling of power systems provides a systematic way of modelling the coupling between harmonic components due to non-linearities and modulating elements, as reviewed in [Arrillaga *et al.* 1995]. The harmonic domain, combined with iterative techniques such as Newton-Raphson methods, gives a steady-state solution to the interaction of these harmonic sources.

Harmonic domain models have been successfully applied to modelling low-frequency interactions across HVDC links [Larsen *et al.* 1989] [Hume *et al.* 2003]. A comprehensive harmonic domain model for systems containing PWM-switched converters can be found in [Collins 2006], which integrates the load-flow, harmonic, and control mismatches into an iterative numerical model, giving steady-state solutions for unbalanced systems containing a variety of PWM-based converters.

A harmonic domain model forms a complete description of a system in a periodic steady state. For power electronic systems, this implies that the switching instants of the modelled devices are periodically fixed, and that the system has relaxed to a cyclic steady state condition [Love 2007]. It will be seen in Chapter 3 that the harmonic domain solution to an LTP system is the devolution of the fully dynamic harmonic state space solution to the cyclic steady state.

2.2 HARMONIC SIGNAL REPRESENTATION

The foundational principle of harmonic domain modelling is the equivalence of a periodic signal with its Fourier series expansion [Bracewell 2000]. It is represented here as a vector of harmonic coefficients, $X_k \in \mathbb{C}$

$$x(t) = \sum_{k\in\mathbb{Z}} X_k e^{jk\omega_0 t} \tag{2.1}$$

In practical applications, the vector is truncated to a maximum harmonic order h, which is practicable if the spectral content of the signal decreases with frequency. By defining a finite vector of harmonic exponentials, $\mathbf{\Gamma}(t)$, as

$$\mathbf{\Gamma}(t) = \begin{bmatrix} e^{-jh\omega_0 t} & \dots & e^{-j2\omega_0 t} & e^{-j\omega_0 t} & 1 & e^{j\omega_0 t} & e^{j2\omega_0 t} & \dots & e^{jh\omega_0 t} \end{bmatrix} \tag{2.2}$$

the signal may be represented more compactly, as

$$x(t) = \mathbf{\Gamma}(t)\boldsymbol{X} \tag{2.3}$$

The vector $\boldsymbol{X}$ is a constant vector of complex harmonic coefficients, comprised of positive and negative frequency components, which will be conjugate terms for a real signal $x(t)$, as well as a zero-frequency term which will be restricted to real values for a real signal.

2.3 FREQUENCY TRANSFER MATRICES

The Frequency Transfer Matrix (FTM) is introduced as a general construct for the representation of various time-domain operations in the harmonic domain. An output harmonic vector is the result of the product of an FTM and an input harmonic vector, and through this, represents a time-domain operation mapping a periodic input to a periodic output. This thesis makes use of the Operational Matrices formulation of Madrigal and Rico [Madrigal and Rico 2004] to describe operations on LTP signals. Two basis FTMs are defined and discussed here, which will be used to construct FTMs to enable a complete system description in the harmonic domain.

2.3.1 Basis FTM Operators

Diagonal Matrix Given a complex vector $\{a_n\}_{n\in[-h,h]}$, the diagonalising operator $\mathcal{D}$ produces a square FTM of rank $2h+1$, with the diagonal elements of a_n and zeros elsewhere, as in

2.4

$$\begin{aligned}\boldsymbol{D} &= \mathcal{D}\{a_n\}_{n\in[-h,h]} \\ &= \begin{bmatrix} a_{-h} & & & & \\ & \ddots & & & \\ & & a_0 & & \\ & & & \ddots & \\ & & & & a_h \end{bmatrix}\end{aligned} \tag{2.4}$$

Toeplitz Matrix Given a complex vector $\{a_n\}_{n\in[-h,h]}$, the Toeplitz operator $\mathcal{T}$ produces a square FTM of rank $h+1$, which has constant diagonal terms.

$$\begin{aligned}\boldsymbol{T} &= \mathcal{T}\{a_n\}_{n\in[-h,h]} \\ &= \begin{bmatrix} a_0 & a_{-1} & \dots & a_{-h} \\ a_1 & \ddots & \ddots & \ddots \\ \vdots & \ddots & \ddots & a_{-1} \\ a_h & \ddots & a_1 & a_0 \end{bmatrix} \\ \boldsymbol{T}_{k,l} &= a_{k-l}\end{aligned} \tag{2.5}$$

2.3.2 FTMs for Time Domain Operations

Two classes of operations on periodic signals can be defined, which together form a complete description of operations within a periodic system. Those in the first class, that of unary operations, apply a harmonically decoupled transformation to a harmonic vector input. In the most general case, these operations are an arbitrary phase and magnitude transformation between each individual harmonic component of the input and output vectors, and can therefore model any Linear Time Invariant (LTI) operation on harmonic domain signals. Those in the second class, that of binary operations, produce a harmonic vector output from two harmonic vector inputs. This is required to model the time-domain operation of the multiplication of two inputs. Although the two inputs are mathematically interchangeable, one is selected to become the operator, and the other the operand, in a choice which reflects the structure of the modelled system.

Harmonically Decoupled FTM The general form of the harmonically decoupled transfer

is described by multiplication with the diagonalised matrix of 2.4. For the input vector $\boldsymbol{U}$ and output vector $\boldsymbol{W}$, the operation describing the decoupled transfer is multiplication with the diagonally-structured FTM $\boldsymbol{V}$.

$$\begin{aligned} \boldsymbol{W} &= \boldsymbol{V}\boldsymbol{U} \\ \boldsymbol{V} &\triangleq \mathcal{D}\{v_n\}_{n\in[-h,h]} \end{aligned} \tag{2.6}$$

All LTI operations such as scaling, transformation by harmonic admittance, integration and differentiation are special cases of this FTM.

Integration FTM For the periodic input vector $\boldsymbol{U}$ with fundamental angular frequency ω_0, the FTM $\boldsymbol{\Lambda}_{\int}$ of the transfer to its time integral is described as:

$$\begin{aligned} y(t) &= \int u(t)\,dt \\ Y_n &= \frac{1}{jn\omega_0}U_n \\ \boldsymbol{\Lambda}_{\int} &\triangleq \mathcal{D}\left\{\frac{1}{jn\omega_0}\right\}_{n\in[-h,h]} \end{aligned} \tag{2.7}$$

Differentiation FTM For the periodic input vector $\boldsymbol{U}$ with fundamental angular frequency ω_0, the FTM $\boldsymbol{\Lambda}_D$ of the transfer to its time derivative is described as:

$$\begin{aligned} y(t) &= \frac{du(t)}{dt} \\ Y_n &= jn\omega_0 U_n \\ \boldsymbol{\Lambda}_D &\triangleq \mathcal{D}\{jn\omega_0\}_{n\in[-h,h]} \end{aligned} \tag{2.8}$$

Phase Shift FTM A time-domain shift of the periodic signal $\boldsymbol{U}$ by τ seconds is equivalent to a shift by $\phi = \frac{\tau}{\omega_0}$ radians at the fundamental frequency, and therefore $n\phi$ radians at every n^{th} harmonic component, which may be represented in the following decoupled FTM:

$$
\begin{aligned}
y(t) &= u(t + \frac{\phi}{\omega_0}) \\
Y_n &= e^{jn\phi} U_n \\
\mathbf{\Lambda}_\Phi(\phi) &\triangleq \mathcal{D}\{e^{jn\phi}\}_{n\in[-h,h]}
\end{aligned} \tag{2.9}
$$

Three-Phase Shift FTM A special case of the phase shift FTM can be applied in the modelling of three-phase power systems. Phase signals (currents or voltages) in balanced and periodic three-phase systems are identical, but shifted in time by one third of the fundamental period. This implies that any of the three phase signals may be described as time-shifted variations of the reference phase a, or equivalently in the harmonic domain as the harmonic vector of a modified by the harmonic-dependent phase shift defined in equation 2.9.

The positive sequence phase shift ψ relative to phase a is therefore defined as $\psi_a = 0$, $\psi_b = \frac{-2\pi}{3}$ and $\psi_c = \frac{2\pi}{3}$ over the three phases. The general vectorial representation of this FTM is gained by applying this phase-dependent shift ψ to the general phase shift FTM:

$$\mathbf{\Psi} = \mathbf{\Lambda}_\Phi(\psi) \tag{2.10}$$

$$\mathbf{\Psi} \triangleq \mathcal{D}\{e^{jn\psi}\}_{n\in[-h,h]} \tag{2.11}$$

In this manner, the FTM may be applied to give a generalised harmonic domain expression for any phase $\boldsymbol{U}_\psi$ in a symmetric system, based on the single harmonic domain vector for the phase a signal, $\boldsymbol{U}_a$:

$$\boldsymbol{U}_\psi = \mathbf{\Psi}\boldsymbol{U}_a \tag{2.12}$$

Multiplication FTM Implementing multiplication of periodic signals represented as harmonic vectors is achieved by exploiting the convolution theorem, which states that the Fourier series expansion of the time-domain product of two signals $v(t)$ and $u(t)$ is equal to the convolution of their respective Fourier series expansions, the harmonic vectors $\boldsymbol{V}$ and $\boldsymbol{U}$.

$$w(t) = v(t)u(t) \tag{2.13}$$

$$\sum_{k=-h}^{h} W_k e^{jk\omega_0 t} = \sum_{m=-h}^{h} V_m e^{jm\omega_0 t} \sum_{n=-h}^{h} U_n e^{jn\omega_0 t} \tag{2.14}$$

The Toeplitz structure rationalises the product of sums to a matrix multiplication.

$$\begin{aligned} \boldsymbol{\Gamma}(t)\boldsymbol{W} &= \boldsymbol{\Gamma}(t)\boldsymbol{\mathcal{T}}\{\boldsymbol{V}\}_{m\in[-2h,2h]}\boldsymbol{U} \\ \boldsymbol{W} &= \boldsymbol{\mathcal{T}}\{\boldsymbol{V}\}_{m\in[-2h,2h]}\boldsymbol{U} \end{aligned} \tag{2.15}$$

The term selected as the multiplicand, from which the FTM $\boldsymbol{V}$ is formed, requires harmonic content of twice the order of the input vector to fully populate the FTM. In the terms of the positive and negative spectral representation, this is required to model in-band transfers from an input harmonic component at $p\omega_0$ to an output harmonic component at $-q\omega_0$ for $p, q \leq h$ (and likewise from $-p\omega_0$ to $q\omega_0$).

Chapter 3

HARMONIC STATE SPACE MODELLING

3.1 INTRODUCTION

This chapter introduces the HSS as a general framework for the solution of LTP systems, and shows how it can be applied to power system modelling. It will demonstrate that existing harmonic domain modelling techniques are a subset of the HSS formulation, and thus the unifying potential of the HSS framework.

The HSS was developed by Wereley [Wereley 1991] as a framework for the analysis of LTP systems. The target of Wereley's analysis was the modelling of helicopter rotor blades, which exhibit periodic dynamics as they rotate alternately into and out of the direction of travel, driving a harmonic response which the control system must be designed for. The helicopter blade system has a clear analogy to a power system containing switching converters, in which a dominant fundamental frequency input gives rise to harmonic interaction through the switching action of the converter.

This mode of analysis has its roots in earlier methods for the analysis of periodic systems. Floquet theory [Floquet 1883], introduced in 1883, provides a time-dependent change of coordinates for linear systems with periodically time-varying coefficients, resulting in a linear system with constant coefficients in the new reference frame. Importantly, all the dynamics of the original system are preserved in the modified reference frame, and stability results can be demonstrated from within the modified frame. This technique was used by Hill [Hill 1886] for the analysis of celestial objects, in which periodically varying dynamics arise through their orbits. The common idea is to use a modified reference frame in which periodic dynamics become constant. In Floquet theory, this is achieved through a factorisation of the response into the product of a periodic transition matrix with an exponential response [Alvarez Martin *et al.* 2011]. In the HSS, this is achieved through an extension of the conventional LTISS by expanding its domain of signals to explicitly include harmonic components.

Other authors reach a similar formulation to the HSS under the names of the Dynamic Harmonic

Domain (DHD) [Chavez 2010] or Extended Harmonic Domain (EHD) [Rico *et al.* 2003]. In this thesis, the terminology of the HSS is used in acknowledgement of the original formulation, and also in light of the goal of extending state-space analysis to a harmonic model of the VSC.

3.2 HARMONIC STATE SPACE

The Harmonic State Space is an extension of the conventional LTISS to describe LTP systems. The LTISS is first characterised here, so that the HSS can be logically extended from it.

3.2.1 LTI State Space

An LTI system may be modelled as a set of first-order linear differential equations of its state variables, allowing the formulation of a compact algebraic representation as an LTISS system.

$$\dot{x}(t) = Ax(t) + Bu(t) \tag{3.1}$$
$$y(t) = Cx(t) + Du(t) \tag{3.2}$$

The unilateral Laplace transform provides an integral transformation of the signals $x(t)$ of the LTISS system, and thus of the state-space formulation itself, with the use of the differential operator s giving a completely algebraic representation of the LTISS within the s-domain. The algebraic description allows analysis of the dynamic behaviour of the system through mechanisms such as the s-domain pole-zero and root-locus techniques.

$$x(s) = \mathcal{L}\{x(t)\} = \int_{0_-}^{\infty} e^{-st} x(t)\, dt \tag{3.3}$$

$$sx(s) = Ax(s) + Bu(s) \tag{3.4}$$
$$y(s) = Cx(s) + Du(s) \tag{3.5}$$

The basis function for the LTISS is the kernel function of the Laplace operator, e^{-st}, where $s = \sigma + j\omega$. It is by extension of this basis function into harmonic components that the HSS gains the power to model periodic systems. The integrability of signals on the region of $[0, \infty)$ determines the set of signals that can be described in the s-domain. This set, the complex frequency or s-domain, maps to all physically realizable signals of an LTI system, with the

exception of the resonant response to an undamped mode [Love 2007]. The form of the signals of an LTI system in the s-domain are shown in Table 3.1, where $u_0 \in \Re^{p\times 1}$.

Table 3.1 The signals of an LTI system.

LTI Signal	Symbol	Formula
Input	u(t)	$u_0 e^{st}$
Forced response (steady-state response)	$x_{ss}(t)$	$(sI - A)^{-1}Bu_0 e^{st}$
Transient response	$x_{tr}(t)$	$e^{At}(x(t_0) - x_{ss}(t_0))$
Steady state output	$y_{ss}(t)$	$Cx_{ss}(t)$
Transient output	$y_{tr}(t)$	$Cx_{tr}(t)$
System transfer function	$H(s)$	$C(sI - A)^{-1}B$

These equations reveal several important qualities of the LTI system. The response of the LTI system to an s-domain input is seperable into two parts; the transient response, which evolves at the eigenvalues of the system A matrix, and the forced or steady-state response, which evolves at the frequencies of the inputs. An important property of such a system is the relaxation of the transient response. If the system is asymptotically stable, as can be determined by the eigenvalues of the A matrix, then the transient response tends towards zero as $t \to \infty$. This property allows for the calculation of the steady state response as a direct algebraic solution of the state space description of the system for its input, a property that should be retained in any expanded framework.

In the steady state, the frequencies of the input are those of the output, but transformed through the gain and phase modifications of the mapping between inputs and outputs, as represented by the system transfer function. The linear separability of those transfers is confirmed by the equivalent representation of the p-input, q-output system as $p.q$ distinct s-domain transfer functions, though with the loss of generality and manipulability afforded by the algebraic representation. This general property of linearity, in which input frequencies map one-to-one with output frequencies, assures that an LTI system model in any single reference frame cannot describe a modulator, which couples signals at multiple frequencies through time-variant action, but hints at the expression of a domain which can.

3.2.2 Exponentially Modulated Periodic Signals

By introducing a periodic extension to the kernel function of the Laplace transform, a new signal representation is gained, the Exponentially Modulated Periodic (EMP) signal:

$$z(t) = \sum_{k\in\mathbb{Z}} Z_k e^{s_k t} \tag{3.6}$$

where $s_k = s + jk\omega_0$, giving

$$z(t) = e^{st} \sum_{k \in \mathbb{Z}} Z_k e^{jk\omega_0 t} \tag{3.7}$$

This signal representation is the product of the periodic signal of 2.1 and the complex exponential basis of the s-domain. Each component of the signal is modulated exponentially at an integer multiple of the fundamental frequency. In doing so, this creates a multiplicity of harmonic reference frames as illustrated in Fig. 3.1, allowing any fixed periodic signal to be represented by a stationary vector $\boldsymbol{Z}$ in the degenerate case where $s = 0$, and also dynamically time-varying signals in the general case.

Unlike the conventional s-domain, the dynamic signal representation is non-unique, because of the multiplicity of equivalent signals. Any s-domain signal $Z_0 e^{st}$ can be represented in any k-th order harmonic reference frame $e^{jk\omega_0}$ as $Z_k e^{(s-jk\omega_0)t}$

This signal can be equivalently expressed using the harmonic vector of 2.2, as:

$$z(t) = e^{st} \boldsymbol{\Gamma}(t) \boldsymbol{Z} \tag{3.8}$$

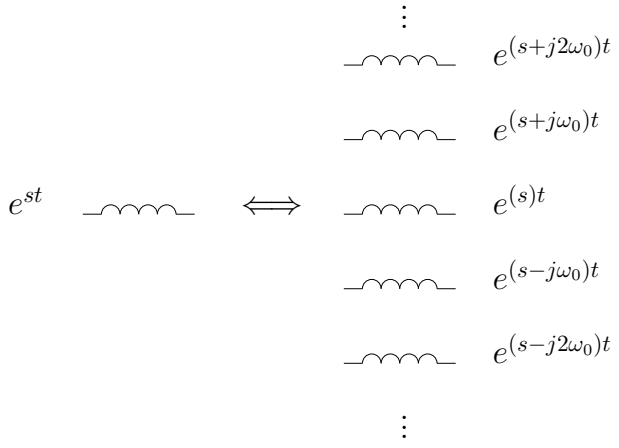

Figure 3.1 Figurative expansion of an s-domain signal into multiple harmonic reference frames.

3.2.3 Products of EMP Signals

This signal representation retains the multiplication-convolution duality of the static harmonic domain representation. This allows for the same implementation of convolution as a matrix product of a Toeplitz-structured matrix of the harmonic coefficients of the multiplicand,

$$y(t) = A(t)z(t)$$
$$e^{st}\mathbf{\Gamma}(t)\boldsymbol{Y} = e^{st}\mathbf{\Gamma}(t)\boldsymbol{\mathcal{T}}\{\boldsymbol{A}\}\boldsymbol{Z} \tag{3.9}$$
$$\boldsymbol{Y} = \boldsymbol{A}_{\mathcal{T}}\boldsymbol{Z} \tag{3.10}$$

where the shorthand $\boldsymbol{A}_{\mathcal{T}}$ is equal to the Toeplitz operator of 2.5 applied to the harmonic vector $\boldsymbol{A}$.

3.2.4 Derivative of EMP Signals

In order to form an explicit description of the state-space dynamic equations in terms of harmonic vectors, it is required to define the derivative of the harmonic modulation vector $\mathbf{\Gamma}(t)$:

$$\dot{\mathbf{\Gamma}}(t) = \mathbf{\Gamma}(t)\boldsymbol{N} \tag{3.11}$$

where $\boldsymbol{N}$ is the diagonally structured derivative matrix of 2.8. Using this form, the derivative of the EMP signal of 3.8 can be generated using the product rule as:

$$\dot{z}(t) = e^{st}\mathbf{\Gamma}(t)s\boldsymbol{Z} + e^{st}\mathbf{\Gamma}(t)\boldsymbol{N}\boldsymbol{Z} \tag{3.12}$$

3.2.5 Harmonic State Space Equations

The state-space description of a LTP system is written below, in which the system matrices $A(t)$, $B(t)$, $C(t)$ and $D(t)$ are T_0-periodic functions.

$$\dot{x}(t) = A(t)x(t) + B(t)u(t) \tag{3.13}$$
$$y(t) = C(t)x(t) + D(t)u(t) \tag{3.14}$$

By expressing the dynamic state-space equations of 3.13 and 3.14 using the EMP signals and operators defined in 3.8-3.12, the dynamic Harmonic State Space equations are produced as follows:

$$
\begin{aligned}
e^{st}\boldsymbol{\Gamma}(t)s\boldsymbol{X} + e^{st}\boldsymbol{\Gamma}(t)\boldsymbol{N}\boldsymbol{X} &= e^{st}\boldsymbol{\Gamma}(t)\boldsymbol{A}_{\mathcal{T}}\boldsymbol{X} + e^{st}\boldsymbol{\Gamma}(t)\boldsymbol{B}_{\mathcal{T}}\boldsymbol{U} \\
s\boldsymbol{X} + \boldsymbol{N}\boldsymbol{X} &= \boldsymbol{A}_{\mathcal{T}}\boldsymbol{X} + \boldsymbol{B}_{\mathcal{T}}\boldsymbol{U} \\
s\boldsymbol{X} &= (\boldsymbol{A}_{\mathcal{T}} - \boldsymbol{N})\boldsymbol{X} + \boldsymbol{B}_{\mathcal{T}}\boldsymbol{U} \qquad (3.15)
\end{aligned}
$$

$$
\begin{aligned}
e^{st}\boldsymbol{\Gamma}(t)\boldsymbol{Y} &= e^{st}\boldsymbol{\Gamma}(t)\boldsymbol{C}_{\mathcal{T}}\boldsymbol{X} + e^{st}\boldsymbol{\Gamma}(t)\boldsymbol{D}_{\mathcal{T}}\boldsymbol{U} \\
\boldsymbol{Y} &= \boldsymbol{C}_{\mathcal{T}}\boldsymbol{X} + \boldsymbol{D}_{\mathcal{T}}\boldsymbol{U} \qquad (3.16)
\end{aligned}
$$

These equations map the time-periodic LTP system matrices to their fixed HSS equivalents, defining the general procedure for the translation of a pure LTP system into an HSS system by means of the Toeplitz transform and time derivative matrix.

$$\bar{\boldsymbol{A}} = \boldsymbol{A}_{\mathcal{T}} - \boldsymbol{N} \qquad (3.17)$$

$$\bar{\boldsymbol{B}} = \boldsymbol{B}_{\mathcal{T}} \qquad (3.18)$$

$$\bar{\boldsymbol{C}} = \boldsymbol{C}_{\mathcal{T}} \qquad (3.19)$$

$$\bar{\boldsymbol{D}} = \boldsymbol{D}_{\mathcal{T}} \qquad (3.20)$$

Of note is the presence in the system dynamic matrix of equation 3.15 of the $-\boldsymbol{N}\boldsymbol{X}$ term, which can be interpreted as forcing a rotation of the nth component of the harmonic state variable at $e^{-jn\omega_0}$, which is equivalent to the reality that in the stationary reference frame, the unforced state variables will remain constant.

3.2.6 HSS Properties

Just as a stable LTISS system was defined to relax to a steady-state condition for a constant input vector, in this form it can be seen that the HSS system relaxes to a similar steady-state condition, specifically the cyclical or harmonic steady state where $s\boldsymbol{X} = \boldsymbol{0}$. From this, the steady-state solution to an arbitrary harmonic input can be solved through manipulation of the state-space matrices:

$$
\begin{aligned}
s\boldsymbol{X} &= \bar{\boldsymbol{A}}\boldsymbol{X} + \bar{\boldsymbol{B}}\boldsymbol{U} \\
\boldsymbol{Y} &= \bar{\boldsymbol{C}}\boldsymbol{X} + \bar{\boldsymbol{D}}\boldsymbol{U}
\end{aligned}
$$

$$
\begin{aligned}
\mathbf{0} &= \bar{\boldsymbol{A}}\boldsymbol{X} + \bar{\boldsymbol{B}}\boldsymbol{U} \\
\boldsymbol{X} &= -\bar{\boldsymbol{A}}^{-1}\bar{\boldsymbol{B}}\boldsymbol{U} && (3.21) \\
\boldsymbol{Y} &= (-\bar{\boldsymbol{C}}\bar{\boldsymbol{A}}^{-1}\bar{\boldsymbol{B}} + \bar{\boldsymbol{D}})\boldsymbol{U} && (3.22)
\end{aligned}
$$

3.3 PASSIVE NETWORK MODELLING

The HSS modelling techniques described above are applied here to LTI component networks that will later be used as part of a larger VSC system model. The result is a self-contained HSS block suitable for the modular system construction described in Section 4.4.4.

Series RL Network

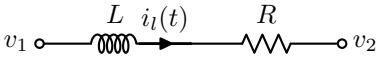

Figure 3.2 Series RL network.

As a linear network, describable using first-order differential equations, the series RL network as shown in Fig. 3.2 can be written in state-space form, using the following state mapping:

$$
\begin{aligned}
x(t) &= \begin{bmatrix} i_l(t) \end{bmatrix} && (3.23) \\
y(t) &= \begin{bmatrix} i_l(t) \end{bmatrix} && (3.24) \\
u(t) &= \begin{bmatrix} v_1(t) \\ v_2(t) \end{bmatrix} && (3.25)
\end{aligned}
$$

$$
\begin{aligned}
\begin{bmatrix} \dot{i_l}(t) \end{bmatrix} &= \begin{bmatrix} \frac{-R}{L} \end{bmatrix} \begin{bmatrix} i_l(t) \end{bmatrix} + \begin{bmatrix} \frac{1}{L} & \frac{-1}{L} \end{bmatrix} \begin{bmatrix} v_1(t) \\ v_2(t) \end{bmatrix} && (3.26) \\
\begin{bmatrix} i_l(t) \end{bmatrix} &= \begin{bmatrix} 1 \end{bmatrix} \begin{bmatrix} i_l(t) \end{bmatrix} + \begin{bmatrix} 0 & 0 \end{bmatrix} \begin{bmatrix} v_1(t) \\ v_2(t) \end{bmatrix} && (3.27)
\end{aligned}
$$

When these time-invariant matrices are generalised as constant LTP matrices, the resultant

Toeplitz transforms of their spectra are constant diagonal matrices of dimension $n = [-h, h]$, which when combined with the LTP to HSS mapping procedure of equations 3.17-3.20 gives the HSS frequency transfer matrices and associated harmonic state vectors, resulting in a self-contained state-space block with defined harmonic inputs and outputs:

$$\bar{\boldsymbol{A}} = \boldsymbol{A}_{\mathcal{T}} - \boldsymbol{N}$$

$$= \begin{bmatrix} \frac{-R}{L} & & & & \\ & \ddots & & & \\ & & \frac{-R}{L} & & \\ & & & \ddots & \\ & & & & \frac{-R}{L} \end{bmatrix} - \begin{bmatrix} -jh\omega_0 & & & & \\ & \ddots & & & \\ & & 0 & & \\ & & & \ddots & \\ & & & & +jh\omega_0 \end{bmatrix}$$

$$\bar{\boldsymbol{A}} = \begin{bmatrix} \frac{-R}{L} + jh\omega_0 & & & & \\ & \ddots & & & \\ & & \frac{-R}{L} & & \\ & & & \ddots & \\ & & & & \frac{-R}{L} - jh\omega_0 \end{bmatrix} \tag{3.28}$$

$$\bar{\boldsymbol{B}} = \begin{bmatrix} \frac{1}{L} & & \frac{-1}{L} & & \\ & \ddots & & \ddots & \\ & \frac{1}{L} & & \frac{-1}{L} & \\ & & \ddots & & \ddots \\ & & \frac{1}{L} & & \frac{-1}{L} \end{bmatrix} \tag{3.29}$$

$$\bar{\boldsymbol{C}} = \begin{bmatrix} 1 & & & \\ & \ddots & & \\ & & 1 & \\ & & & \ddots \\ & & & 1 \end{bmatrix} \tag{3.30}$$

$$\bar{\boldsymbol{D}} = \begin{bmatrix} 0 & & 0 & & \\ & \ddots & & \ddots & \\ & 0 & & 0 & \\ & & \ddots & & \ddots \\ & & 0 & & 0 \end{bmatrix} \tag{3.31}$$

$$\boldsymbol{X} = \begin{bmatrix} \dots & I_{l,-1} & I_{l,+0} & I_{l,+1} & \dots \end{bmatrix}^T \tag{3.32}$$

$$\boldsymbol{Y} = \begin{bmatrix} \dots & I_{l,-1} & I_{l,+0} & I_{l,+1} & \dots \end{bmatrix}^T \tag{3.33}$$

$$\boldsymbol{U} = \begin{bmatrix} \begin{bmatrix} \dots & V_{1,-1} & V_{1,+0} & V_{1,+1} & \dots \end{bmatrix} & \begin{bmatrix} \dots & V_{2,-1} & V_{2,+0} & V_{2,+1} & \dots \end{bmatrix} \end{bmatrix}^T \tag{3.34}$$

The HSS models of these LTI networks are diagonal in structure, the individual harmonic components therefore being independent of each other. This implies these HSS constructions are not dependent on any specific three-phase signal representation or choice of modelled harmonics. They can therefore be constructed for any subset of harmonic components, as included in the state space vectors and matrices.

Series RC Network

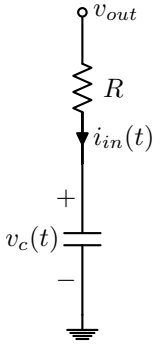

Figure 3.3 Series RC network.

The series RC network, as illustrated in Fig. 3.3, has the following state-space form which similarly translates into a decoupled HSS system:

$$\begin{bmatrix} \dot{v_c}(t) \end{bmatrix} = \begin{bmatrix} 0 \end{bmatrix} \begin{bmatrix} v_c(t) \end{bmatrix} + \begin{bmatrix} \frac{1}{C} \end{bmatrix} \begin{bmatrix} i_{in}(t) \end{bmatrix} \tag{3.35}$$

$$\begin{bmatrix} v_{out}(t) \end{bmatrix} = \begin{bmatrix} 1 \end{bmatrix} \begin{bmatrix} v_c(t) \end{bmatrix} + \begin{bmatrix} R \end{bmatrix} \begin{bmatrix} i_{in}(t) \end{bmatrix} \tag{3.36}$$

Parallel RC Network

The parallel RC network, as illustrated in Fig. 3.4, has the following state-space form which similarly translates into a decoupled HSS system:

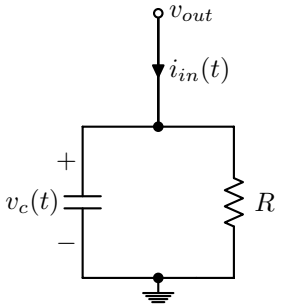

Figure 3.4 Parallel RC network.

$$\left[\dot{v_c}(t)\right] = \left[\tfrac{-1}{RC}\right]\left[v_c(t)\right] + \left[\tfrac{1}{C}\right]\left[i_{in}(t)\right] \tag{3.37}$$

$$\left[v_{out}(t)\right] = \left[1\right]\left[v_c(t)\right] + \left[0\right]\left[i_{in}(t)\right] \tag{3.38}$$

Chapter 4

THREE PHASE VSC MODELLING

4.1 INTRODUCTION

This chapter introduces the three-phase VSC as the subject of analysis in the HSS domain. The principles of the operation and control of pulse-width modulated (PWM) VSC systems are introduced generally and then used to describe a harmonic domain modelling framework suited for three-phase vector control.

The switching action of the VSC is described using the numerical switching function model developed in Section 4.4, at first using a fixed control vector and switching function, which is extended to modelling varying control inputs in Chapter 5. The output of the numerical switching function model is then used in Section 4.4.3 to define the harmonic-domain transfers which describe the uncontrolled VSC in the HSS.

Existing harmonic domain models of VSCs usually make use of analytic derivations of the switching spectra, defined as Fourier coefficients of pulse trains as determined by a set of switching instants [Collins 2006], where control variation is an element of the steady-state solution combining load-flow and harmonic solutions. To date most HSS (or equivalently EHD/DHD) models of VSCs similarly model fixed switching functions, using individual phase networks to provide the generality for the modelling of non-characteristic harmonics and unbalanced system conditions [Madrigal *et al.* 2000] [Rico *et al.* 2003].

The goal of the VSC model developed in this chapter is to provide a flexible framework which is organised around the principles of vector control, and which satisfies a unified interpretation of three-phase quantities in the harmonic state space, allowing for subsequent extension to a controlled model.

4.1.1 VSC Applications

The Voltage Source Converter is a highly versatile topology. By modulating a dc bus with three sets of switches, it acts as a synthetic voltage source of variable magnitudes, phases and frequencies. As a controllable voltage source, it can indirectly control current and power flows between the ac and dc terminals. As discussed in Section 4.3, with a suitable control scheme this allows for the decoupled control of real and reactive power flows, allowing the VSC to be controlled as a virtual machine.

As an intermediating link between ac and dc systems, this ability to control decoupled power flows gives the VSC use as a grid-tie inverter for dc energy sources such as photovoltaic power systems, as a STATCOM, or a controlled rectifier. When two converters are combined with a shared dc link, the same structure can serve as a variable-speed machine drive, or VSC-HVDC link.

4.2 VSC STRUCTURE AND OPERATION

4.2.1 Structure and Operation

The fully-controlled two-level three-phase bridge forms the kernel of the three-phase voltage-source converter. It consists of three converter legs, each connecting an ac phase to the positive and negative rails of the dc bus through a pair of fully-controlled switching devices. These devices may be of any force-commutated type, including MOSFETs, IGBTs or GTOs, and may be connected in any combination of parallel or series configurations in order to achieve higher current or voltage ratings, so long as they are switched unitarily to give the effect of a monolithic switching device.

The switching devices are controlled between an on-state (conducting) and an off-state (blocking). When the upper switching device is on, the phase is connected to the top rail of the dc bus, and similarly for the lower switching device. The state of the switches on an individual leg may be described by a switching function for each phase, $s_\psi(t)$, which takes the value 1 when the top switch is conducting, and -1 when the bottom switch is conducting.

4.2.2 Dead-time Compensation

The switching devices are paired with antiparallel diodes such that there always exists a path for the phase current, even when both switching devices in a leg are off. This state necessarily occurs during the dead-time period, where both devices on a leg are simultaneously driven off, to allow the previously conducting device time to commutate to its full off-state blocking voltage

before the alternate device is switched on, in order to prevent simultaneous conduction and the catastrophic shoot-through that would accompany it. During this dead-time period, the state of conduction in either the upper or lower antiparallel diode, and thus which dc rail is connected to the phase, is dependent on the direction of the current in the phase. If left unchecked, this will result in a departure of the effective switching function from the ordered switching signal, and thus in the terms of angular or vector control schemes, a departure from the ordered fundamental frequency phase vector.

Various schemes are available for the active compensation of this effect, the net result of which is an effective switching function which matches the ordered switching signal. The converter model considered in this thesis assumes the implementation of one of these schemes, such that the effect of the dead-time may be ignored in the modelling of both the converter and control system [Holmes and Lipo 2003]. This assumption is justified based on the capabilities of these schemes to be transparently integrated into the control system.

4.3 VSC CONTROL

The versatility and controllability of the fully-controlled VSC comes from the ability to apply arbitrary switching functions to its individual converter legs. This enables a control bandwidth in proportion to the maximum switching frequency of the devices, which allows for the fundamentally high-bandwidth applications such as active harmonic filtering, as well as a fast response in fundamental frequency control applications. It is these fundamental frequency control applications which this thesis is concerned with, in which the objective is control over fundamental frequency voltages, currents, and power flows.

This section introduces the converter control techniques required for basic fundamental frequency control applications, and their treatment in the harmonic domain model of the VSC.

4.3.1 PWM Control

4.3.1.1 Carrier-Based PWM

Carrier-based PWM is the oldest and most straightforward technique for the translation of a control reference signal into a switching function, well-described in sources such as [Mohan and Undeland 2007] and [Holmes and Lipo 2003]. The switching function for an individual phase $s_\psi(t)$ is produced from the comparison of two signals, the carrier signal $v_c(t)$ and reference signal $v_{ref-\psi}(t)$. The carrier signal is a sawtooth or triangular waveform of frequency ω_c, which must be an integer multiple m_f of the fundamental frequency ω_0 to produce a switching function with a fundamental period T_0. In single-phase applications, it is sufficient for m_f to be an odd number

so as to avoid the production of even harmonics. For three-phase converters, m_f is chosen as an odd third multiple [Mohan and Undeland 2007].

The reference signal is in the most basic case a set of three sinusoids with the desired amplitude, or modulation index m_a and phase. For the generation of a balanced three-phase switching function, reduces to a single space vector $\vec{M}$ in either a static or synchronous reference frame. The resultant switching signal, sharing the fundamental period, may be expressed as its Fourier series expansion, and equivalently as a harmonic vector:

$$s_\psi(t) = \sum_{k\in\mathbb{Z}} S_{\psi,k} e^{jk\omega_0 t} \tag{4.1}$$

$$s_\psi(t) = \mathbf{\Gamma}(t)\boldsymbol{S}_\psi \tag{4.2}$$

When analysed in the frequency domain, the resulting switching signal in the ideal case has a fundamental frequency component with an identical magnitude and phase to the reference signal. This is equivalent to stating that the transfer function from m_a to $|S_{\psi 1}|$ has a linear gain. There are two criteria to be satisfied for this linearity to be achieved. Firstly, the reference signal must be constrained to the domain $(-1, 1)$ over the entire period, or the switching signal will enter an overmodulation state, resulting in not only a loss of linear gain, but the introduction of low-order harmonic content. For sinusoidal PWM, this requires that the modulation index m_a be less than 1. Secondly, the modulation frequency ratio must be sufficiently high as to present a reference waveform evolving linearly compared to the slope of the triangular carrier, in order to give a linear fundamental component transfer function. It will be seen in Section 4.4 that the numerical model developed here is equally capable of describing operation in the overmodulation region.

4.3.1.2 Space Vector Modulation

Space Vector Modulation is a newer technique for the synthesis of a three-phase PWM waveform, amenable to digital implementation. It maps a scheduled output voltage space vector in the $\alpha-\beta$ reference frame to a time-weighted combination of the eight possible switching states (and thus instantaneous output space vectors) of the three-phase two-level bridge. For a given vector, the weighted combination of switching states is non-unique because of the choice of utilisation of the two zero vectors, [000] and [111], which are equivalently zero-valued in the zero-sequence agnostic $\alpha - \beta$ reference frame [Kolar *et al.* 1991].

It has been demonstrated that one of these sub-types of SVM, symmetrical SVM with equal use of the zero vectors, is equivalent to carrier-based PWM with a 3rd harmonic triangle wave

superimposed on the reference signal [Zhou and Wang 2002]. Whether achieved in the inherently zero-sequence agnostic SVM framework or augmented to a carrier-based system, the result is an extension to the linear modulation range to $m_a \leq 2/\sqrt{3} \approx 1.154$, a 15% improvement in maximum ac voltage, and thus dc bus utilisation, which has now been widely applied. This equivalence allows SVM schemes to be easily implemented in the numerical switching model described in Section 4.4, through the modification of the reference signal with a phase-matched triangular waveform, or sinusoid for THIPWM.

4.3.2 Vector Control

Vector control in VSCs, and power electronic systems in general, allows measured power system signals to be represented as maximally decoupled quantities, suitable for treatment as independent control variables. This decoupling takes two primary forms, both achieved through the main tools of vector control, the $dq0$ and $\alpha\beta\gamma$ transforms, Park's and Clark's transformations respectively. The magnitude-preserving form of Park's transformation is given as:

$$\begin{bmatrix} v_d \\ v_q \\ v_0 \end{bmatrix} = \frac{2}{3} \begin{bmatrix} \cos(\theta) & \cos(\theta - \frac{2\pi}{3}) & \cos(\theta + \frac{2\pi}{3}) \\ -\sin(\theta) & -\sin(\theta - \frac{2\pi}{3}) & -\sin(\theta + \frac{2\pi}{3}) \\ \frac{1}{2} & \frac{1}{2} & \frac{1}{2} \end{bmatrix} \begin{bmatrix} v_a \\ v_b \\ v_c \end{bmatrix} \tag{4.3}$$

The first form of decoupling achieved through the application of Park's transformation is the conversion of the balanced component of the measured three-phase fundamental frequency signal to a static vector in the synchronous reference frame, where $\theta = \omega_{sys}t + \phi$. This decouples changes in the phase of the vector from the periodic rotation of the vector, assuming a constant system frequency, and reduces the signal dimension from three scalars to a single 2-vector. The second form of decoupling is achieved when the phase angle ϕ matches that of the remote voltage source, which may be the grid voltage at the point of common connection, or an electrical machine EMF (by definition the direct axis) in drive applications. In this synchronous reference frame, the axial d and q components of the converter current resolve directly to real and reactive power flow (or equivalently to torque and flux for a machine drive), and when the remote voltage source and the controllable voltage source of the converter are connected through a predominantly inductive impedance, these components may be effectively controlled through the quadrature manipulation of converter voltage.

This introduces the problem of achieving an accurate and stable reference for the remote voltage, which may vary in phase and frequency, so as to provide the correct signal ϕ, as any error in this signal will translate to an angular error in the reference frame, and all control signals developed within it. In practise, this is commonly achieved with a phase-locked loop (PLL) mechanism, which functions as an observer of θ and controls the error between the reference oscillator and

the external measurement. The STATCOM model presented by Wood and Osauskas in [Wood and Osauskas 2004] embeds a linearised PLL model.

As a harmonic domain model, absolute periodicity at the nominal system frequency must be assumed, which allows ω_{sys} to be fixed at ω_0. Furthermore, the phase reference is assumed to be similarly absolute, fixing the synchronous reference frame as an integral part of the model, resulting in a global fixed reference frame, and effectively ignoring PLL dynamics. This has obvious implications when modelling power systems subject to a remote source with a varying phase, which will be dealt with appropriately.

4.4 HARMONIC DOMAIN VSC MODEL

Using the general principles of harmonic domain modelling introduced in Chapter 2, and the specific considerations of VSC construction and control detailed in this chapter, the harmonic domain model of the VSC is constructed in this section in accordance with the interpretation of EMP signals for polyphase applications developed below. The numerical switching function model is developed to provide the link between the specified operating point and the switching spectrum that forms the harmonic-domain FTMs.

4.4.1 Three-Phase Signal Representation

Key to using a harmonic domain formulation for the description of a three-phase power system comprised of LTP elements is the choice of signal representation for three-phase signals. Three-phase electric power systems are the target of our analysis, as they dominate the landscape for the generation, transmission and utilisation of electrical energy at high power levels. The three-phase system is the simplest polyphase system which allows energisation in a sequence creating a rotating vector in the phase plane. It is this particular sequence of energisation, as revealed by the linear separation into the symmetrical components of Fortescue [Fortescue 1918], that imbues the three-phase power system with the privileged reference frame associated with the fundamental frequency phase vector, and which should then be considered explicitly when developing a harmonic domain model.

Harmonic signal representation in single-phase systems require no extra consideration beyond the general framework presented in Chapter 2, as their harmonic components are simple phasors with no sequence-dependent behaviour. Accordingly, it is possible to construct a three-phase harmonic domain model comprised of three single-phase networks interconnected appropriately, as in [Rico *et al.* 2003]. This can be improved upon, for the same reasons that motivated the development of the method of decomposition to symmetric components. One significant motivation for developing sequence-dependent models is the potential for reduction in the size and thus

computational load of the model, which can be realised by taking advantage of analytical results in the symmetrical framework. As a most immediate example, in a basic three-wire system, no path is available for zero-sequence current, and consequently, power flows (caveats apply, such as shared dc-side connections [Pöllänen and Others 2003]). This means that the ac harmonic state variables of order $0 + 3n$ may be eliminated without any loss of descriptive power of the model.

This thesis aims to advance a coherent treatment of three-phase harmonic domain modelling suitable for use in dynamic (i.e. HSS) models, through some simplifying assumptions about the system. The first of these is by equating the ac harmonic domain vector $\boldsymbol{\Gamma}(t)\boldsymbol{X}_{\boldsymbol{\psi}}$ with a vector of balanced harmonic phasors. For a component of a harmonic phasor to be balanced is equivalent to it being equal over all three phases by a phase shift defined by the sequence of fundamental frequency energisation, as represented by the three-phase shift FTM of 2.11.

$$\boldsymbol{X}_{\psi} = \boldsymbol{\Psi}\boldsymbol{X}_{a} \tag{4.4}$$

Under this balanced phasor construction, a single harmonic vector, nominally the a phase for simplicity, is able to simultaneously represent all three phases of an ac quantity such as the voltage applied to one side of a three-phase inductance, or the set of state variables for the currents flowing in it. It will be seen in Section 4.4.6.3 that this simplification does not preclude the modelling of imbalanced components (or other non-characteristic signals).

Secondly, the ac network itself is assumed to be balanced, that is that the impedances on each phase are assumed to be identical. This property is required for the balance of three-phase signals to be reflexive across transformation by the network impedances.

The third assumption is the steady state balance of the individual phase switching functions $s_{\psi}(t)$, in the same way as the ac harmonic domain vector was defined to be, allowing all of the phase switching functions to be described as phase-shifted variants of the phase a switching function $s_a(t)$. This assumption is concordant with a single control vector $\vec{M}$ in a fundamental frequency positive-sequence reference frame. This covers a subset of possible vector control schemes, but does not include control schemes which control the phases individually (and thus implicitly allow negative sequence control), or schemes which include a negative-sequence fundamental reference frame and associated control vector such as in [Etxeberria Otadui *et al.* 2007] to allow direct vector control over unbalanced fundamental power flows.

With these assumptions in place, the ac and dc characteristic harmonic sets of balanced phasors can be derived. Using the definition of the balanced switching function, the general form of the harmonic-domain signal over all phases for $\psi_a = 0$, $\psi_b = \frac{-2\pi}{3}$ and $\psi_c = \frac{2\pi}{3}$ may be written as:

$$\begin{aligned} x_\psi(t) &= \boldsymbol{\Gamma}(t)\boldsymbol{X}_\psi \\ x_\psi(t) &= \boldsymbol{\Gamma}(t)\boldsymbol{\Psi}\boldsymbol{X}_a \\ x_\psi(t) &= \sum_{k\in\mathbb{Z}} X_k e^{j(k\omega_0 t + k\psi)} \end{aligned} \tag{4.5}$$

The following identity holds over all ψ, allowing harmonic components of the same set to be modulated by terms of order e^{j3n} while maintaining the consistent $k\psi$ phase relation to the fundamental component, which is the defining feature of the balanced set:

$$(m + 3n)\psi = m\psi \tag{4.6}$$

Because all switching functions in the network possess half-wave symmetry, then all even ac terms may be eliminated, giving the more sparse definition:

$$(m + 6n)\psi = m\psi \tag{4.7}$$

By applying this definition to the two conjugate elements X_{+1} and X_{-1} which together define the fundamental ac component, as well as to the base dc element X_0, three sets of characteristic harmonics are defined, which are sufficient to describe all ac and dc signals in a system obeying the assumptions detailed earlier:

$$\{X_{+1}\} = \begin{bmatrix} \vdots \\ X_{-5} \\ X_{+1} \\ X_{+7} \\ \vdots \end{bmatrix}, \{X_{-1}\} = \begin{bmatrix} \vdots \\ X_{-7} \\ X_{-1} \\ X_{+5} \\ \vdots \end{bmatrix}, \{X_0\} = \begin{bmatrix} \vdots \\ X_{-6} \\ X_{+0} \\ X_{+6} \\ \vdots \end{bmatrix} \tag{4.8}$$

These characteristic harmonic sets will be used in Section 4.4.3 to enable the description of a balanced three-phase modulator as a combination of two conjugate transfers, operating linearly with respect to frequency.

4.4.2 Numerical Switching Function Model

At the core of the VSC model of this thesis is the numerical switching function model. This maps a given converter operating point, specified as a modulation vector $\vec{M}$ and carrier frequency multiple m_f to a switching function $s_a(t)$ and associated spectrum $\boldsymbol{S}_a$.

This is achieved through the direct numerical solution of the switching function, evaluated discretely at N points. The carrier signal is a symmetrical sawtooth, centred at the origin of the d-axis.

$$v_{carrier}[n] = saw(m_f n \frac{2\pi}{N}) \tag{4.9}$$

The reference signal is generated as

$$v_{ref-a}[n] = M_d \cos(n\frac{2\pi}{N}) - M_q \sin(n\frac{2\pi}{N}) \tag{4.10}$$

where $\vec{M} = M_d + jM_q$, in the fixed global synchronous reference frame defined in Section 4.3.2. The switching function is then computed discretely through a Boolean operation on the magnitude of the two signals as

$$s_a[n] = 2(v_{ref-a}[n] > v_{carrier}[n]) - 1 \tag{4.11}$$

The discrete approximation to the true switching spectrum is then computed as the FFT (Fast Fourier Transform) of the discrete switching function as

$$\boldsymbol{S}_a = \mathcal{F}\{S_a\} \tag{4.12}$$

and truncated to $k = \pm 2h$, twice the maximum harmonic order in the system, the requirement for population of the truncated Toeplitz FTMs as per equation 2.15.

The direct numerical solution of the switching function is used because of its generality and suitability for use in computer modelling. Arbitrary accuracy can be achieved with a sufficiently large choice of N, and the specific choice of carrier signal or alternate modulation method as per 4.3.1.2 can be easily achieved through modification to the reference signals. Analytical solutions of varying power and generality are available [Holmes 1998], but cannot match the flexibility afforded by the numerical method in this environment. The question of the sensitivity to the parameter N is discussed in Section 5.2.3.

This process for generating the numerical switching function is illustrated in Fig. 4.1. The switching spectrum of Fig. 4.2 is shown for just the characteristic harmonics which will form the FTMs. It demonstrates the roll-off skew property described in [Sandberg *et al.* 2005] allowing for the arbitrarily close modelling of the switching action through an FTM generated from this spectrum.

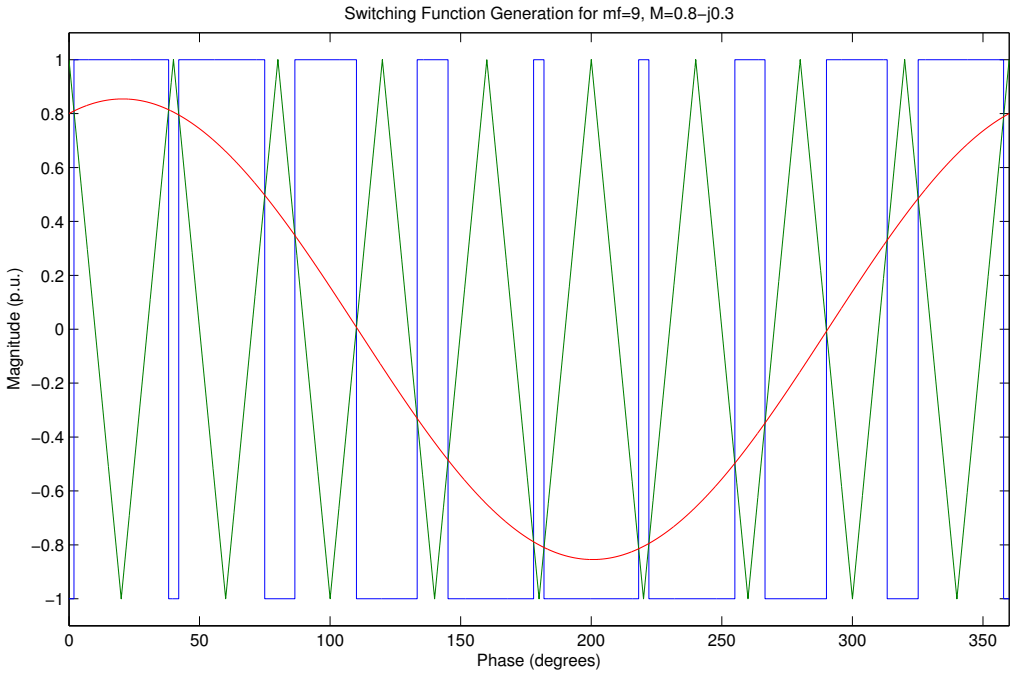

Figure 4.1 Numerical switching function generation showing the reference, carrier, and switching signals.

4.4.3 Derivation of Three-Phase Transfers

In this section, the frequency transfer matrices for the voltage and current transfers are derived from their time-domain relations. Although the general procedure for the translation of a generic LTP system to the harmonic state space is given by the HSS equations of Section 3.2.5, these are insufficient on their own for the description of the three-phase VSC in the reduced-order balanced harmonic phasor framework. Instead, the transfers will be developed using specific results from the principles of the balanced modulator.

The VSC is described by two sets of transfers; from the dc-side voltage to the ac-side voltage, and from the ac-side current to the dc-side current. These transfers are unrelated to each other except as they are described by the same patterns of conduction and thus switching functions. Both of these transfers are stateless, and are therefore described by a static $\bar{\boldsymbol{D}}$ matrix in the HSS. The derivation of these transfers proceeds as for a harmonic domain formulation with no

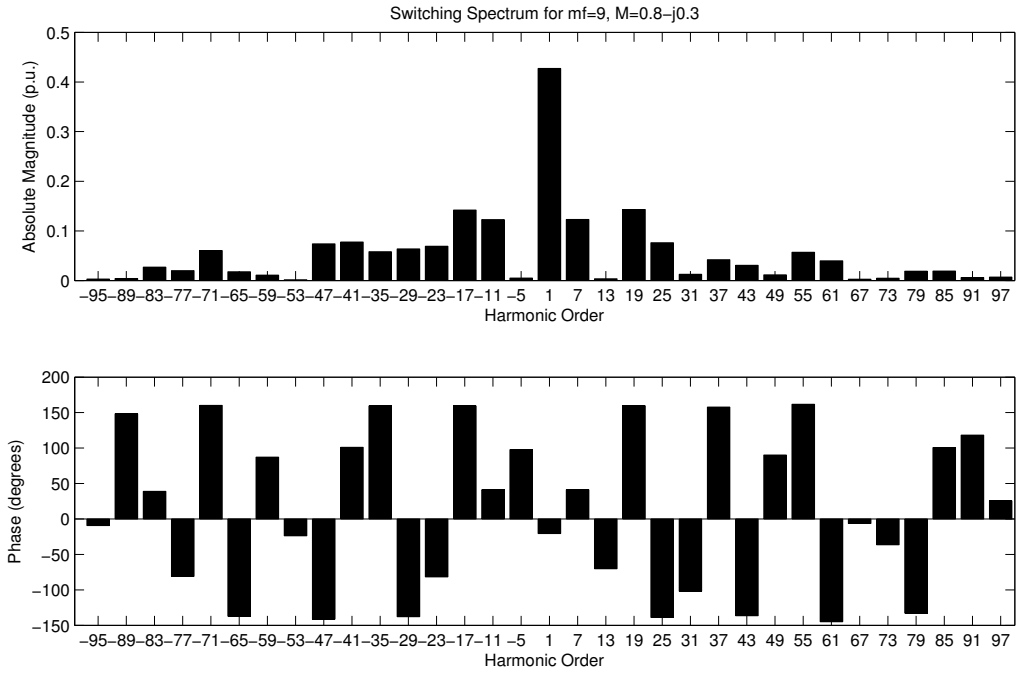

Figure 4.2 Spectrum of the switching function for the characteristic harmonics, exhibiting the roll-off characteristic.

dynamically varying components, but it will be seen that because of the statelessness of the modulator, the harmonic domain description is equivalent to the HSS model.

The phase voltages v_ψ, defined with reference to the dc-side mid-point, may be written generally as the time-domain products of the individual phase switching functions s_ψ and the dc bus voltage (also relative to the dc-side mid-point), which have the harmonic domain formulations:

$$v_\psi(t) = s_\psi(t)\frac{v_{dc}(t)}{2} \tag{4.13}$$

$$s_\psi(t) = \sum_{k\in\mathbb{Z}} S_{\psi,k} e^{jk\omega_0 t} \tag{4.14}$$

$$v_{dc}(t) = \sum_{m\in\mathbb{Z}} V_{dc,m} e^{jm\omega_0 t} \tag{4.15}$$

The phase switching functions, because of the balanced condition of the modulator, may be described as time-shifted variations of the reference phase a switching function $s_a(t)$, and equivalently in the harmonic domain as a harmonic-dependent (and thus implicitly sequence-dependent) phase shift of $k\psi$, where $\psi_a = 0$, $\psi_b = \frac{-2\pi}{3}$ and $\psi_c = \frac{2\pi}{3}$, in accordance with the

derivation of the three-phase shift FTM of equation 2.11:

$$s_\psi(t) = \boldsymbol{\Gamma}(t)\boldsymbol{S}_\psi \tag{4.16}$$

$$s_\psi(t) = \boldsymbol{\Gamma}(t)\boldsymbol{\Psi}\boldsymbol{S}_a$$

$$s_\psi(t) = \sum_{k\in\mathbb{Z}} S_{a,k}e^{j(k\omega_0 t+k\psi)} \tag{4.17}$$

This is now the fully general equation of the dc voltage to phase voltage transfer in the form of the harmonic domain product of equation 2.14, which may be expanded to yield the exponents of the resulting harmonic domain phase voltages:

$$v_\psi(t) = \frac{1}{2}\left(\sum_{k\in\mathbb{Z}} S_{a,k}e^{j(k\omega_0 t+k\psi)}\right)\left(\sum_{m\in\mathbb{Z}} V_{dc,m}e^{jm\omega_0 t}\right) \tag{4.18}$$

$$\sum_{k,m\in\mathbb{Z}} V_{a,k+m}e^{j((k+m)\omega_0 t+k\psi)} = \frac{1}{2}\sum_{k,m\in\mathbb{Z}} S_{a,k}e^{j(k\omega_0 t+k\psi)}V_{dc,m}e^{jm\omega_0 t} \tag{4.19}$$

With the restriction, assumed for now, of the dc harmonic vector to terms of order $m = 0{+}6p, p \in \mathbb{Z}$, the substitution $(k{+}m)\psi$ for $k\psi$ is performed, as $(1{\pm}3n)\psi = \psi$ over all phases. This preserves the ability of the other phases to be described by the phase a harmonic vector in combination with the same phase shift, dependent only on the harmonic order n:

$$v_\psi(t) = \sum_{n\in\mathbb{Z}} V_{a,n}e^{j(n\omega_0 t+n\psi)} = \frac{1}{2}\sum_{k,m\in\mathbb{Z}} S_{a,k}e^{j(k\omega_0 t+k\psi)}V_{dc,m}e^{jm\omega_0 t} \tag{4.20}$$

The establishment of this condition for the balanced identity of the phases allows for the construction of the equivalent vectorial expression, using the phase-dependent shift matrix of equation 2.11, which gives the form of the harmonic transfer when reduced:

$$\boldsymbol{\Gamma}(t)\boldsymbol{V}_{\boldsymbol{\psi}} = \frac{1}{2}\boldsymbol{\Gamma}(t)\boldsymbol{\mathcal{T}}\{\boldsymbol{S}_\psi\}\boldsymbol{V}_{dc} \tag{4.21}$$

$$\boldsymbol{\Gamma}(t)\boldsymbol{\Psi}\boldsymbol{V}_a = \frac{1}{2}\boldsymbol{\Gamma}(t)\boldsymbol{\Psi}\boldsymbol{\mathcal{T}}\{\boldsymbol{S}_a\}\boldsymbol{V}_{dc}$$

$$\boldsymbol{V}_a = \frac{1}{2}\boldsymbol{\mathcal{T}}\{\boldsymbol{S}_a\}\boldsymbol{V}_{dc} \tag{4.22}$$

This transfer could be implemented using a single sparse Toeplitz FTM, where the inputs and

outputs consist of full-rank harmonic vectors, giving a square FTM of dimension $2h$ containing $4h^2$ terms, where h is the highest harmonic order of the model. It is also possible to partition this transfer using two conjugate networks, the characteristic harmonic sets $1+6p$ and $-1+6p$, giving two FTMs of dimension $\frac{2h}{6}$ containing $\frac{h^2}{9}$ terms, an 18-fold reduction in the number of complex multiplications required, and therefore a 72-fold reduction in the number of scalar multiplications required when using the tensor representation of complex values described in Section 4.4.4, and a 216-fold reduction when compared to a full-rank transfer for each phase.

$$\begin{bmatrix} \vdots \\ V_{a,-5} \\ V_{a,+1} \\ V_{a,+7} \\ \vdots \end{bmatrix} = \frac{1}{2} \begin{bmatrix} \ddots & & & & \\ & S_{a,+1} & S_{a,-5} & S_{a,-11} & \\ & S_{a,+7} & S_{a,+1} & S_{a,-5} & \\ & S_{a,+13} & S_{a,+7} & S_{a,+1} & \\ & & & & \ddots \end{bmatrix} \begin{bmatrix} \vdots \\ V_{dc,-6} \\ V_{dc,+0} \\ V_{dc,+6} \\ \vdots \end{bmatrix} \tag{4.23}$$

$$\begin{bmatrix} \vdots \\ V_{a,-7} \\ V_{a,-1} \\ V_{a,+5} \\ \vdots \end{bmatrix} = \frac{1}{2} \begin{bmatrix} \ddots & & & & \\ & S_{a,-1} & S_{a,-7} & S_{a,-13} & \\ & S_{a,+5} & S_{a,-1} & S_{a,-7} & \\ & S_{a,+11} & S_{a,+5} & S_{a,-1} & \\ & & & & \ddots \end{bmatrix} \begin{bmatrix} \vdots \\ V_{dc,-6} \\ V_{dc,+0} \\ V_{dc,+6} \\ \vdots \end{bmatrix} \tag{4.24}$$

Such a partitioning also makes explicit the sequence-dependent frequency shifting behaviour of the modulator. It results in two complex ac networks, each the complex conjugate of the other in both state-space equations and signals, which combine to provide the necessarily real-valued signals for real-valued inputs.

A similar transfer can now be derived, from the phase currents to the dc-side current, which may be written as the sum of the phase currents multiplied by their respective conduction functions, which give dc currents $i_{dc-\psi}$ as the contribution from each phase. These currents can be physically mapped to the upper part of each converter leg, flowing nominally into the common positive rail, in accordance with the passive sign convention adopted for the phase currents.

$$i_{dc}(t) = \sum_{\psi \in a,b,c} i_{dc-\psi}(t) \tag{4.25}$$

When mapping the phase currents to their contributions to the dc current, the appropriate transformation is the conduction function of the upper-leg switches $c_\psi(t)$, which may be defined relative to the previously defined switching function as $c_\psi(t) = \frac{s_\psi(t)}{2} + \frac{1}{2}$. The constant term is neglected when constructing the transfer, as both positive and negative sequence phase currents,

when multiplied by this constant, will cancel on the dc side. Because of the assumption of a three-wire system, no zero-sequence current which would result in a net contribution to dc current will be present. To construct a similar model which does allow for zero-sequence flows, due to a four-wire system or dc-side interconnections, the transfer would necessarily have to be based on the conduction function including the constant term, and also disallowing the FTM reduction techniques described earlier. With this assumption present, the transfer in time-domain and harmonic-domain forms is therefore:

$$i_{dc-\psi}(t) = \frac{s_\psi(t)}{2} i_\psi(t) \tag{4.26}$$

$$i_{dc}(t) = \frac{1}{2} \sum_{\psi \in a,b,c} s_\psi(t) i_\psi(t) \tag{4.27}$$

Because of the linearity and balance of the ac network, if the phase voltages share the balanced condition of the phase switching functions, it can be concluded that the phase currents are similarly balanced, and the harmonic domain forms of both the switching function (as per equation 4.17) and current may be written as harmonic-dependent variations of their respective phase a harmonic series:

$$i_\psi(t) = \boldsymbol{\Gamma}(t) \boldsymbol{I}_\psi \tag{4.28}$$

$$i_\psi(t) = \boldsymbol{\Gamma}(t) \boldsymbol{\Psi} \boldsymbol{I}_a$$

$$i_\psi(t) = \sum_{m \in \mathbb{Z}} I_{a,m} e^{j(m\omega_0 t + m\psi)} \tag{4.29}$$

$$i_{dc}(t) = \frac{1}{2} \sum_{\psi \in a,b,c} \left(\sum_{k \in \mathbb{Z}} S_{a,k} e^{j(k\omega_0 t + k\psi)} \right) \left(\sum_{m \in \mathbb{Z}} I_{a,m} e^{j(m\omega_0 t + m\psi)} \right) \tag{4.30}$$

which when expanded into the form of the dc current sub-component harmonic vectors, provides the general relation of the exponents:

$$\sum_{\psi \in a,b,c} \left(\sum_{k,m \in \mathbb{Z}} I_{dc-a,k+m} e^{j((k+m)\omega_0 t + (k+m)\psi)} \right) = \frac{1}{2} \sum_{\psi \in a,b,c} \left(\sum_{k,m \in \mathbb{Z}} S_{a,k} e^{j(k\omega_0 t + k\psi)} I_{a,m} e^{j(m\omega_0 t + m\psi)} \right) \tag{4.31}$$

If the harmonic indices of the input harmonic vectors S_a and I_a are restricted to that of our two

partioned networks, i.e. the non-zero terms $k = \pm 1 + 6p$ and $m = \pm 1 + 6q$, their harmonic domain products may be divided into two classes; the exponential sum terms where $k + m = \pm 2 + 6r$, and the exponential difference terms where $k + m = 0 + 6r$.

$$i_{dc}(t) = \sum_{\psi \in a,b,c} \left(\sum_{k+m=6r} I_{dc-a,k+m} e^{j((k+m)\omega_0 t + (k+m)\psi)} + \sum_{k+m=\pm 2+6r} I_{dc-a,k+m} e^{j((k+m)\omega_0 t + (k+m)\psi)} \right) \tag{4.32}$$

A simple relation holds for the sum terms, in which the phase shifted exponentials cancel over the summed phases. The associated terms can be physically interpreted as harmonic currents which circulate in the converter bridge, but which do not contribute to the net dc current.

$$\sum_{\psi \in a,b,c} e^{(\pm 2+6r)\psi} = \sum_{\psi \in a,b,c} e^{(\pm 2)\psi} = e^0 + e^{\pm \frac{2\pi}{3}} + e^{\mp \frac{2\pi}{3}} = 0 \tag{4.33}$$

The result is that the exponential sum terms can be removed from the harmonic domain product, leaving only difference terms $k + m = 0 + 6r$, and therefore justifying, through the linearity of the dc network, the initial assumption of the restricted dc voltage harmonic set. Recalling the identity $3n\psi = 0$, it is clear that $n\psi = 0$ for all $n = 6p$, which is to say that the virtual dc current contributions from each phase $i_{dc-\psi}$ are identical, and so the sum over the phases reduces to a multiplication by three:

$$\sum_{\psi \in a,b,c} \left(\sum_{n \in \mathbb{Z}} I_{dc-a,n} e^{j(n\omega_0 t + n\psi)} \right) = \frac{1}{2} \sum_{\psi \in a,b,c} \left(\sum_{k,m \in \mathbb{Z}} S_{a,k} e^{j(k\omega_0 t + k\psi)} I_{a,m} e^{j(m\omega_0 t + m\psi)} \right) \tag{4.34}$$

$$i_{dc}(t) = 3 \left(\sum_{n \in \mathbb{Z}} I_{dc-a,n} e^{jn\omega_0 t} \right) = \frac{3}{2} \left(\sum_{k,m \in \mathbb{Z}} S_{a,k} e^{j(k\omega_0 t + k\psi)} I_{a,m} e^{j(m\omega_0 t + m\psi)} \right) \tag{4.35}$$

The equivalent construction of this transfer in vector form, making use of the results for the selective cancellation of harmonic products based on the restricted indices, can be expressed in the following form, where $\boldsymbol{A}^*$ denotes the complex conjugate of $\boldsymbol{A}$:

$$\boldsymbol{\Gamma}(t)\boldsymbol{I}_{dc} = \frac{1}{2}\sum_{\psi\in a,b,c}\boldsymbol{\Gamma}(t)\boldsymbol{\mathcal{T}}\{\boldsymbol{S}_{\psi}\}\boldsymbol{I}_{\psi} \tag{4.36}$$

$$\boldsymbol{\Gamma}(t)\boldsymbol{I}_{dc} = \frac{1}{2}\sum_{\psi\in a,b,c}\boldsymbol{\Gamma}(t)\boldsymbol{\mathcal{T}}\{\boldsymbol{\Psi}\boldsymbol{S}_{a}\}\boldsymbol{\Psi}\ \boldsymbol{I}_{a} \tag{4.37}$$

$$\boldsymbol{\Gamma}(t)\boldsymbol{I}_{dc} = \frac{3}{2}\boldsymbol{\Gamma}(t)\boldsymbol{\mathcal{T}}\{\boldsymbol{S}_{a}^{*}\}\boldsymbol{I}_{a} \tag{4.38}$$

$$\boldsymbol{I}_{dc} = \frac{3}{2}\boldsymbol{\mathcal{T}}\{\boldsymbol{S}_{a}^{*}\}\boldsymbol{I}_{a} \tag{4.39}$$

With the ac current input vectors in the form of the partitioned conjugate networks, the familiar Toeplitz structure emerges from the $k+m = 6r$ condition. The conjugate ac networks recombine on the dc side, as their respective contributions to the dc current add according to their nominal harmonic index to give the real dc signal, which then necessarily has a purely real zero-frequency component, and conjugate harmonic terms:

$$\begin{bmatrix} \vdots \\ I_{dc,-6} \\ I_{dc,+0} \\ I_{dc,+6} \\ \vdots \end{bmatrix} = \frac{3}{2}\begin{bmatrix} \ddots & & & & \\ & S_{a,-1} & S_{a,-7} & S_{a,-13} & \\ & S_{a,+5} & S_{a,-1} & S_{a,-7} & \\ & S_{a,+11} & S_{a,+5} & S_{a,-1} & \\ & & & & \ddots \end{bmatrix}\begin{bmatrix} \vdots \\ I_{a,-5} \\ I_{a,+1} \\ I_{a,+7} \\ \vdots \end{bmatrix} + \frac{3}{2}\begin{bmatrix} \ddots & & & & \\ & S_{a,+1} & S_{a,-5} & S_{a,-11} & \\ & S_{a,+7} & S_{a,+1} & S_{a,-5} & \\ & S_{a,+13} & S_{a,+7} & S_{a,+1} & \\ & & & & \ddots \end{bmatrix}\begin{bmatrix} \vdots \\ I_{a,-7} \\ I_{a,-1} \\ I_{a,+5} \\ \vdots \end{bmatrix} \tag{4.40}$$

With this formulation, the self-consistency of the characteristic harmonic set under the balanced phasor interpretation of the harmonic domain signals has been demonstrated, while maintaining the dynamic generality of the model. By partitioning the system into conjugate networks which are modulated linearly, the sequence-dependent frequency folding behaviour of earlier harmonic domain models is achieved, but without the need for convoluted transforms, which allows the state-space description and simulation output to be more legible and intuitive. This shows the simplifying power of the central assumption of the balanced modulator and associated ac network.

4.4.4 Implementation of LTI Model

The HSS model is implemented in MATLAB as a real-valued LTI state-space system. This is constructed using a modular approach, with state-space sub-blocks being connected by shared inputs and outputs using the MATLAB 'connect' command, as illustrated in Fig. 4.3. Though not illustrated, the ac network in itself is comprised of series RL and RC sections, themselves split into the conjugate characteristic harmonic sets identified in Section 4.4.3. Each sub-block is a self-contained state-space system, formed from the $\bar{\boldsymbol{A}}$, $\bar{\boldsymbol{B}}$, $\bar{\boldsymbol{C}}$ and $\bar{\boldsymbol{D}}$ matrices of the transformed system using the LTP to HSS methods described in Chapters 2 and 3.

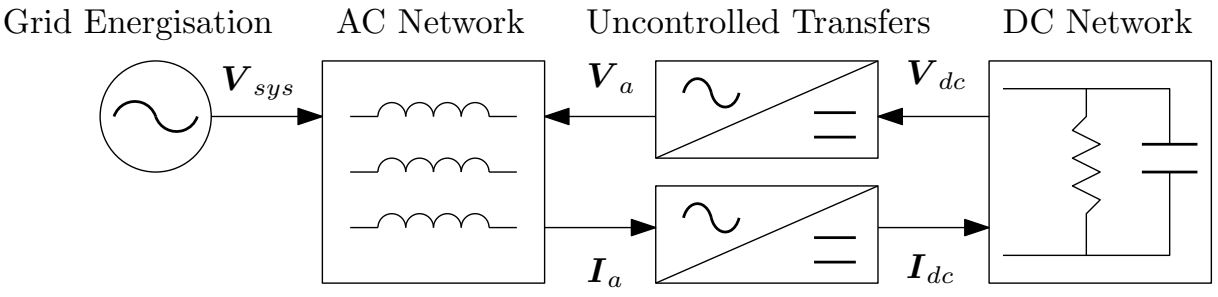

Figure 4.3 Block diagram of the state-space structure of the uncontrolled model.

An additional step is required to form real-valued matrices from the original complex ones. This is done by separating the real and imaginary parts of the signal, and using a 2x2 tensor to represent each complex coefficient. A complex multiplication $x = yz$, $x, y, z \in \mathcal{C}$ is represented using real signals as:

$$\begin{bmatrix} \Re x \\ \Im x \end{bmatrix} = \begin{bmatrix} \Re y & -\Im y \\ \Im y & \Re y \end{bmatrix} \begin{bmatrix} \Re z \\ \Im z \end{bmatrix} \tag{4.41}$$

When the state-space blocks are joined, the aggregate system is defined by identifying which signals are to form the inputs and outputs. All signals that are to be stored for processing are set as outputs. For the uncontrolled system, just the grid side of the ac voltage network is exposed as an input, giving the form of the input vector as the two conjugate grid voltage vectors:

$$\boldsymbol{U} = \begin{bmatrix} \begin{bmatrix} \vdots \\ V_{grid,-5} \\ V_{grid,+1} \\ V_{grid,+7} \\ \vdots \end{bmatrix} \\ \begin{bmatrix} \vdots \\ V_{grid,-7} \\ V_{grid,-1} \\ V_{grid,+5} \\ \vdots \end{bmatrix} \end{bmatrix} \tag{4.42}$$

4.4.5 Time-Domain Signal Reconstruction

The LTI implementation of the HSS model described here produces sets of harmonic vectors, one at each solution time-step, as its output. These harmonic output vectors are processed into time-domain signals by multiplying the harmonic vector at each time-step by the vector of complex harmonic exponentials $\boldsymbol{\Gamma}(t)$. Theoretically, no distinction is made between a generic full-rank harmonic vector, and the same vector partitioned into the two characteristic harmonic sets, but for clarity the process for reconstructing the time-domain a-phase voltage signal is presented in equation 4.44, directly as it appears in the model. The two vectors of the characteristic harmonic sets along with their respective $\boldsymbol{\Gamma}(t)$ vectors being complex conjugates of each other, add to form a single purely real time series.

$$v_a(t) = \boldsymbol{\Gamma}(t)\boldsymbol{V}_a(t) \tag{4.43}$$

$$v_a(t) = \begin{bmatrix} \dots & e^{-j5\omega_0 t} & e^{j\omega_0 t} & e^{j7\omega_0 t} & \dots \end{bmatrix} \begin{bmatrix} \vdots \\ V_{a,-5} \\ V_{a,+1} \\ V_{a,+7} \\ \vdots \end{bmatrix} (t) + \begin{bmatrix} \dots & e^{-j7\omega_0 t} & e^{-j\omega_0 t} & e^{j5\omega_0 t} & \dots \end{bmatrix} \begin{bmatrix} \vdots \\ V_{a,-7} \\ V_{a,-1} \\ V_{a,+5} \\ \vdots \end{bmatrix} (t) \tag{4.44}$$

This reconstruction for ac quantities is specific to the a phase. To generate the time-domain series for other phases, it is necessary to apply the harmonic-dependent phase shifts of equation 2.11, which recovers the time series of any phase for dynamically varying signals.

$$v_\psi(t) = \mathbf{\Gamma}(t)\mathbf{\Psi}\boldsymbol{V}_a(t) \tag{4.45}$$

As the output an of LTI model, the EMP-domain signals evolve continuously (and in the degenerate steady-state case, are static), and therefore may be linearly interpolated before reconstructing the time-domain signal without penalty in a way that the time-domain output could not. This allows the time-domain reconstruction of the HSS simulation carried out at a time-step of 100 µs to match the output of the EMTDC simulation at a time-step of 10 µs.

4.4.6 Verification of Individual Transfers

To validate the converter model, the individual voltage and current transfers described in Section 4.4.3 are characterised in isolation, without the feedback from the coupling ac and dc networks. These transfers demonstrate the accuracy of the numerical model used, and illustrate the characteristic of the VSC as a linear frequency modulator.

4.4.6.1 PSCAD Model

The benchmark for the accuracy of the HSS model is an equivalent PSCAD/EMTDC testbench, constructed of ideal components and with an identical carrier-based PWM scheme. The system showing the relevant measurement locations is illustrated in Fig. 4.4. So as to match the assumptions of the HSS model, the PSCAD model derives its phase reference for both the triangular carrier and the synchronous reference frame from a PLL attached to a fixed three-phase source, separated from the active grid to provide a constant phase reference irrespective of the conditions of the test network. Fixed current and voltage sources provided the test inputs for the steady-state transfers.

4.4.6.2 Steady-State Transfers

The following results were obtained with the converter operating point defined by the dq-frame modulation vector of $M_d = 0.8$, $M_q = 0.2$, a switching frequency of 450 Hz ($m_f = 9$), and using test inputs of 10 kA rms (leading the reference frame by 90 degrees) and 10 kV dc respectively. The HSS model was energised with the static harmonic vector inputs $V_{dc,+0} = 10000$, $I_{a,+1} = -j5000\sqrt{2}$ and $I_{a,-1} = +j5000\sqrt{2}$, resulting in a set of static harmonic vector outputs in accordance with the stateless input-output characteristic of the converter. These static harmonic outputs were converted to time-domain series for display, and then the same FFT was applied to the EMTDC and converted MATLAB time series.

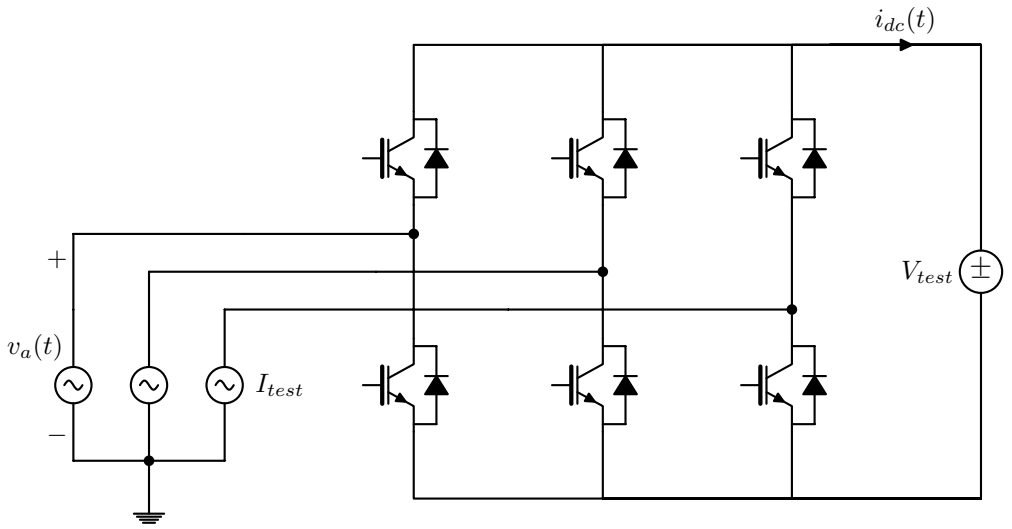

Figure 4.4 PSCAD testbench for individual transfers.

Fig. 4.5 displays the voltage transfer from a zero-frequency dc component only; the resultant ac voltage is simply the phase a switching function itself, less the common-mode elements, and is therefore visible as the phase-to-neutral component. This transfer, simulated with a maximum harmonic order of 157 in order to give clear visual time-domain agreement, nevertheless displays the Gibbs phenomenon near its multiple periodic jump discontinuities.

The harmonic-domain comparison of the phase a voltage transfer, Fig. 4.6, is indexed linearly according to the characteristic harmonic set $1 \pm 6n$, to display only the extant harmonics in the signal. The full FFT of this real signal necessarily contains energy at positive and negative frequencies for all present harmonics, but these are not shown in preference to the linear index.

As seen in Fig. 4.8, a small amount of energy at non-characteristic harmonic frequencies is present in the EMTDC data, which based on the harmonic model developed in this chapter should not be present in the idealised system; this may be due to numerical error in the control system. The harmonic and time-domain analyses show otherwise clear agreement.

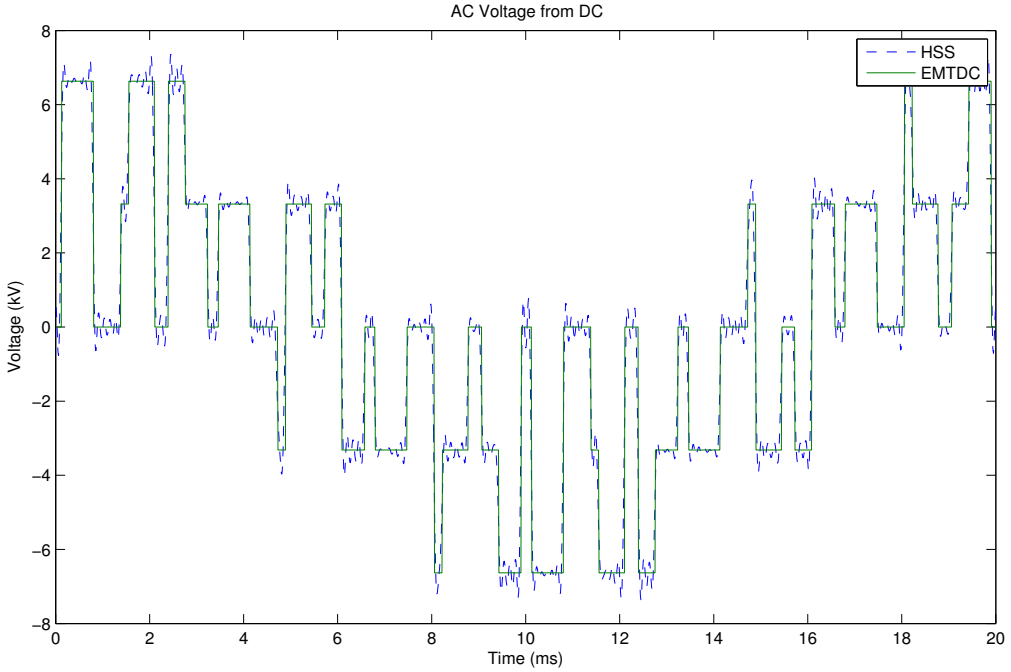

Figure 4.5 Time-domain comparison of ac voltage transfer from a constant dc bus voltage.

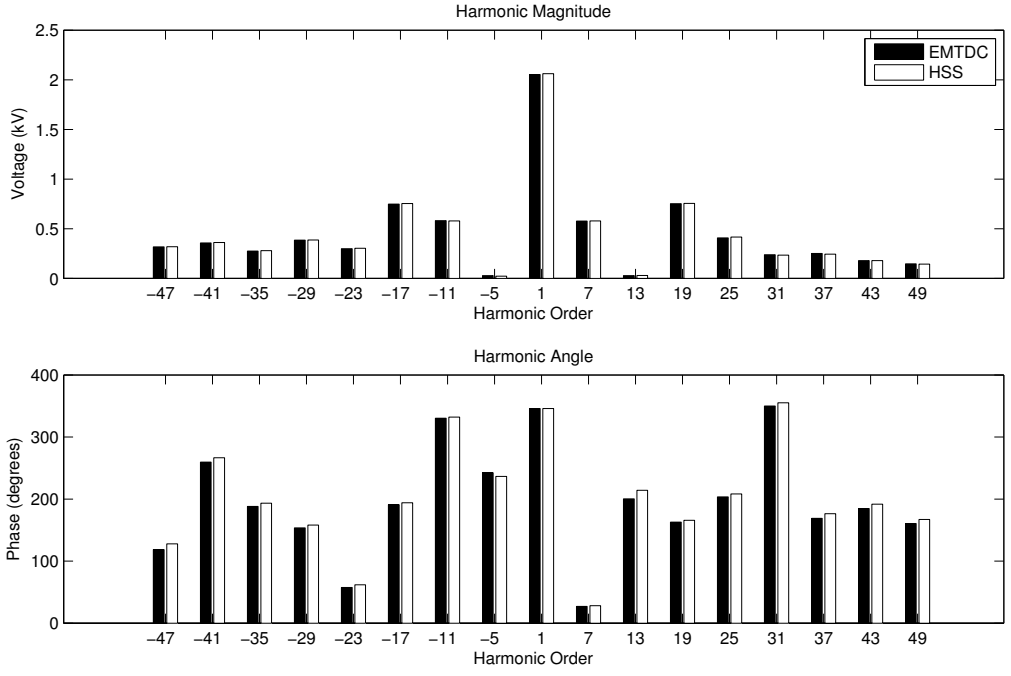

Figure 4.6 Harmonic comparison of ac voltage transfer from a constant dc bus voltage.

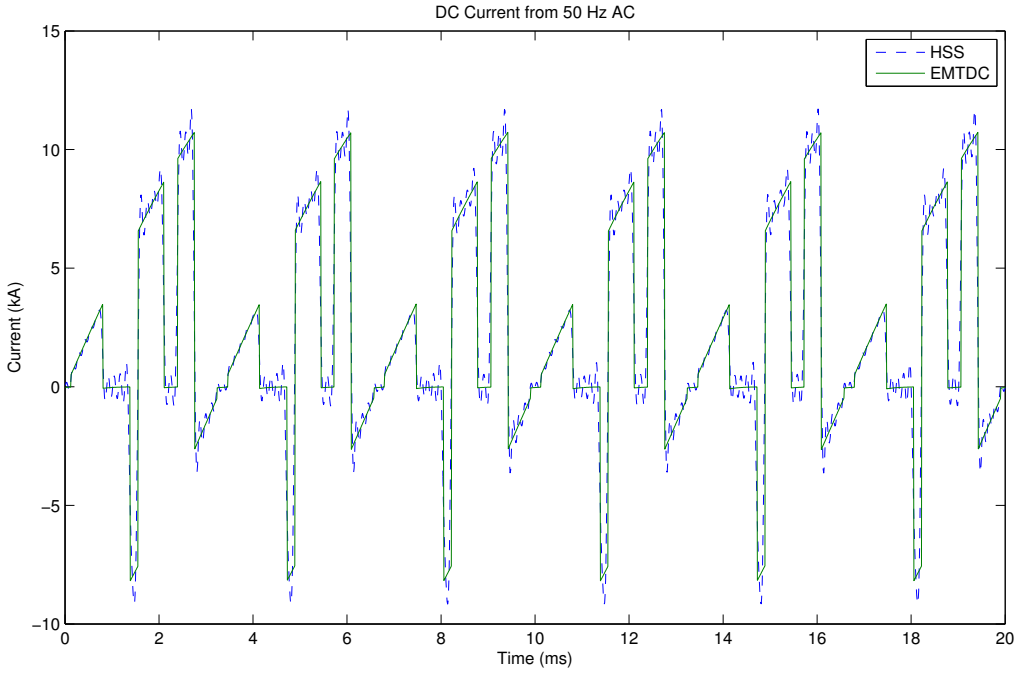

Figure 4.7 Time-domain comparison of dc current transfer from a positive sequence ac current.

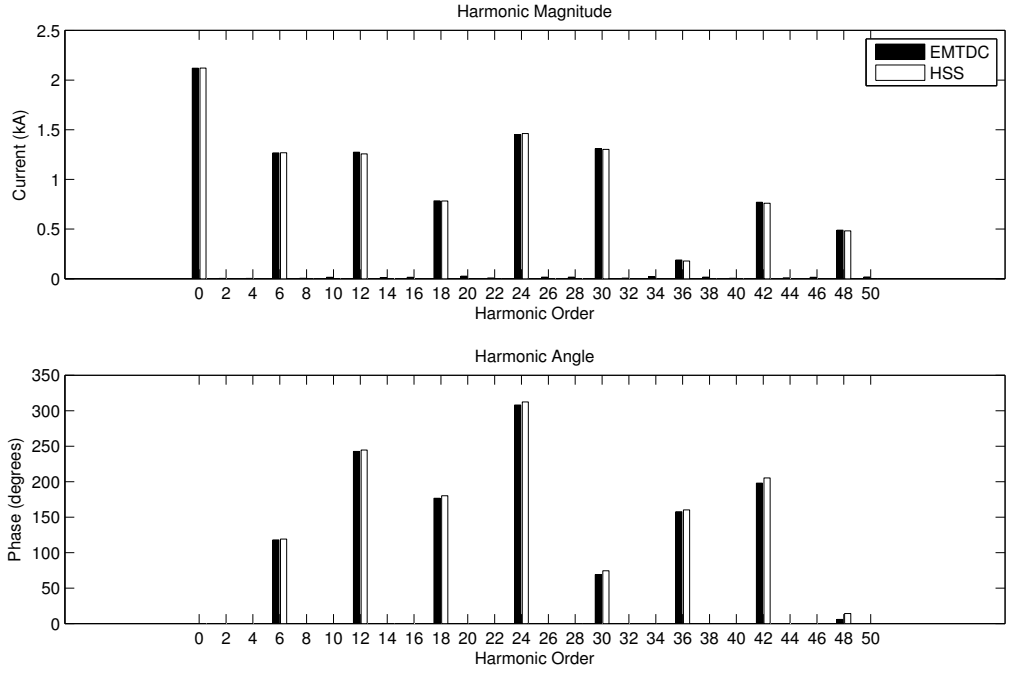

Figure 4.8 Harmonic comparison of dc current, all even terms.

4.4.6.3 Dynamic Transfers

As described in Chapter 3, the dynamically time-varying form of the general EMP signal allows the representation of non-characteristic harmonics through the modulation of, in theory, any of the available harmonic reference frames. This method is used here to extend the reduced-order converter model to include non-characteristic harmonic signals, principally for the purpose of modelling the effects of fundamental frequency system voltage imbalances, an important network condition to study. To create this non-characteristic signal, the fundamental frequency current input was modulated at $-2\omega_0$, in effect reversing the rotation of the positive sequence phasor associated with the fundamental frequency harmonic reference. This is encoded here using the complex inputs $I_{a,+1} = +j5000\sqrt{2}e^{-j2\omega_0 t}$ and $I_{a,-1} = -j5000\sqrt{2}e^{j2\omega_0 t}$

As an LTI model, the principle of superposition is obeyed, and using this method, any linear combination of positive and negative sequence fundamental components could be created using a superposition of constant and modulated complex inputs, respectively. Additionally, by the non-uniqueness of the EMP domain, the non-characteristic signal could be generated from a modulated input in any reference frame, with the strict Toeplitz structure of the transfer matrix ensuring that the time-domain transfer is equivalent. This characteristic of linearity with respect to frequency demonstrates how the validity of the transfer for general dynamically varying signals guarantees the ability to model the transfer of non-characteristic components.

By adopting this convention of a reduced model containing only the characteristic harmonic set of a balanced system, a sharp distinction is drawn between the steady state of the state-space model, which must necessarily be balanced, and the dynamic excursions of the state-space model which may include as a special case non-characteristic harmonics, which are necessarily unbalanced. In Chapter 5, this distinction is employed when developing the small-signal converter model, including dynamic control of the converter.

The comparison of negative sequence current transfers in Figs. 4.9 and 4.10 demonstrate the same high degree of conformity. In the harmonic analysis, the phase components of the nominally zero $6n$ terms have been zeroed out so as to not show spurious phase terms.

Figs. 4.11 and 4.12 demonstrate the equivalence of the same signal achieved through the modulation of two different reference frames; the reconstructed signals are exactly identical. In the 7th harmonic reference frame, a negative sequence fundamental signal is generated by the complex inputs $I_{a,+7} = +j5000\sqrt{2}e^{-j8\omega_0 t}$ and $I_{a,-7} = -j5000\sqrt{2}e^{j8\omega_0 t}$. Similarly, by the phasor interpretation of the balanced harmonic reference frames, to generate the same signal in the 5th harmonic reference frame (associated with a phasor at $-5\omega_0$), the complex input required is $I_{a,-5} = +j5000\sqrt{2}e^{+j4\omega_0 t}$ and $I_{a,+5} = -j5000\sqrt{2}e^{-j4\omega_0 t}$. It is instructive to note that both the reference frames (and thus the order of the associated term in the $\mathbf{\Gamma}(t)$ vector used for time-domain reconstruction) and the frequency complex inputs are separated by $12\omega_0$.

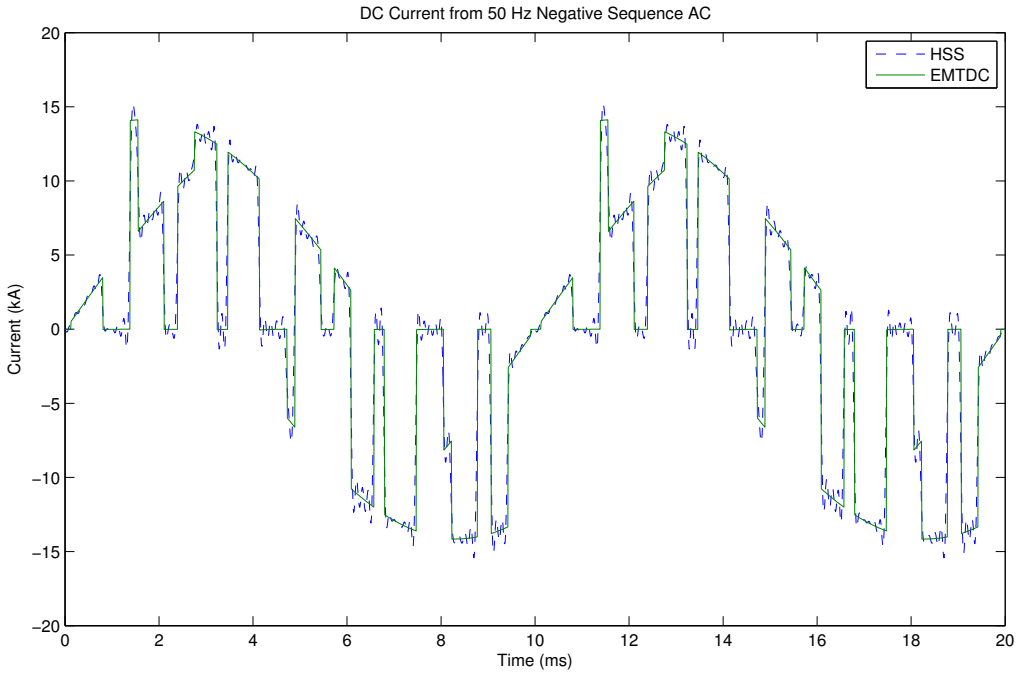

Figure 4.9 Time-domain comparison of transfer from a modulated negative sequence ac current to dc current.

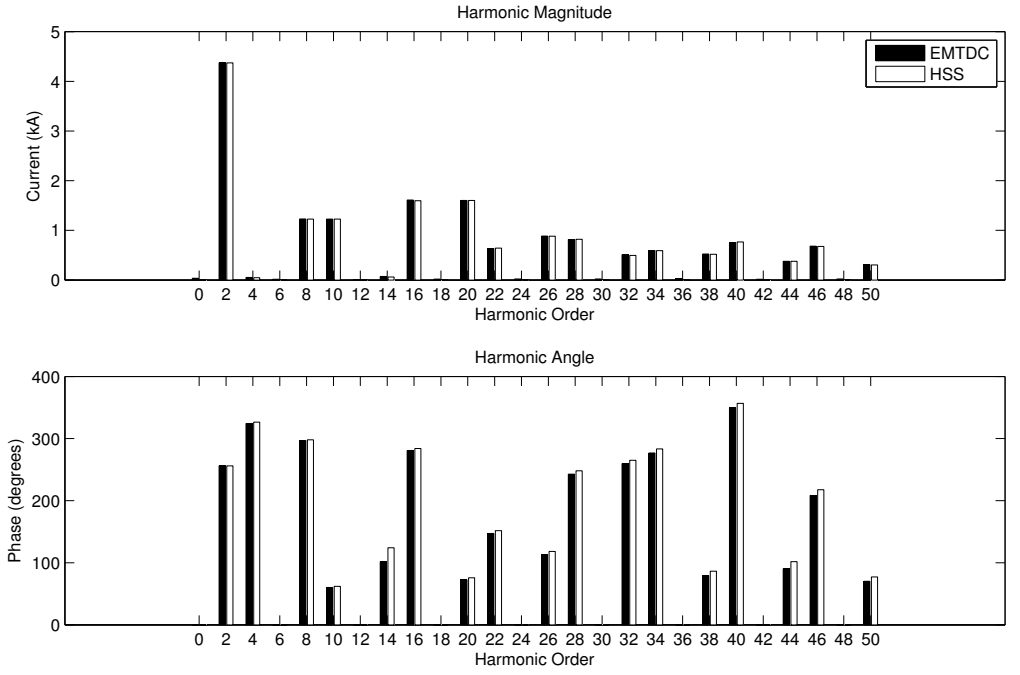

Figure 4.10 Harmonic comparison of transfer from a modulated negative sequence ac current to dc current.

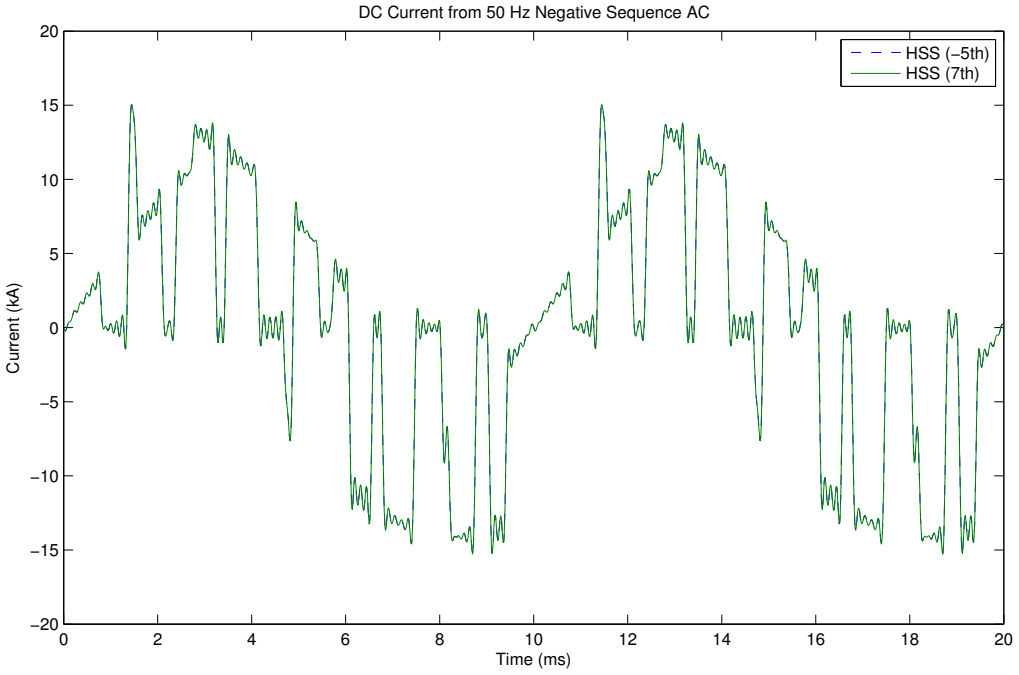

Figure 4.11 Time-domain comparison of negative-sequence current transfer by modulated inputs in the -5th and 7th harmonic reference frames.

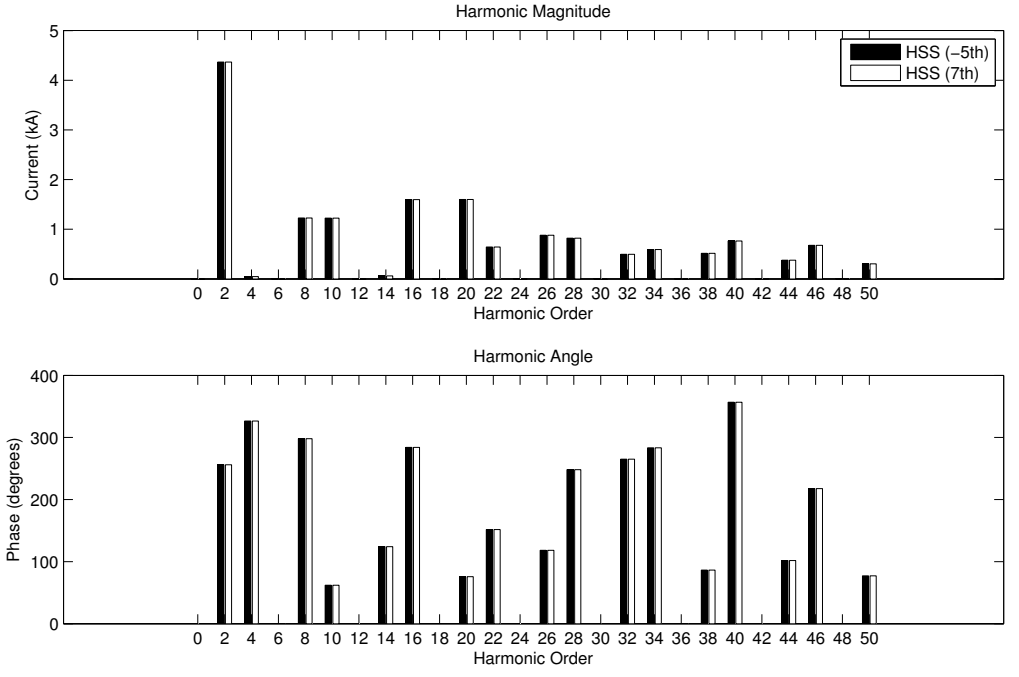

Figure 4.12 Harmonic comparison of negative-sequence current transfer by modulated inputs in the -5th and 7th harmonic reference frames.

4.5 UNCONTROLLED SYSTEM MODEL

The previous section demonstrated the validity of the uncontrolled harmonic domain VSC model for steady-state and dynamic inputs. With this functionality satisfied, the VSC model may be evaluated as a component in a larger HSS model also incorporating passive elements.

The test system, illustrated in Fig. 4.13 consists of a three-phase remote voltage source with an RL network impedance, interfacing to the VSC through its own RL impedance, with a shunt RC network providing harmonic filtering. The harmonic response of the filter can be approximately described by the LC network formed from the filter capacitor and the converter-side inductance, which eliminates the majority of the harmonic content of the VSC voltage as seen by the grid, and thus limits harmonic current flows to the grid. The filters, by virtue of being shunt-connected capacitors, passively supply a small component of reactive power (157 kVA or 0.0785 p.u. at rated voltage in the simulation to follow) to the network. The dc side of the VSC has a parallel RC network to model the dc link capacitor, as well as either a small switching loss or alternately a resistive load. Depending on the chosen system parameters and component values, this basic structure may be used as a STATCOM, controlled rectifier, or a simplified model of a VSC-HVDC terminal.

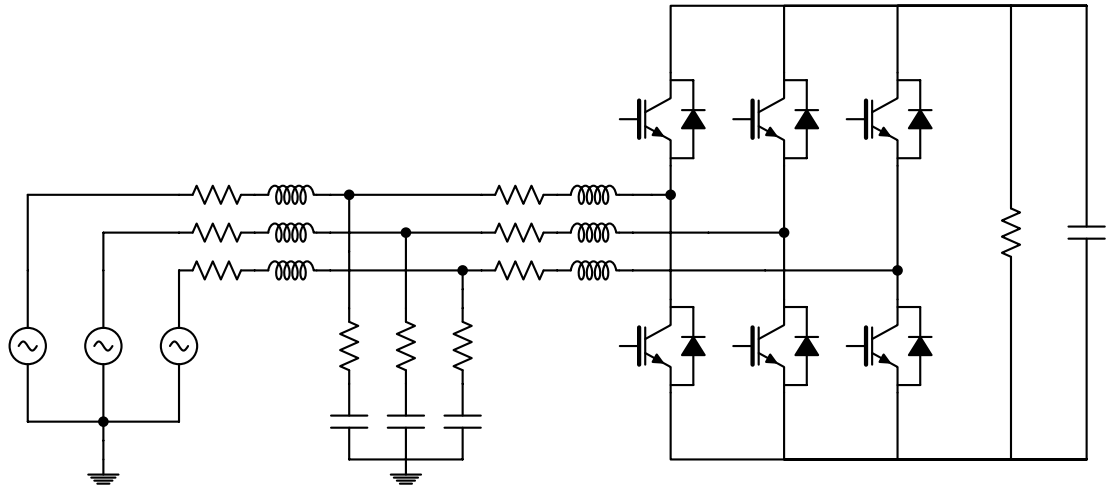

Figure 4.13 Test network circuit diagram.

The analysis undertaken here uses this system in a STATCOM (Static Synchronous Compensator) configuration, with the VSC acting as a controllable voltage source to deliver a controllable level of reactive power to the fixed grid. As the simulation is an evaluation of the uncontrolled model with fixed switching instants, the modulation vector M is chosen in advance such that the system settles to a steady-state condition where reactive power is being injected into the grid.

4.5.1 STATCOM Operation and Control

In order to place the simulation of STATCOM system dynamics in context, a phasor-based fundamental-frequency model of the dynamic STATCOM in equilibrium is presented here. This simplified model illustrated in Fig. 4.14 lacks the shunt filter and dc-side loss component, compared with the full system. The dynamic STATCOM is distinguished from the conventional STATCOM by having direct control over the magnitude and angle of the synthesized voltage, contrasted with power angle control only.

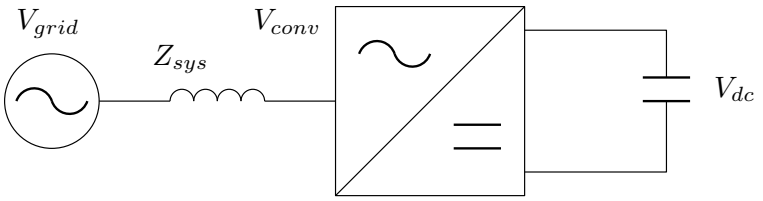

Figure 4.14 Single-line diagram of simplified network, without shunt filter or dc-side loss for the analysis of the VSC system at equilibrium.

In the steady state, the dc-side capacitor voltage is constant, implying that the real power flow across the converter is near-zero, with a small component to supply the shunt resistance loss, which is neglected here. Assuming a constant M_d component, manipulation of the M_q component controls the power angle of the synthesised converter voltage against the remote source. This in turn sets the equilibrium of dc-side capacitor voltage achieved at zero real power flow through the converter (and therefore a converter current orthogonal to the converter voltage), as visualised in Fig. 4.15. In this manner, control of the power angle sets the level of reactive power flow through the dc voltage.

This equilibrium may be interpreted geometrically as the intersection of a phasor of variable length following the fixed power angle versus the grid voltage plus the voltage drop along the interconnecting impedance following the slope of the line X/R ratio (the line impedance angle θ_z). This geometric interpretation allows intuition about the relative passive stability of the uncontrolled system for different X/R ratios, with respect to changing power angles between the grid and the synthetic voltage source of the VSC.

Generalising this analysis to systems not in equilibrium illustrates the operational flexibility of the dynamic STATCOM made possible by the decoupled vector control of the d- and q-axis voltage components, compared to the STATCOM with power angle control only. Fig. 4.16 shows the same system after the M_d voltage component has been reduced, but before the system can re-equilibriate. This allows the reactive power flow to be reduced immediately, without the delay required for the dc voltage to adjust as for a conventional STATCOM. The system current and thus apparent power flow into the converter then contains a real component, which in time would drive a new equilibrium at the new, slightly larger power angle. To stabilise the reactive power

flow at this present level, the power angle could be reduced to the point of zero real power flow. It should be noted that in terms of the power angle, the control action required to satisfy the equilibrium is contra the short-term action. Because of the two degrees of freedom available for control, the same equilibrium can be achieved for any absolute value of the modulation vector M, as the dc voltage will adjust accordingly. The absolute magnitude of the modulation vector to be maintained at the equilibrium level will therefore be determined by the constraints of the maximum capacitor voltage (and thus minimum modulation vector magnitude), and the output voltage held in reserve to provide an immediate increase in reactive power output [Sao *et al.* 2002]. The STATCOM-based simulations in this chapter therefore use a baseline modulation vector of 0.8.

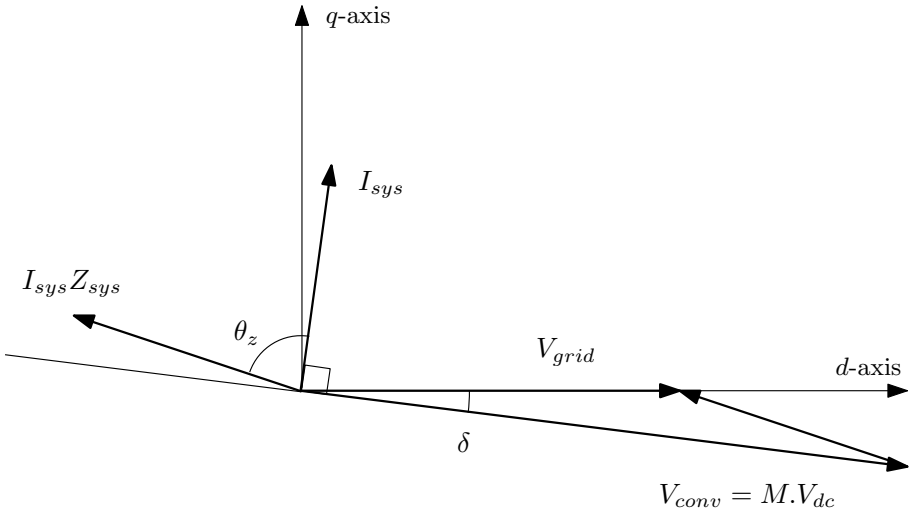

Figure 4.15 Phasor diagram showing VSC system at equilibrium, supplying reactive power.

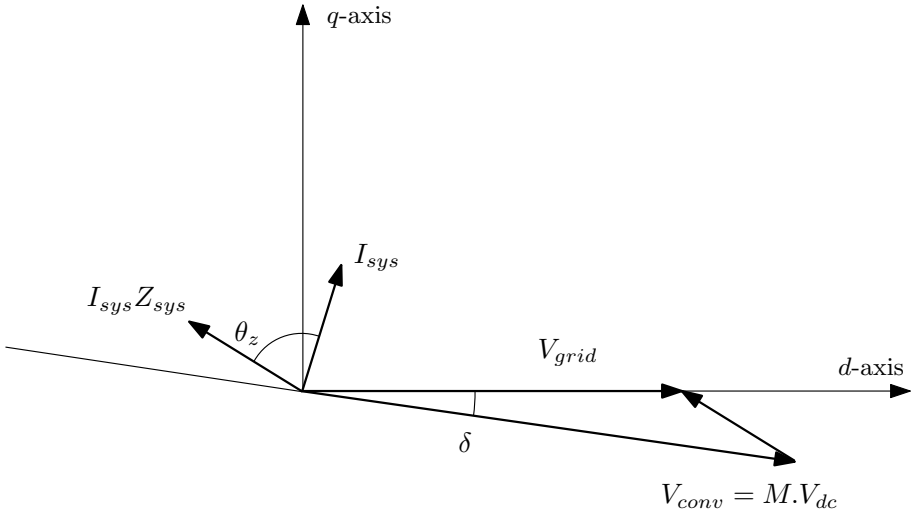

Figure 4.16 Phasor diagram showing VSC system not at equilibrium after adjusting modulation vector, reducing reactive power supply.

4.5.2 Uncontrolled System Verification

As for the verification of the individual converter transfers, the benchmark for the evaluation of the uncontrolled system HSS model is a PSCAD/EMTDC simulation constructed of ideal components and with an identical control scheme in an independent synchronous frame. The HSS model results were produced with a maximum harmonic order of 109. Table 4.1 lists the parameters for the test system configured to function as a STATCOM supplying reactive power to the grid.

Table 4.1 Uncontrolled test system parameters.

Parameter	Value	Per-unit basis
Base voltage	$V_{base} = 10\,\text{kV}$	
Base MVA	$S_{base} = 2\,\text{MVA}$	
Fundamental frequency	$f_0 = 50\,\text{Hz}$	
Switching frequency	$f_{sw} = 750\,\text{Hz}$	15 p.u.
Modulation vector	$M = 0.8 - j0.03$	
Source resistance	$R_s = 0.25\,\Omega$	0.005 p.u.
Source inductance	$L_s = 0.01\,\text{H}$	0.0628 p.u.
Converter resistance	$R_c = 1\,\Omega$	0.02 p.u.
Converter inductance	$L_c = 0.04\,\text{H}$	0.251 p.u.
Filter resistance	$R_f = 0.1\,\Omega$	0.002 p.u.
Filter capacitance	$C_f = 5\,\mu\text{F}$	12.7 p.u.
DC-side capacitance	$C_{dc} = 300\,\mu\text{F}$	0.212 p.u.
DC-side resistance	$R_{dc} = 10\,\text{k}\Omega$	2000 p.u.
Converter LC corner frequency	$f_{co} = 355.881\,\text{Hz}$	7.12 p.u.
Steady-state MVA	$S_{ss} = 2.8\,\text{MVA}$	1.4 p.u.
Steady-state dc voltage	$V_{ss} = 29.5\,\text{kV}$	

The dc capacitor voltage is a useful measure of the accuracy of the simulation, because it tracks the integral of the real power flow through the converter (less dc-side losses). In Fig. 4.17, very close agreement of the dc voltage is observed between the EMTDC and HSS models, demonstrating the ability of the model to closely track the power flow during the start-up transient from an initial state of all variables zeroed. This measurement allows the observation of a decaying oscillation close to the fundamental frequency, driven by the initial asymmetry between the phases in the presence of an increasing dc voltage. Visualising the ac voltage in Fig. 4.18 similarly demonstrates the dynamic accuracy of the model.

A further test of the validity of the dynamic model of the full system involves perturbing the model with a negative sequence grid voltage component, achieved through the modulation of a grid voltage harmonic input. The modulated harmonic voltage signal results in the propagation of modulated signals through the converter as currents, interacting on the dc-side network to

give a modulated bus voltage, which is then fed back onto the ac network through the voltage transfer FTM, forming a feedback loop. Correct modelling of the system in the HSS for these inputs therefore relies on the complete linearity with respect to frequency of all parts of the model, which is implied by the validity of the dynamic model.

This is achieved using the superposition of constant (giving the positive sequence fundamental frequency phasor) and exponentially modulated (giving the negative sequence fundamental frequency phasor) inputs to the fundamental frequency harmonic input, written here as $V_{grid,+1} = 5000\frac{\sqrt{2}}{\sqrt{3}}(1 + 0.1e^{-j2\omega_0 t})$ and $V_{grid,-1} = 5000\frac{\sqrt{2}}{\sqrt{3}}(1 + 0.1e^{+j2\omega_0 t})$, to give a 10% imbalance which was switched in at $t = 250\,\text{ms}$, once the start-up transient had begun to stabilise.

Fig. 4.19 shows the response of the dc voltage to this imbalance, which clearly demonstrates the accuracy of the response of the model to the imbalance, though showing an already present small discrepancy in the average level of the dc voltage. The comparison of the dc converter current in Fig. 4.20 shows that the exponentially modulated signals at all stages of the feedback loop described above provide meaningful time-domain reconstructions.

4.6 CONCLUSION

The numerical harmonic state space model of the VSC was demonstrated to accurately model uncontrolled current and voltage transfers, in isolation and as part of a full converter system. Importantly, it was demonstrated that by constructing the VSC model as a linear modulator acting on conjugate characteristic harmonics sets, the frequency-coupling action of the VSC can be captured in full dynamic generality by a reduced-order model. The controlled VSC model developed in the next chapter will rely on the orthogonality of the numerical vector control scheme and decoupled three-phase signal representation as implemented here to achieve an accurate linearised model.

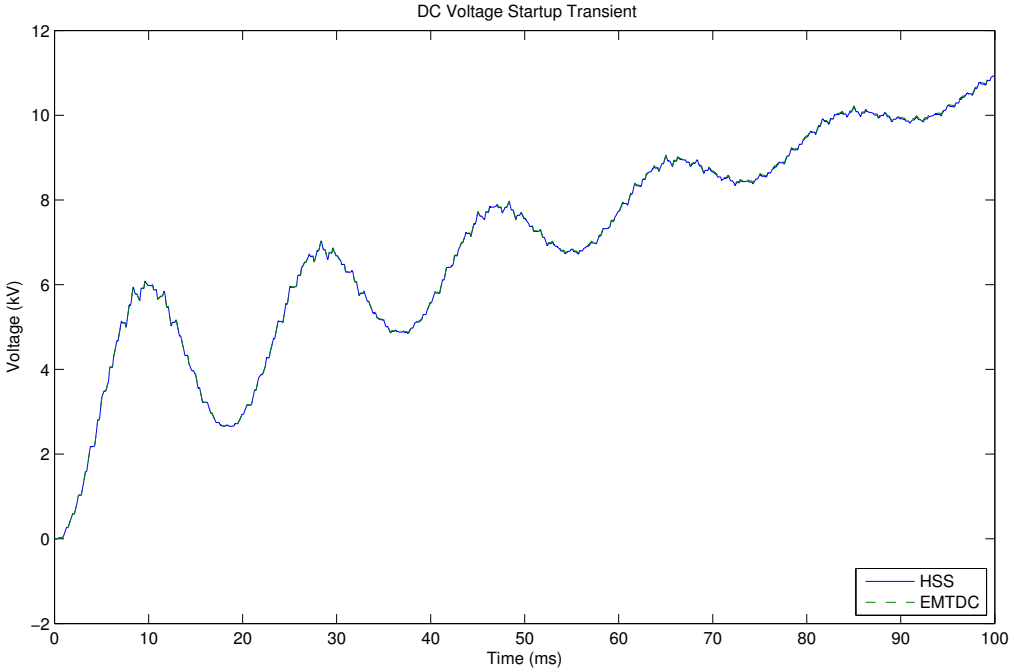

Figure 4.17 Transient evolution of dc voltage during STATCOM start-up.

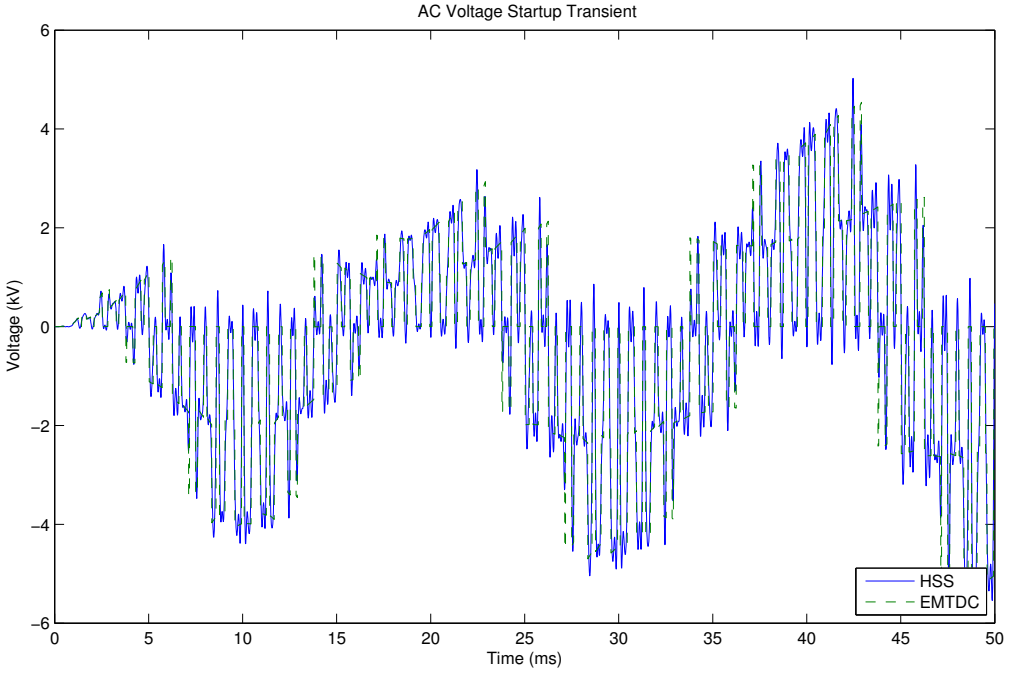

Figure 4.18 Transient evolution of phase a voltage during STATCOM start-up.

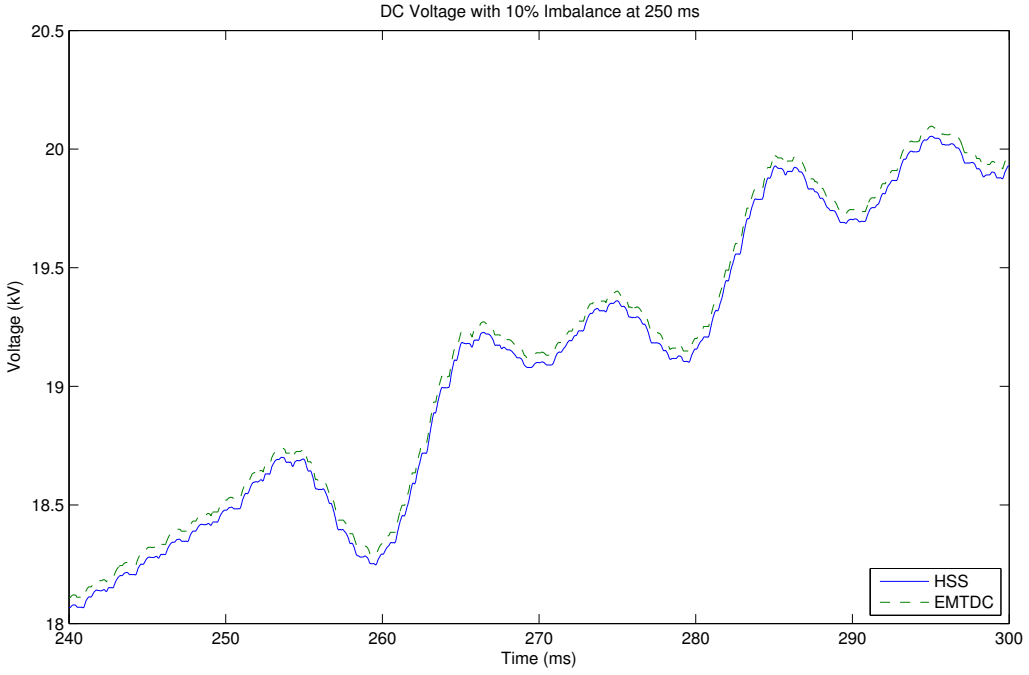

Figure 4.19 Transient evolution of dc voltage following introduction of 10% imbalance at 250 ms.

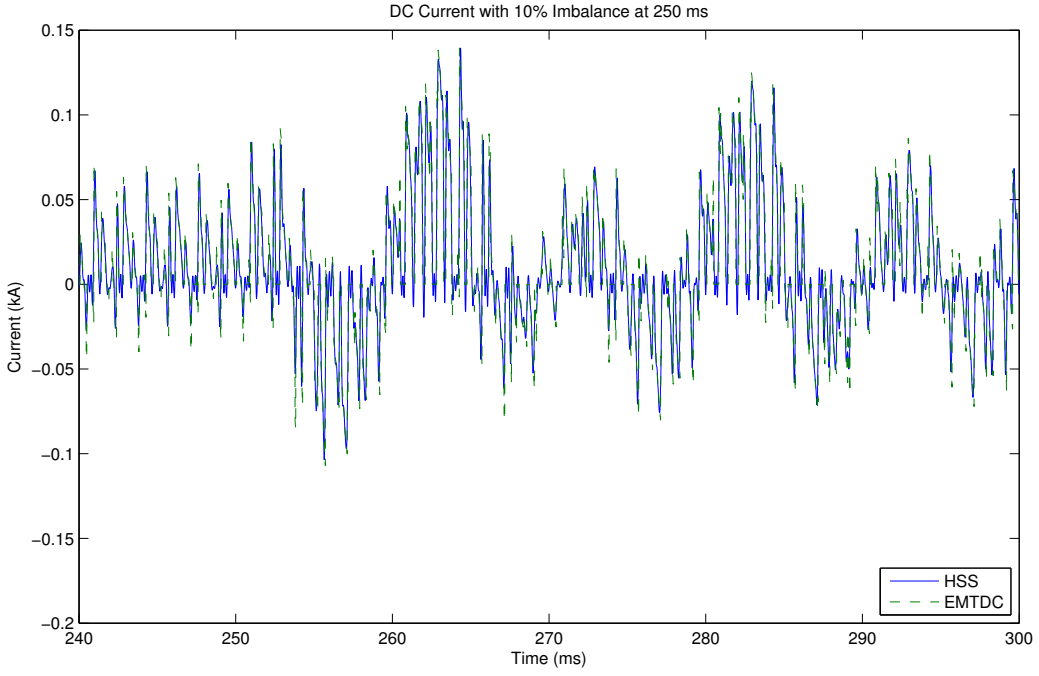

Figure 4.20 Transient evolution of dc current following introduction of 10% imbalance at 250 ms.

Chapter 5

VSC MODEL WITH CONTROL

5.1 INTRODUCTION

With the development and verification of the VSC model in Chapter 4, the ability of the HSS to completely capture the dynamics of a power system comprised of linear elements and an uncontrolled VSC defined by a fixed switching function has been demonstrated. By formulating the VSC as a linear time-invariant system, the VSC system gains the properties of the LTI state-space described in Section 3.2.1; the system may be solved directly for its steady state solution for arbitrary inputs, and its dynamics may be evaluated through examination of its eigenvalues. These properties allow new analyses for uncontrolled VSC systems, however the most important studies of converter system dynamics require the closed-loop controlled response to be modelled.

This requires the extension of the VSC model to include the response to changes in the control input. As discussed in Section 5.2, this is a problem of linearisation. In this chapter, it will be shown how the numerical switching model and synchronous reference frame for the uncontrolled VSC developed in Chapter 4 provides an ideal basis for extension to a small-signal controlled HSS model for analysing harmonic interaction.

Controlled state-space models have been developed for various converters, using state-space averaging techniques. In a precursor to modern HSS formulations, [Möllerstedt and Bernhardsson 2000] presented an HSS model of a controlled locomotive rectifier with idealised switching based on linearised pre-computed waveforms, able to produce closed-loop stability criteria. A significant class of averaged state-space model for ac systems are the Dynamic Phasor models, as formulated by Stankovic et al. [Stanković *et al.* 2000], in which generalised averaging techniques are applied over a small chosen set of harmonic reference frames to the governing differential equations of the system. The resulting equations, generally developed for individual phases, are time-invariant but not required to be linear. This means that more complicated non-linear time-invariant controllers may be included as in [Deore *et al.* 2012], and non-linear system dynamics and measurement techniques may be included without linearisation. To gain analysis for these models in the s-domain however, requires a secondary linearisation step to be

carried out. This is contrasted with the inherently linear HSS model developed in this chapter that results from the extension of the uncontrolled harmonic-domain model, and the similarly linearised implementation of Switching Instant Variation applied to TCR and line-commutated HVDC systems by Orillaza and Hwang in [Orillaza *et al.* 2010].

In this chapter, the controlled small-signal model of the VSC is derived through a process of linearisation of the numerical switching model using the orthogonal dq-axis control structure developed in Chapter 4, and the limits of the linearisation process are characterised. The structure of the complete small-signal model is described in Section 5.2.1 as a linear combination of modular transfers, delineating the large-signal and small-signal modes of the model. Concepts for the measurement of dynamic harmonic signals for use as control inputs are introduced in Section 5.4.1, and applied to the measurement and control of reactive power and capacitor voltage in a simple closed-loop STATCOM control system. The resulting system is validated against time-domain simulation in PSCAD in Section 5.5, used to demonstrate the relevance of LTI analysis techniques when applied to the HSS model, and to perform a test of the dependence on the closed-loop control response to harmonic coupling terms.

5.2 LINEARISATION STRATEGY

This section describes the application of linearisation techniques to the uncontrolled VSC model of Chapter 4, in order to gain a fully LTI harmonic state-space model of the controlled converter.

Using the harmonic-domain vector notation, equation 5.1 shows the form of the dynamic transfer to the phase a voltage for a fixed switching function, representative of the dynamic transfer for all phases in the balanced network.

$$\boldsymbol{V}_a(t) = \frac{1}{2}\boldsymbol{\mathcal{T}}\{\boldsymbol{S}_a\}\boldsymbol{V}_{dc}(t) \tag{5.1}$$

The transfer is defined by the switching function $s_a(t)$, and equivalently in the harmonic domain, the Toeplitz matrix formed from its spectrum $\boldsymbol{S}_a$. For fully general control, the switching function becomes a function of the time-variant control inputs $M_d(t)$ and $M_q(t)$.

$$\boldsymbol{V}_a(t) = \frac{1}{2}\boldsymbol{\mathcal{T}}\{\boldsymbol{S}_a(M_d(t), M_q(t))\}\boldsymbol{V}_{dc}(t) \tag{5.2}$$

This equation, although accurately describing the general controlled transfer, is neither linear (as the switching function is a non-linear function of the control inputs), nor time-invariant.

Formulation of the LTI state-space model therefore requires a dual linearisation around both the switching function and the converter state variables.

Firstly, the switching function as a function of the control vector input must be linearised around small changes each of the decoupled control vector components. This requires the construction of the partial differential switching spectra $\frac{\partial \boldsymbol{S}_a}{\partial M_d}$ and $\frac{\partial \boldsymbol{S}_a}{\partial M_q}$. The differential switching spectra are obtained using the numerical switching function model, by computing the switching functions and associated spectra for the base case control vector, and for the base case control vector plus a small finite differential control input ΔM_d, and then normalising the resulting differential spectra to the magnitude of the differential control input. Because of the linearity of the FFT, it does not matter whether the difference taken is between the time-domain switching functions, or the resultant spectra, although both the description here and implemented model use the differential spectra.

$$\frac{\partial \boldsymbol{S}_a}{\partial M_d} = \frac{(\boldsymbol{S}_a(M_{d-base} + \Delta M_d, M_{q-base}) - \boldsymbol{S}_a(M_{d-base}, M_{q-base}))}{\Delta M_d} \tag{5.3}$$

$$\frac{\partial \boldsymbol{S}_a}{\partial M_q} = \frac{(\boldsymbol{S}_a(M_{d-base}, M_{q-base} + \Delta M_q) - \boldsymbol{S}_a(M_{d-base}, M_{q-base}))}{\Delta M_q} \tag{5.4}$$

The partial differential spectra obtained in 5.3 and 5.4, when substituted into the original dynamic transfer of 5.1, yield the formulation of equation 5.5. The switching spectrum, previously a non-linear function of the control inputs is now replaced by a linear superposition of the base case spectrum and the two partial differential switching spectra, scaled by the instantaneous values of the scalar control inputs $M_d(t)$ and $M_q(t)$.

This structure is time-invariant, with the constant-valued linearised frequency transfer matrices being suitable for embedding in a dynamic model. This structure is not linear however, as the output is dependent on the multiplication of two dynamic variables, namely the scalar control inputs $M_d(t), M_q(t)$ with the dc voltage harmonic vector $\boldsymbol{V}_{dc}(t)$.

$$\boldsymbol{V}_a(t) = \frac{1}{2}\left(\boldsymbol{\mathcal{T}}\{\boldsymbol{S}_a\} + \delta M_d(t)\boldsymbol{\mathcal{T}}\left\{\frac{\partial \boldsymbol{S}_a}{\partial M_d}\right\} + \delta M_q(t)\boldsymbol{\mathcal{T}}\left\{\frac{\partial \boldsymbol{S}_a}{\partial M_q}\right\}\right)\boldsymbol{V}_{dc}(t) \tag{5.5}$$

The solution to this is the linearisation of the converter state variables around the base-case operating point. By assuming that the harmonic state variables remain constant over small variations in the control inputs or changes in the external energisation applied to the system, the relation can be reformulated to be completely linear and time-invariant.

$$\boldsymbol{V}_a(t) = \frac{1}{2}\left(\boldsymbol{\mathcal{T}}\{\boldsymbol{S}_a\}\boldsymbol{V}_{dc}(t) + \delta M_d(t)\boldsymbol{\mathcal{T}}\left\{\frac{\partial \boldsymbol{S}_a}{\partial M_d}\right\}\boldsymbol{V}_{dc-base} + \delta M_q(t)\boldsymbol{\mathcal{T}}\left\{\frac{\partial \boldsymbol{S}_a}{\partial M_q}\right\}\boldsymbol{V}_{dc-base}\right) \quad (5.6)$$

The harmonic vectors for the base-case state variables are multiplied at build-time by the partial differential switching FTM, giving the partial differential output vectors:

$$\frac{\partial \boldsymbol{V}_a}{\partial M_d} = \frac{1}{2}\boldsymbol{\mathcal{T}}\left\{\frac{\partial \boldsymbol{S}_a}{\partial M_d}\right\}\boldsymbol{V}_{dc-base} \quad (5.7)$$

$$\frac{\partial \boldsymbol{V}_a}{\partial M_q} = \frac{1}{2}\boldsymbol{\mathcal{T}}\left\{\frac{\partial \boldsymbol{S}_a}{\partial M_q}\right\}\boldsymbol{V}_{dc-base} \quad (5.8)$$

Together with the original large-signal FTM, these partial differential output vectors add to form the total controlled transfer, giving a single harmonic vector output which may be connected to a passive ac network.

$$\boldsymbol{V}_a(t) = \frac{1}{2}\boldsymbol{\mathcal{T}}\{\boldsymbol{S}_a\}\boldsymbol{V}_{dc}(t) + \delta M_d(t)\frac{\partial \boldsymbol{V}_a}{\partial M_d} + \delta M_q(t)\frac{\partial \boldsymbol{V}_a}{\partial M_q} \quad (5.9)$$

A similar procedure may be applied to the current transfer, resulting in a similar controlled transfer, linearised around the base case inductor current.

$$\frac{\partial \boldsymbol{I}_{dc}}{\partial M_d} = \frac{3}{2}\boldsymbol{\mathcal{T}}\left\{\frac{\partial \boldsymbol{S}_a^*}{\partial M_d}\right\}\boldsymbol{I}_{a-base} \quad (5.10)$$

$$\frac{\partial \boldsymbol{I}_{dc}}{\partial M_q} = \frac{3}{2}\boldsymbol{\mathcal{T}}\left\{\frac{\partial \boldsymbol{S}_a^*}{\partial M_q}\right\}\boldsymbol{I}_{a-base} \quad (5.11)$$

$$\boldsymbol{I}_{dc}(t) = \frac{3}{2}\boldsymbol{\mathcal{T}}\{\boldsymbol{S}_a^*\}\boldsymbol{I}_a(t) + \delta M_d(t)\frac{\partial \boldsymbol{I}_{dc}}{\partial M_d} + \delta M_q(t)\frac{\partial \boldsymbol{I}_{dc}}{\partial M_q} \quad (5.12)$$

These linearisations correspond to two modes of error as the small-signal model diverges from the base-case operating point. Firstly, the linearised model of how the switching function changes as a result of control inputs becomes less accurate with increasing deviation. This contribution to model error will be discussed in Section 5.2.3, and will be ultimately overshadowed by the second mode of error. This second mode of error is the result of the fact that any change in the converter state variables away from the harmonic steady-state of the base case will not be

reflected in the base-case harmonic vectors built in to the partial differential transfer vectors.

5.2.1 Small-Signal Model Structure

As described in Chapter 4, the three-phase bridge which forms the kernel of the VSC is a stateless modulator, capable of indiscriminately coupling voltages and currents through its terminals. It is the linking of the modulator with the ac-side inductances and dc-side capacitance that lends these voltages and currents a unilateral inertia, and therefore gives the VSC its structure as a directional modulator of currents and voltages. The same inertia of these state variables, when extended to the harmonic state space, provides the basis of the linearisation described above.

This marks the distinction between the uncontrolled model with fixed switching instants, which is valid for all real signals applied to the system, and the small-signal controlled model, which is valid only for the region of signal-space surrounding the base case operating point. Because the linear model obeys the principle of superposition, it is possible to separate the open-loop model into three orthogonal modes and associated responses, setting aside for the moment the presence of measurement and control elements:

1. The model with uncontrolled transfers only, energised with the base-case inputs, yielding the base-case state variables.
2. The model with uncontrolled transfers only, energised with a disturbance to the base-case inputs (e.g. step change in grid voltage magnitude or angle, or a dynamic negative-sequence disturbance), yielding the deviation from the base case state variables (which cannot be incorporated in the linearised transfers).
3. The model with controlled and uncontrolled transfers, energised with externally derived control inputs, yielding the small-signal deviation from the base case due to control action.

Fig. 5.1 illustrates this linearised converter structure as a harmonic state-space model, showing how the contribution from the control action is realised as a set of exogenous forcing components. It is important to note that even in the small-signal model, all energy flow in the system still passes through the large-signal uncontrolled transfers and passive networks, including the small-signal component induced in the ac and dc networks and subsequently coupled back to the converter. This reveals the dual nature of the linearisation error as the converter departs from the base-case operating point:

1. Deviations in the linked converter state variables are not reflected in the static control transfers.

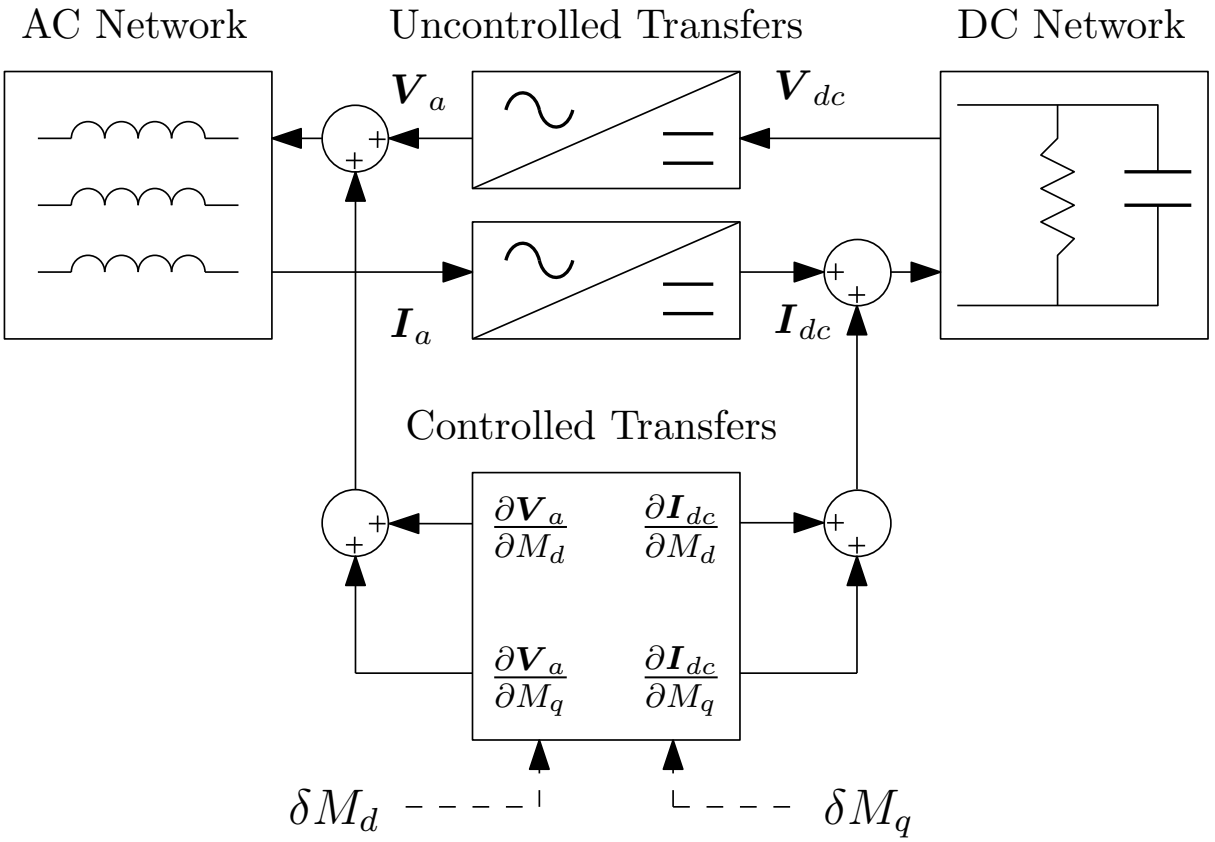

Figure 5.1 Block diagram of small-signal open-loop control model.

2. The induced small-signal components, once coupled back through the passive networks, are modulated by the base-case uncontrolled transfer only.

The open-loop model of Fig. 5.1 does not allow for the coupling of the system state variables to the control inputs, and therefore between the orthogonal modes of the system.

5.2.2 PWM Sampling Error

There exists another mode of error which is directly related to the nature of the switching converter, and its description in this thesis as an LTI system using the HSS formulation. This is the problem of sampling, as during the operation of the converter, any updates in the ordered control vector and thus switching function are only realised at the time of the next switching instant, giving the closed-loop operation of the PWM converter the characteristic of a continuous sampled-data system [Fang and Abed 1999]. The linearised model described in Section 5.2 actuates on control inputs instantaneously. The worst case is sampling at $2f_0$, as in the case of thyristor-controlled networks, with a maximum delay of $\frac{T}{2}$ before the control signal may be sampled by an individual phase. This process may be approximated as a fixed delay [Mathur and Varma 2002], chosen as a midpoint between two possible extremes and assuming sampling can

take place on any phase, as in [Orillaza 2011]. This fixed delay may be then approximated as a rational polynomial in the s-domain through a Padé approximation or similar, introducing a non-minimum phase element[Vajta 2000]. For the PWM-switched converter, the sampling frequency is $2f_c$, twice the carrier frequency, with the maximum delay similarly given by $\frac{T}{2f_c}$. Because this effect is less significant at the switching frequencies of PWM converters, it is neglected in this model.

5.2.3 Switching Function Linearisability

As a first step towards establishing the validity of the linearised control model, the linearisability of the switching function itself is examined. This is the test of the linearisation achieved using the partial differential switching spectra of equations 5.3 and 5.4, of which an example is illustrated in Fig. 5.2. Notably, these spectra do not exhibit the frequency roll-off characteristic associated with the modelling criterion of Sandberg et al. [Sandberg *et al.* 2005], as the base switching functions themselves do.

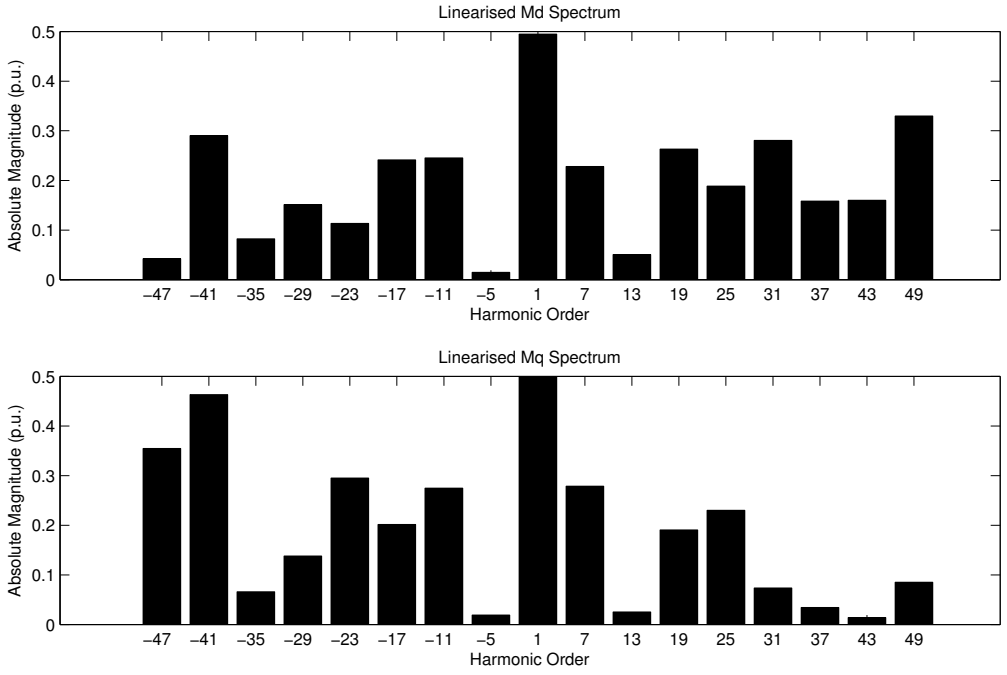

Figure 5.2 Spectra of linearised switching functions, normalised to unit control inputs, for $m_f = 9$, $\vec{M}_{base} = 0.8 - j0.03$

The numerically derived switching function as described in Section 4.4.2 provides a mapping from any given converter control operating point to an output switching spectrum. The linearisability around an operating point is tested by comparing the spectrum produced from the linear combination of the base and the partial differential spectra for a control input shown in equation 5.14, with the one evaluated directly at the new operating point including the control change (5.15).

$$\boldsymbol{S}_{a-base} = \boldsymbol{S}_a(M_{d-base}, M_{q-base}) \tag{5.13}$$

$$\boldsymbol{S}_{a-linearised} = \boldsymbol{S}_{a-base} + \delta M_d \frac{\partial \boldsymbol{S}_a}{\partial M_d} + \delta M_q \frac{\partial \boldsymbol{S}_a}{\partial M_q} \tag{5.14}$$

$$\boldsymbol{S}_{a-direct} = \boldsymbol{S}_a(M_{d-base} + \delta M_d, M_{q-base} + \delta M_q) \tag{5.15}$$

Figs. 5.3, 5.4, and 5.5 show the absolute magnitude of the differences between the individual harmonic components of these two spectra, which are the switching function linearisation errors. The absolute value of the linearisation error is considered here, as this relates directly to the error in the signal introduced to the system through the control action. Only the characteristic harmonics which comprise the switching FTMs are considered.

The results here are produced using a base-case modulation vector of $\vec{M}_{base} = 0.8 - j0.03$, with a switching frequency of 450 Hz. As seen in the figures, with increasing deviation of the control signals, the error in the higher harmonic frequencies increases proportionally greater than the linear trend at the fundamental frequency; this is the result of the non-linearity of the PWM process itself. The significance of error at higher frequencies is reduced, as the admittance to these frequencies in the passive ac and dc networks is respectively low and high.

The absolute linearisation error of the fundamental component is noted in Table 5.1. The error in the fundamental component is crucial, as it contributes to the fundamental frequency power flow. The trend in the absolute error is linearly related to the magnitude of the control input, and the errors for changes in both the M_d and M_q components are predominantly real, summing together when actuated simultaneously.

The accuracy that can be obtained depends on the discrete angular step size used for the numerical switching model detailed in Section 4.4, as the exact switching instant is determined from a numerical comparison of two discrete series. The results presented here and elsewhere in this thesis have used a sample count of $N = 524\,288$ or 2^{19} per cycle, determined empirically to balance computation time with accuracy. A full analysis of the sensitivity of the model to this parameter is outside the scope of this thesis.

Table 5.1 Fundamental component absolute linearisation error (per-unit basis).

Control input (p.u.)	Error for M_d change	Error for M_q change	Error for M_d and M_q change
0.01	5.6919×10^{-5}	5.6661×10^{-5}	1.0862×10^{-4}
0.05	2.6953×10^{-4}	2.9359×10^{-4}	5.5165×10^{-4}
0.10	5.3990×10^{-4}	5.6960×10^{-4}	0.0011
0.20	0.0011	0.0012	0.0022

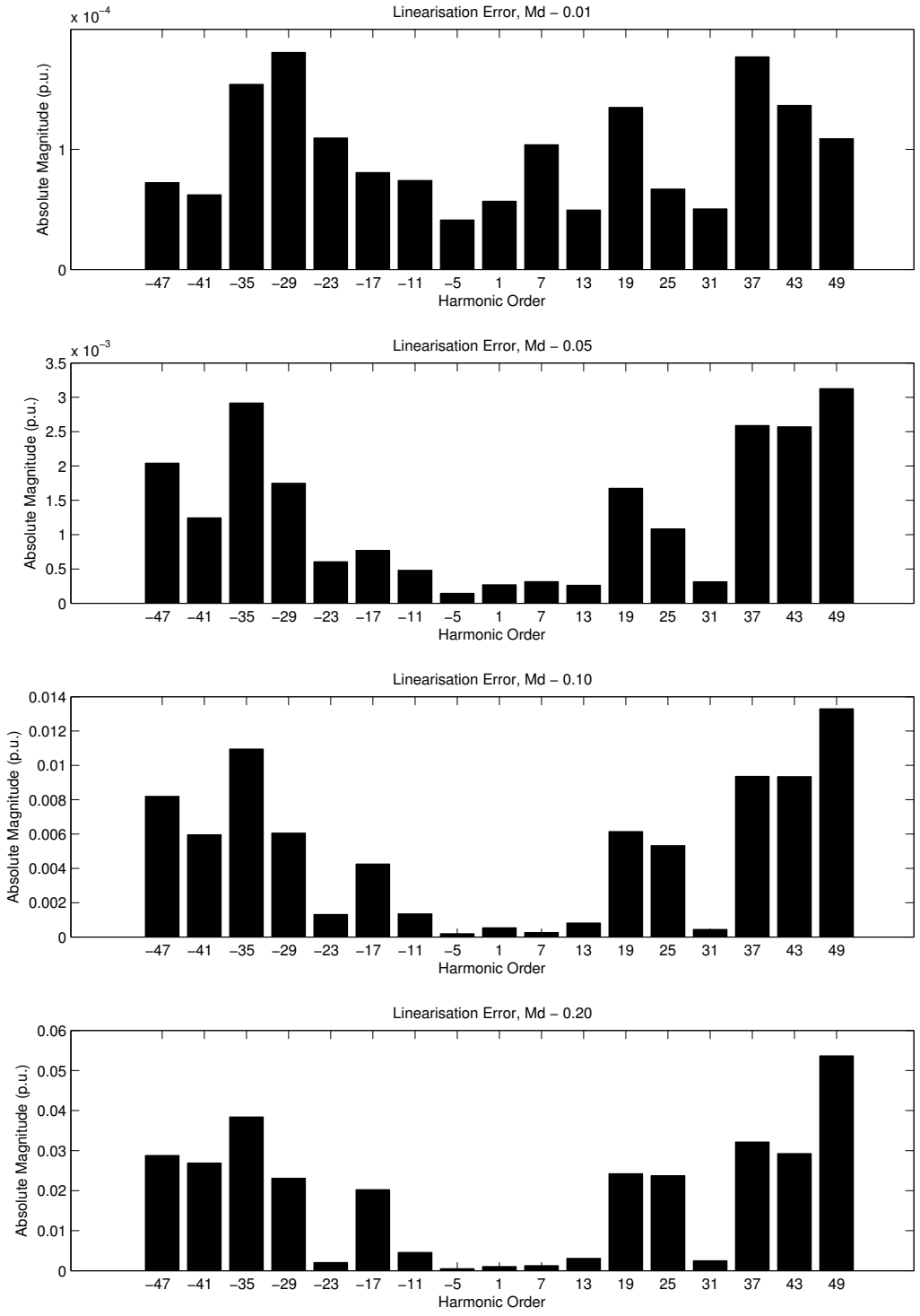

Figure 5.3 Absolute linearisation error for changes in M_d

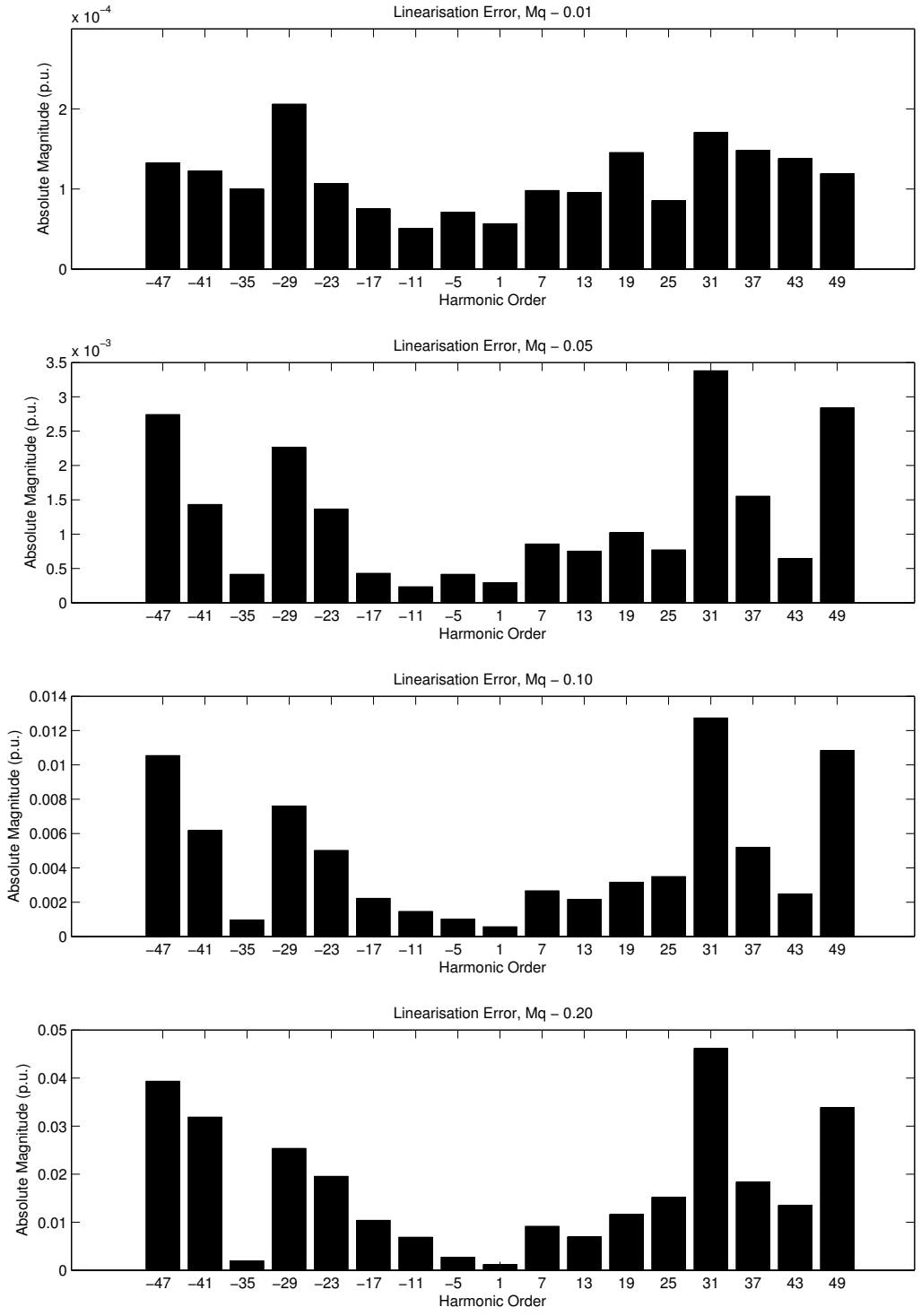

Figure 5.4 Absolute linearisation error for changes in M_q

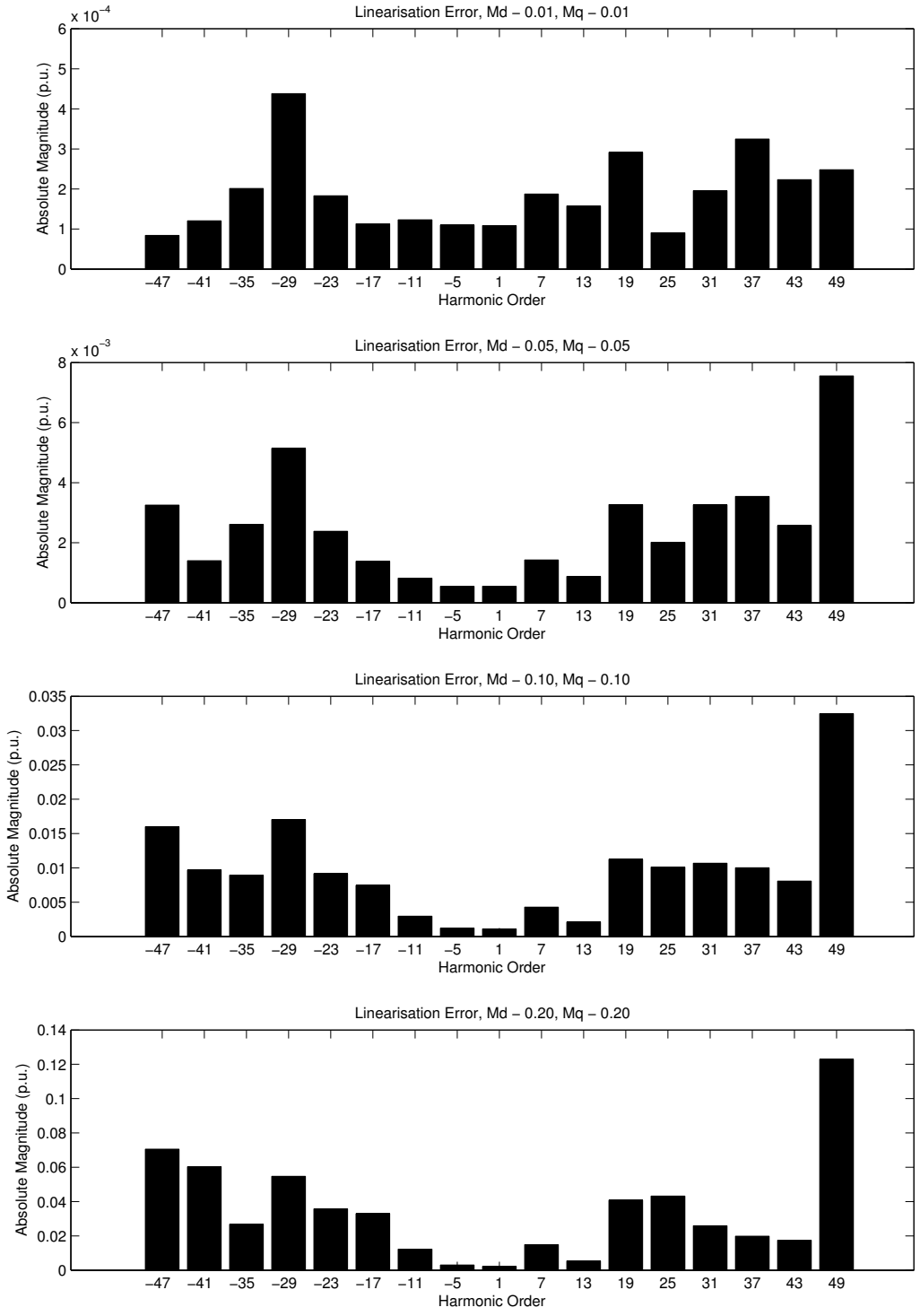

Figure 5.5 Absolute linearisation error for changes in M_d and M_q

5.3 OPEN-LOOP CONTROLLED MODEL

Demonstration of the validity of the linearisation strategy described in Section 5.2, and the characterisation of the limits of the small-signal model created by that linearisation, require the modelled transfers to be evaluated as a component in a full power system, allowing deviation of the state variables away from the harmonic steady state of the base case through coupling to the passive networks.

The system parameters used are that of the uncontrolled STATCOM system verification presented in Section 4.5.2, and both the MATLAB and PSCAD models are initialised to the periodic steady-state of the base case. The MATLAB base case was obtained using the direct solution by inversion of the dynamic matrices detailed in Section 3.2.6, and the PSCAD base case was established by a simulation of the uninitialised system to a periodic steady state at $t = 2\,\mathrm{s}$, and then using the facility for initialising subsequent simulations with its snapshot.

5.3.1 Step Responses in the Time Domain

Step inputs applied to the δM_d and δM_q control inputs give an instantaneous change in the converter power angle and magnitude, resulting in a transient evolution to a new steady state. Figs. 5.6 and 5.7 show the response of the converter model to a step change of the input modulation vector on the direct axis, giving a temporary boost to the direct-axis voltage component, and with reference to the STATCOM dynamics described in Section 4.5.1, providing a fast-acting reactive power support response.

As for the uncontrolled model simulations of Section 4.5.2, the dc voltage measurement is used here to provide a measure of the integral power flow, which is a sensitive indicator of total system dynamics. The simulations identify steady-state offset errors in the dc voltages, detailed in Fig. 5.8 which increase with the magnitude of the control input (approximately $0.05\,\mathrm{kV}$ and $0.2\,\mathrm{kV}$ respectively), however, as identified in Fig. 5.9, the controlled model accurately captures the oscillatory mode of the transient response.

In Figs. 5.10 and 5.11, both the transient response and the steady-state are modelled accurately for step δM_q inputs of both magnitudes.

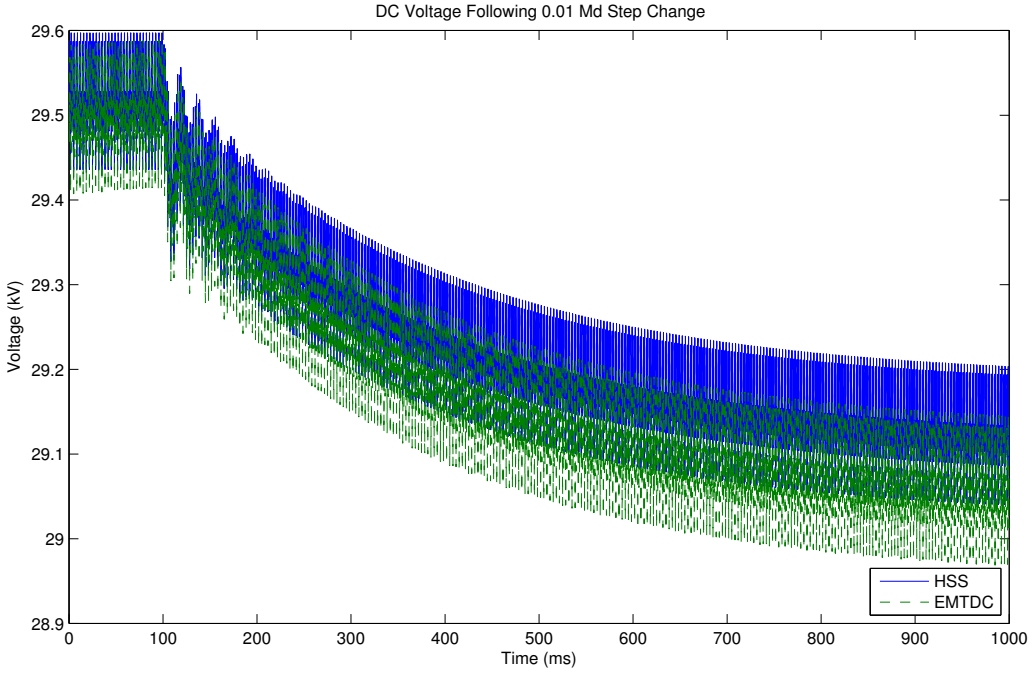

Figure 5.6 DC bus voltage following the application of a step control input of $M_d = 0.01$.

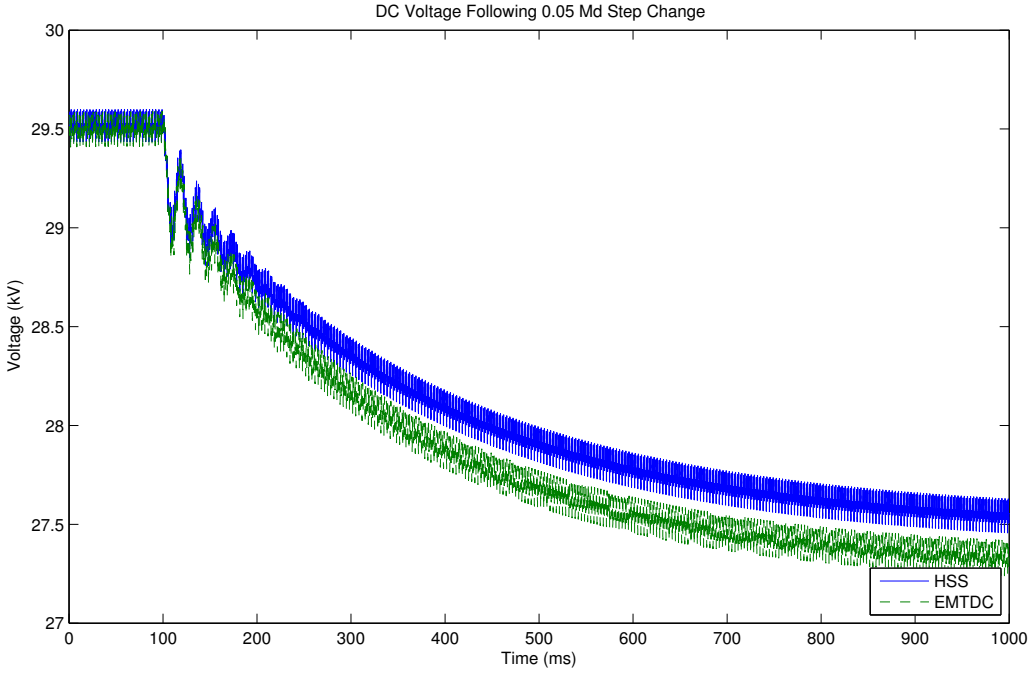

Figure 5.7 DC bus voltage following the application of a step control input of $M_d = 0.05$.

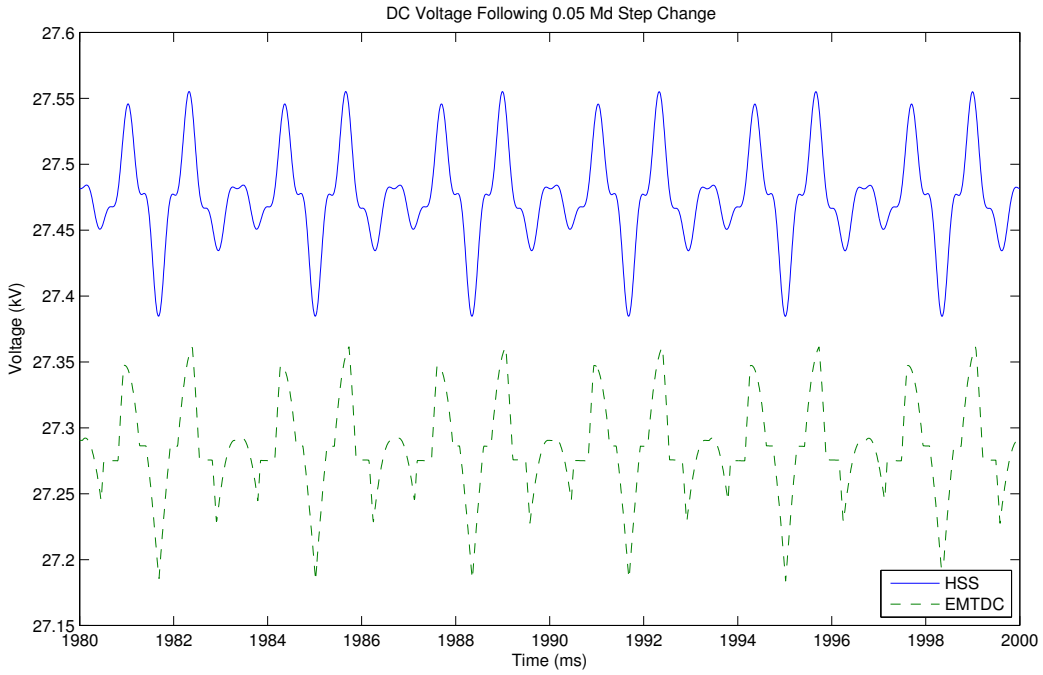

Figure 5.8 DC bus voltage following the application of a step control input of $M_d = 0.05$, detailing the steady-state offset.

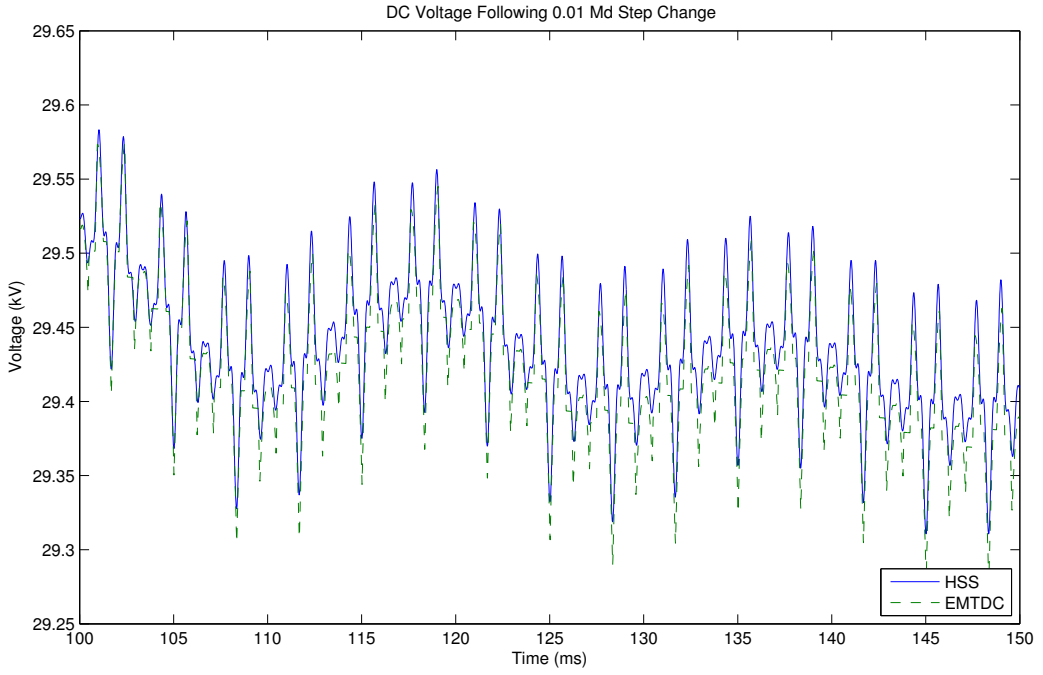

Figure 5.9 DC bus voltage following the application of a step control input of $M_d = 0.01$, detailing the initial transient response.

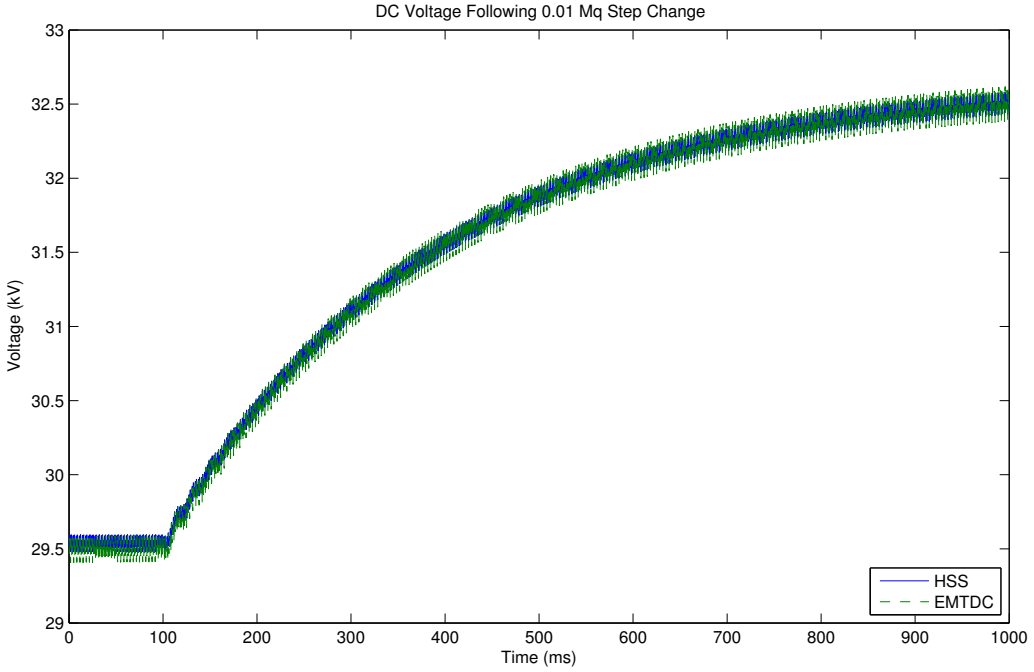

Figure 5.10 DC bus voltage following the application of a step control input of $M_q = 0.01$.

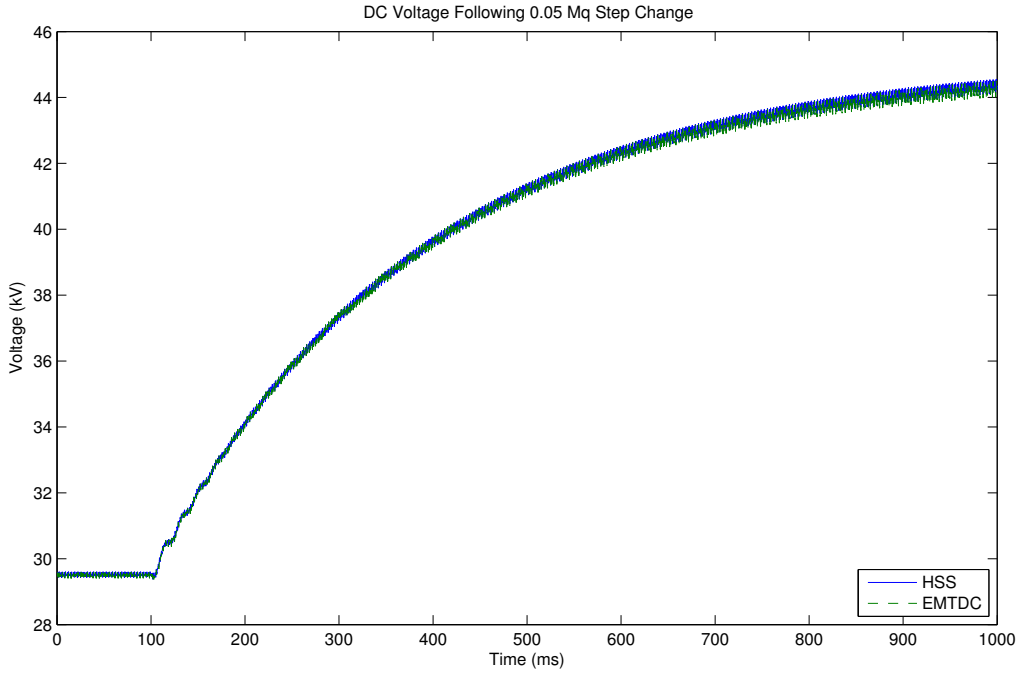

Figure 5.11 DC bus voltage following the application of a step control input of $M_q = 0.05$.

5.3.2 Step Responses in the State Space

With the basic validity of the control transfers established, the special properties of the harmonic state space formulation of the VSC provide previously inaccessible insight to the operation of the converter system. The raw output of the HSS model is available, in the form of the full harmonic vector outputs for each individual state variable and output node of the state-space subsystems. This provides the dynamic evolution of every harmonic component of a given signal, with the advantage that this is obtained without any need for a windowed FFT operation, and the caveat that the dynamic harmonic-domain signal is non-unique. Rico et al. [Rico *et al.* 2003] contains a comparison between measurements of harmonic components achieved through windowed FFT methods and the HSS, demonstrating how the HSS forms an ideal basis for the extension of steady-state harmonic measurement indices to their transient evaluation.

The fundamental component of any state variable, which is the least amenable to conventional Fourier analysis, may be readily extracted in this way. Fig. 5.12 shows the breakdown of the output voltage into the $d-$ and $q-$axis components, which identify with the real and imaginary components of the complex signal in the synchronous reference frame.

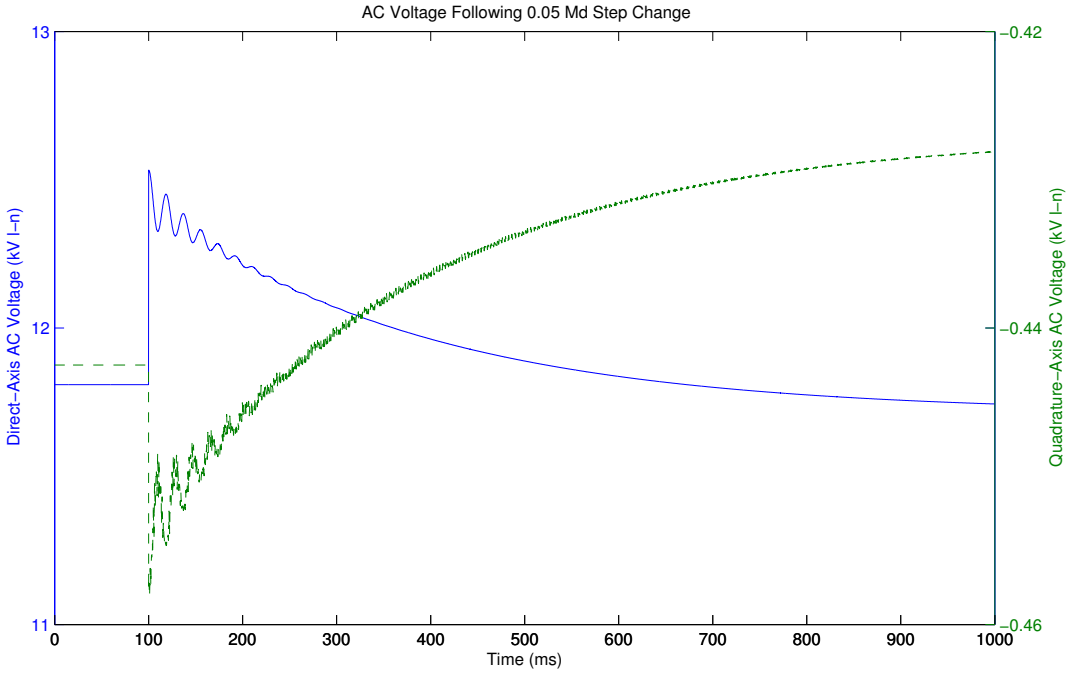

Figure 5.12 Fundamental components of harmonic state-space output.

Under the passive sign convention used for the converter model, positive quadrature-axis converter current indicates a supply of reactive power from the converter to the grid. Fig. 5.13 shows a similar breakdown of the converter current into the orthogonal components of the synchronous dq reference frame, showing the temporary increase in reactive power output. Fig. 5.14 shows the evolution of the dc voltage and current by examination of the zero-frequency component, making it possible to identify the main resonant modes of the system in the time domain without interference from the higher-order harmonic components. This ability to extract the fundamental component in real time will be used when developing the closed-loop control system.

5.3.3 Pole-Zero Analysis of the Open-Loop System

In the time domain, examination of any of these series reveals a dominant resonant pole-pair at a frequency of approximately 54 Hz, as well as an overdamped response. This is borne out by inspection of the pole-zero plot for the open-loop system of Fig. 5.15, in which the dominant poles are identified in Fig. 5.16, and can be identified with the observed time-domain response ($342\,\mathrm{rad\,s^{-1}} = 54.43\,\mathrm{Hz}$). These oscillatory modes are the product of resonances between the dc link capacitor and the inductive ac network, as mediated by the action of the converter.

The large-scale structure of the pole-zero plot shows the same poles repeated up and down the imaginary axis, as the same dynamic response is recreated in multiple harmonic reference frames. This is revealing of the manner in which higher-order resonances in the system may be coupled down to a lower frequency range of interest, such as the control bandwidth.

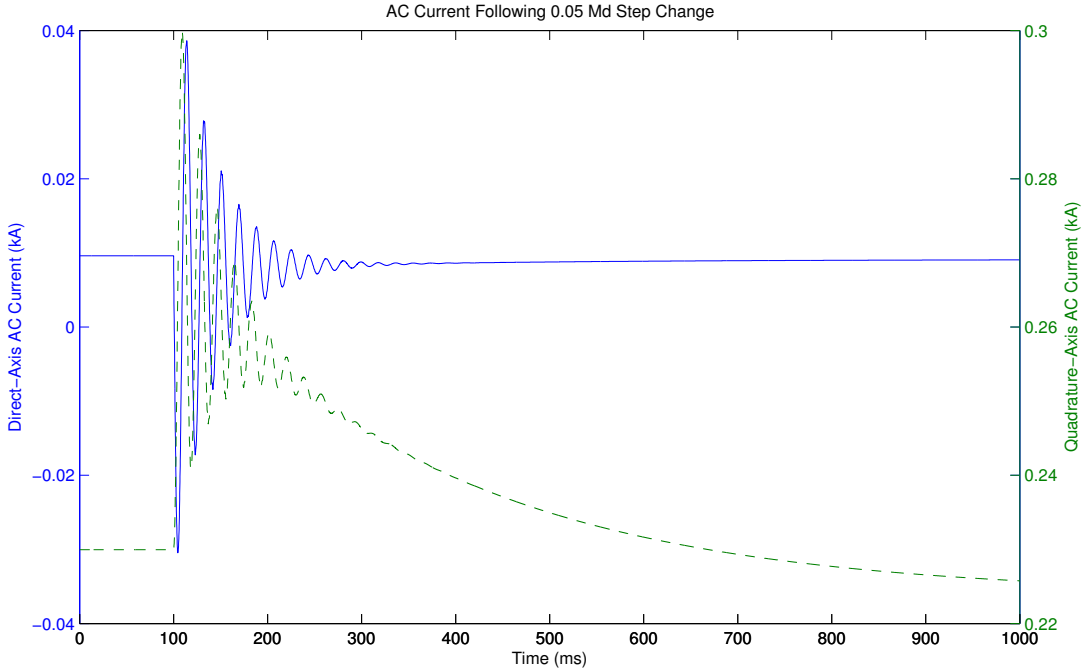

Figure 5.13 Fundamental components of harmonic state-space output.

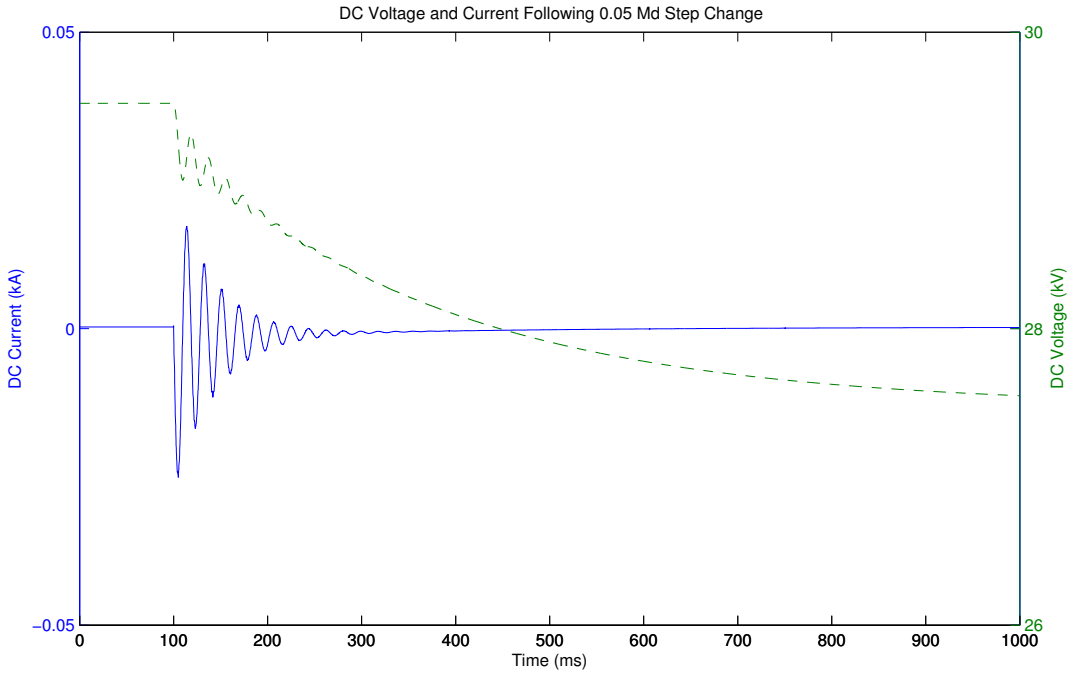

Figure 5.14 Fundamental components of harmonic state-space output.

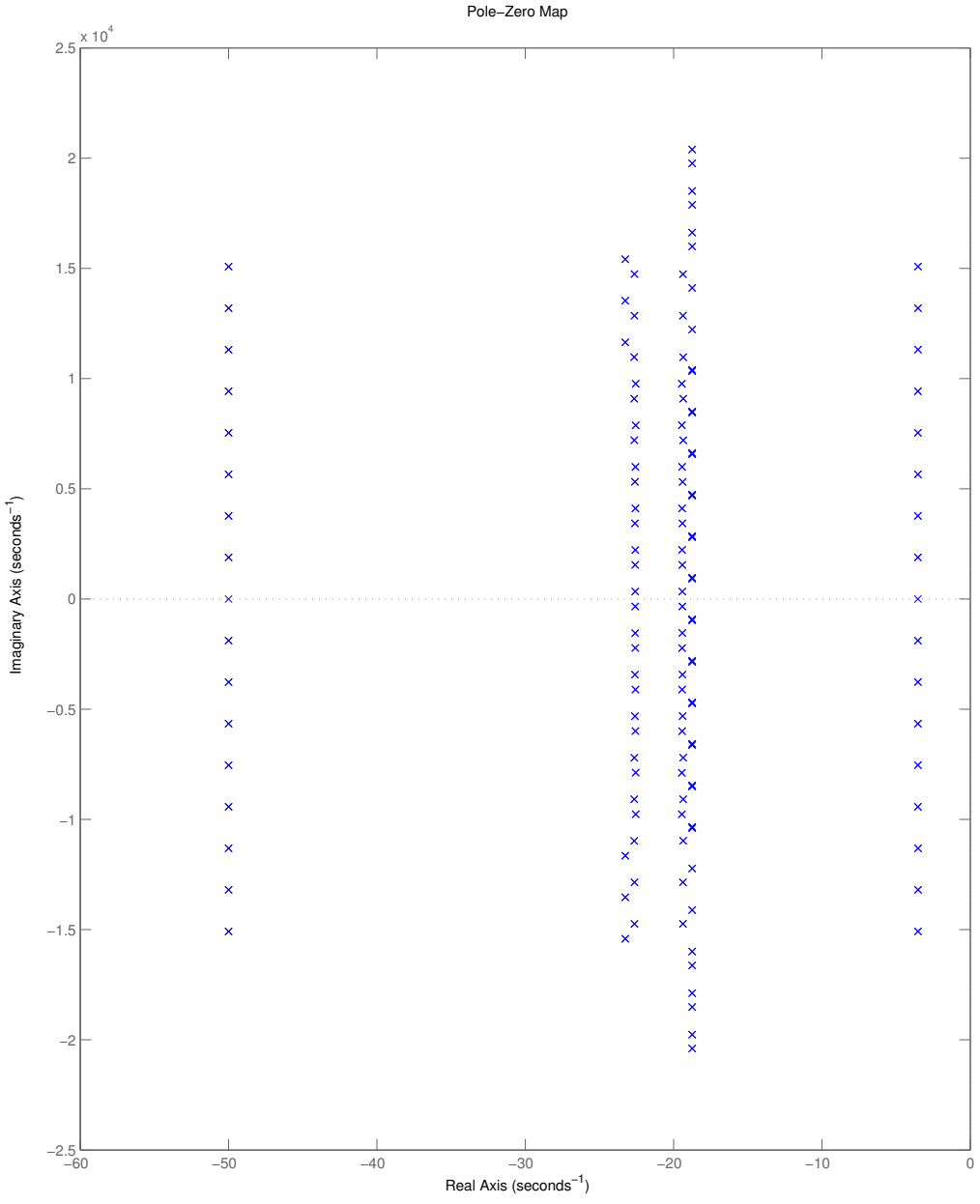

Figure 5.15 Pole-zero map of open-loop controlled system, showing entire system.

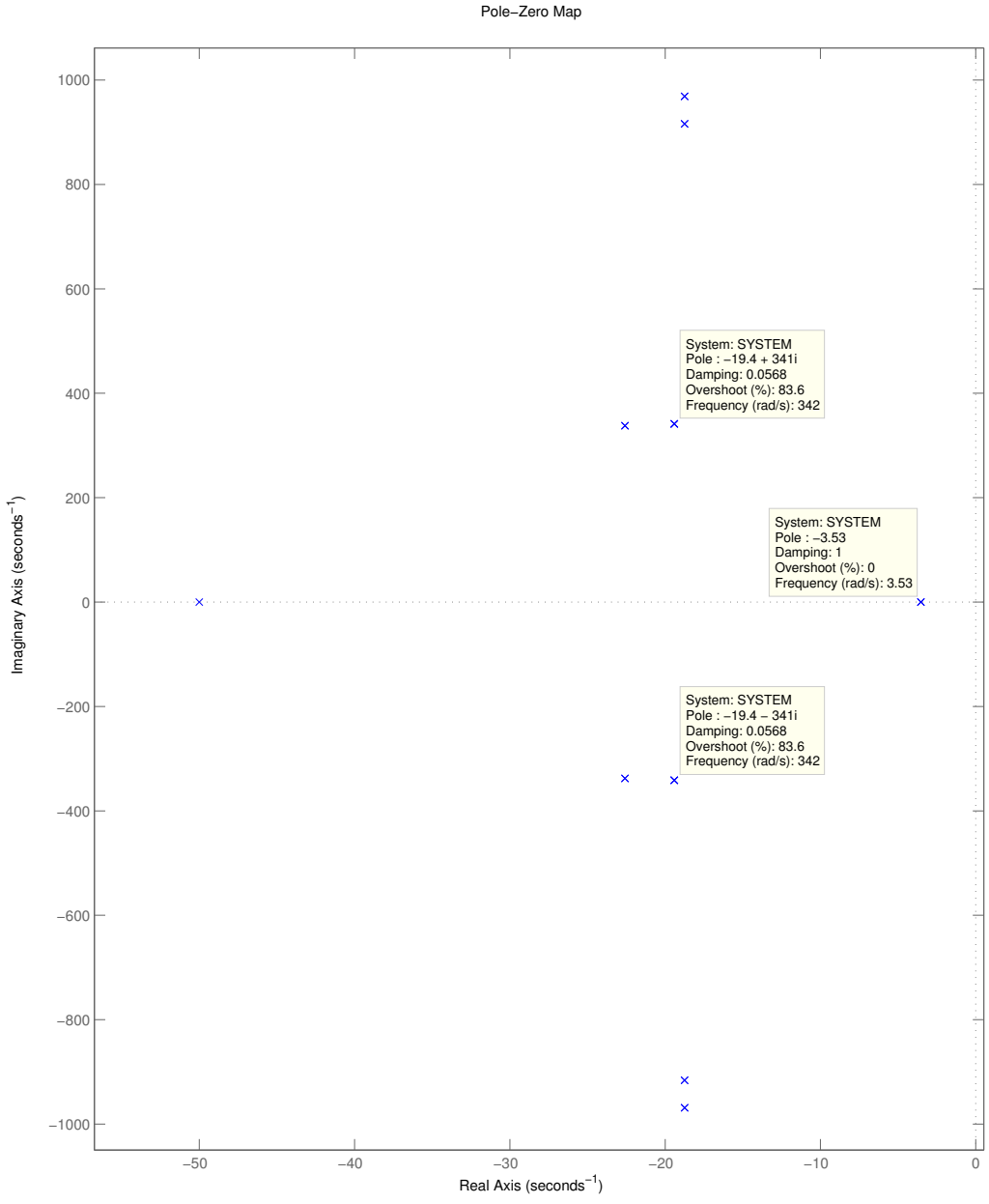

Figure 5.16 Pole-zero map of open-loop controlled system, highlighting dominant poles.

5.4 CLOSED-LOOP CONTROLLED MODEL CONSTRUCTION

The controlled HSS model of the VSC developed in this chapter is an LTI state-space system, accepting two scalar state-space signals as control inputs. This section describes the method for the measurement of the system quantities to be controlled, and the formulation of a simple control system within the state space. This will yield a state-space model of the complete closed-loop converter system including full harmonic coupling effects, and with this, access to LTI analysis techniques. The controlled model is validated for perturbations to the grid and control setpoint, and used to generate results for control analysis and harmonic coupling effects.

5.4.1 Control Variable Measurement

To gain a measurement of a signal in the state-space model, the properties of the HSS signal representation must be considered. Because of the presence of multiple harmonic reference frames, the dynamic EMP signal is non-unique, in contrast to the unique periodic steady-state as defined by the balanced characteristic harmonic phasor set, which the EMP signal degenerates to under steady-state harmonic energisation, in accordance with the transient relaxation property described in Section 3.2.

This property of relaxation may be exploited to gain a measurement of any particular harmonic component of an EMP signal in a stable HSS system, by assuming that the dynamic harmonic signal undergoes a similar continuous relaxation towards a quasi-steady state condition in which signal energy is concentrated in the lowest-order harmonic reference frames. This yields slowly-varying harmonic components which may be used as measurement of individual harmonics as would be derived through windowed FFT methods, though available in real time, without the problems associated with an actual window.

The specific measurements discussed below are the dc voltage and reactive power. Together, these variables can uniquely specify the operating point of the single-converter system, and act as control variables for converter configurations such as the STATCOM-type system used in this chapter, as well as such others as controlled rectifier systems where the goal is to provide a fixed dc output voltage and minimal reactive power draw.

5.4.1.1 DC Voltage

In a STATCOM configuration, dc voltage control is required to ensure that the rated capacitor bank voltage is not exceeded nor run down, but maintained at a level which can deliver or absorb some amount of energy so as to provide a dynamic ride-through capability during transient events [Rao *et al.* 2000]. The capacitor also attenuates the harmonic distortion of the dc bus voltage

from the dc current harmonics as seen in Figs. 5.6 to 5.9. Because of this harmonic distortion, there must be some provision for filtering the signal when used an an input to the control system. This distortion may originate from the harmonic currents of the converters switching action, modulated from the characteristic ac current components (thus giving the characteristic $0 \pm 6n$ components on the dc side, more readily filtered), or a second-harmonic distortion arising from an imbalance in the fundamental current, which being a low frequency is harder to filter, being presented a higher impedance by the dc-side capacitor.

Using the technique described above, the real part of the zero frequency component may be extracted from the dc voltage harmonic vector (the imaginary part will always be zero for conjugate system inputs and thus real signals), and used as a proxy for the averaged value of the dc voltage.

$$v_{dc}(t) = \Re V_{dc,0}(t) \tag{5.16}$$

This signal will be free of the harmonic distortions present of the time-domain signal as evaluated through the harmonic reconstruction of the time series, or as seen in the PSCAD time-domain simulation.

In this model, a single-pole low-pass filter with a time constant of 0.02 s is interposed between the voltage measurement and the control block in both the PSCAD and state-space systems. In the PSCAD model, this filter attenuates the high-frequency content which would be passed through the proportional elements of the control system, and contribute to jitter of the switching instants through the PWM process. There is little high-frequency content to filter in the zero-frequency output from the state-space model, but the same filter element must be present to give the same transient response to the slowly-varying component.

5.4.1.2 Reactive Power

Most modern VSC control systems use a nested system of feedback controllers, with an internal fast *dq*-axis current controller taking its reference input from an external control loop tracking reactive power and dc voltage setpoints. Measurement of reactive power is complicated by the contribution of harmonic and unbalanced flows to the instantaneous reactive power, as supported by the rich literature on power measurement for three-phase systems in the presence of imbalances and distortions [Depenbrock 1993][Watanabe *et al.* 1993][Peng and Lai 1996]. The explicitly balanced HSS formulation permits a powerful simplifying assumption; that the relevant quantity for support of the grid voltage is the fundamental frequency reactive power flow at the

grid connection point. The complex power, defined in positive sequence fundamental phasors, yields the following formulation in a stationary dq reference frame.

$$S = VI^* \tag{5.17}$$
$$= (V_d + jV_q)(I_d - jI_q) \tag{5.18}$$
$$= (V_d I_d + V_q I_q) + j(V_q I_d - V_d I_q) \tag{5.19}$$

In the special case where the dq reference frame is identical with the grid (and thus $V = V_d, V_q = 0$), the reactive power component reduces to

$$\Im S = -V_d I_q \tag{5.20}$$

so that for a constant and normalised V_d, the I_q component functions as a directly proportional proxy for fundamental frequency reactive power levels, with positive I_q equal to reactive power delivered under the passive sign convention adopted here. As a small-signal model, linearisation around a $V = V_d, V_q = 0$ operating point gives second-order terms for changes in the phase of the remote source which are ignored.

As the HSS system is defined in a fixed global dq reference frame, the direct and quadrature components of any fundamental ac signal may be accessed by inspection of the fundamental frequency phasor, again using the assumption of the quasi-steady state relaxation of the harmonic state variables. Compared to time-domain analogues of reactive power measurement which use the full harmonic spectrum, this removes direct dependence on the maximum harmonic order used in the model, allowing for comparison over varying maximum harmonic orders.

Because the real and imaginary parts of the complex EMP phasors are separate state variables, this imaginary component operation is implemented in the state-space model simply through the linear combination of the two conjugate (for real inputs) imaginary variables as given in equation 5.21. The result is equivalent to the magnitude-preserving form of the $dq0$ transform given in 4.3.2, with the steady d and q elements equivalent to peak phase quantities in the ac system.

$$i_q(t) = \Im I_{a,+1}(t) - \Im I_{a,-1}(t) \tag{5.21}$$

For the time-domain PSCAD model, no such built-in reference frame transformation is available, and the quadrature current quantity must be calculated by means of a real-time dq transform block, using the same fixed phase reference from a separated ideal bus as the control system. The dq transform functions as a linear frequency modulator in a very similar way to the switching converter itself, down-modulating the balanced fundamental current component to a pair of i_d and i_q signals. These resultant signals have stationary components from the balanced fundamental component, as well as contributions from down-modulated harmonics and negative-sequence components.

As for the dc voltage measurement, a single-pole filter with a time constant of 0.02 s is used in both models to attenuate these distortions in the PSCAD model while giving the same transient response. As will be demonstrated in Section 5.5.5, if an imbalance were introduced in the HSS model through the modulation of the grid voltage fundamental phasor at -100 Hz, then the same 100 Hz modulation would show up in the state-space measurement as that produced from the down-modulation of the PSCAD dq transform, further validation of the principle of using dynamic variation of balanced HSS phasors to represent imbalanced signals.

5.4.2 Control System

The intention of this control model is not to emulate a practical industrial control system, but to serve as a test system to evaluate closed-loop system dynamics using LTI system analysis techniques. To this end, the control system implemented has a simple feedback structure which satisfies closed-loop stability and controllability criteria, able to reach a steady-state control set-point in an acceptable simulation timeframe.

The structure of this control system is shown in Fig. 5.17, with a 2x2 gain matrix translating control variable errors into control input errors, and then a pair of proportional-integral blocks to track steady-state reference inputs. The error gain matrix is derived numerically by taking the inverse of the open-loop sensitivity matrix $\boldsymbol{S}$ described in the simulation procedure of Section 5.4.4, taken once and then fixed to remove dependence on design variables under test such as the simulation harmonic order. An identical structure is implemented in the PSCAD model through multiplier and PI blocks.

This control network translates directly to the following state-space form:

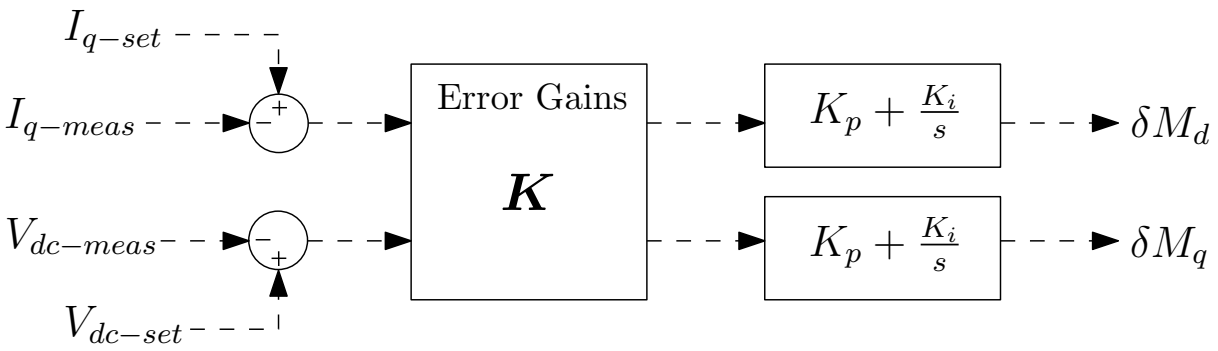

Figure 5.17 Block diagram of feedback network.

$$A = \begin{bmatrix} 0 & 0 \\ 0 & 0 \end{bmatrix} \tag{5.22}$$

$$B = \begin{bmatrix} k_{1,1} & k_{1,2} \\ k_{2,1} & k_{2,2} \end{bmatrix} \tag{5.23}$$

$$C = \begin{bmatrix} K_i & 0 \\ 0 & K_i \end{bmatrix} \tag{5.24}$$

$$D = K_p \begin{bmatrix} k_{1,1} & k_{1,2} \\ k_{2,1} & k_{2,2} \end{bmatrix} \tag{5.25}$$

5.4.3 Complete Closed-Loop Model

Following the procedure of state-space system construction of Section 4.4.4, the complete closed-loop model is constructed from the converter transfer, ac network, dc network, measurement, filtering and control blocks as illustrated in Fig. 5.18.

The input vector to the closed-loop system consists of the grid voltages plus the control setpoints.

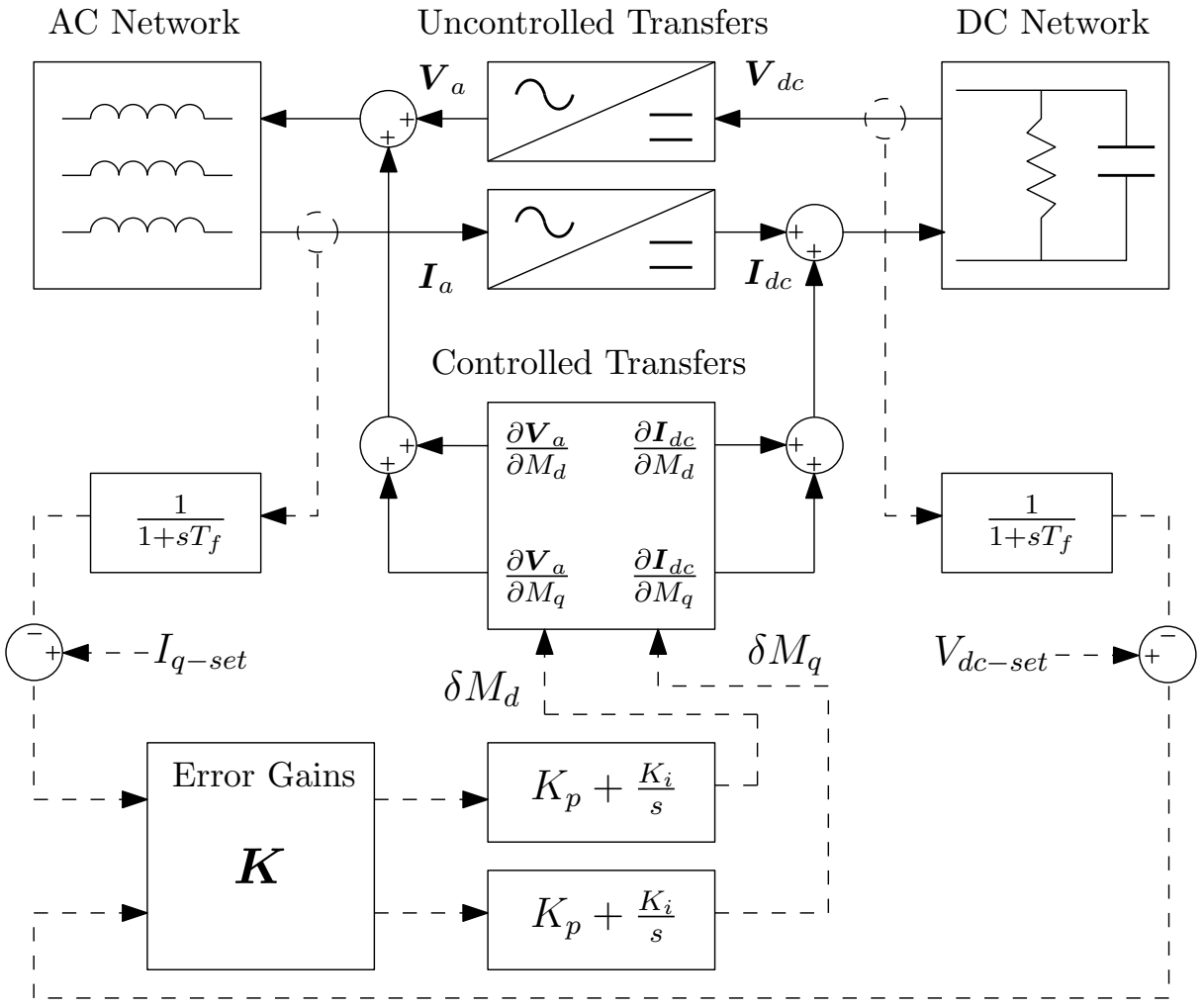

Figure 5.18 Block diagram of small-signal closed-loop control model.

$$\boldsymbol{U} = \begin{bmatrix} \begin{bmatrix} \vdots \\ V_{grid,-5} \\ V_{grid,+1} \\ V_{grid,+7} \\ \vdots \end{bmatrix} \\ \begin{bmatrix} \vdots \\ V_{grid,-7} \\ V_{grid,-1} \\ V_{grid,+5} \\ \vdots \end{bmatrix} \\ I_{q-set} \\ V_{dc-set} \end{bmatrix} \tag{5.26}$$

5.4.4 Simulation Procedure

The procedure for initialising the closed-loop model requires multiple steps. Some of these will be unique to the particular operating point, and require re-computation for any changes; others, such as the dynamic inputs, permit repeated simulation with varying values from the state-space system generated in the prior steps. Aside from the configuration and specification of the passive network, the closed-loop simulation is defined by a set of fixed parameters and time-series:

1. The maximum harmonic order h, defined at $1 + 6n$ for ac vectors.
2. The base-case network inputs $\boldsymbol{V}_{grid-base}$, identified with the first orthogonal mode of Section 5.2.1, normally a single fundamental frequency energisation.
3. The base-case control setpoint, given as the pair I_{q-base} and $V_{dc-base}$
4. The converter base-case modulation vector $\vec{M}_{base}$, chosen to give an uncontrolled steady-state response in the vicinity of the base-case control setpoint (it is not necessary to be exact because the steady-state solution to the closed-loop model will include the adjustment necessary for convergence to the base-case control setpoint).
5. The dynamic network inputs $\boldsymbol{V}_{grid}(t)$, a time series beginning at the base-case value.
6. The dynamic control setpoint inputs $I_{q-set}(t)$ and $V_{dc-set}(t)$, a time series beginning at the base-case value.

The simulation procedure itself is then as follows:

1. Build the open-loop system (as per Fig. 5.1) with control transfers zeroed.
2. Solve for the steady-state solution to the base-case network inputs by inversion of the system matrices.
3. Extract the base-case harmonic vectors for the linked converter state variables $\boldsymbol{I}_{a-base}$ and $\boldsymbol{V}_{dc-base}$.
4. (Optional) Build the open-loop system with the control transfers incorporating the base-case state variables.
5. (Optional) Solve for the steady-state solution to the base-case inputs plus small perturbations of M_d and then M_q to generate the open-loop control sensitivity matrix $\boldsymbol{S}$ as per (5.27).
6. Build the closed-loop system (as per Fig. 5.18) with the same control transfers.

7. Solve the closed-loop system for the base-case network and control reference inputs.
8. Simulate the dynamic closed-loop system for the time-varying network and control reference inputs.

$$\begin{bmatrix} \delta I_q \\ \delta V_{dc} \end{bmatrix} = \begin{bmatrix} s_{1,1} & s_{1,2} \\ s_{2,1} & s_{2,2} \end{bmatrix} \begin{bmatrix} \delta M_d \\ \delta M_q \end{bmatrix} \tag{5.27}$$

In the direct solution by matrix inversion of step 7, the closed-loop stability and controllability of the system is implied by the invertibility of the system $\boldsymbol{A}$ matrix. The system state produced by this solution has the control block integrators pre-set to the level that gives convergence with the base-case setpoint, so that the base-case modulation vector does not need to be precisely set to achieve the base-case control setpoint with no control input.

5.5 CLOSED-LOOP SIMULATION RESULTS

This section presents simulation results obtained using the closed-loop model. Table 5.2 lists the common system parameters for closed-loop simulation. The switching frequency has been lowered to $m_f = 9$ so as to make the effect of low-order harmonic interaction more apparent. The base control gains were selected to give a stable but underdamped response.

The source of the measured I_q plotted in both the HSS and EMTDC data is the output of the single-pole filter, which forms the input to the control system. This allows the transient response to be visually matched between the simulations, although the harmonic content of the time-domain I_q measurement has not been completely attenuated, so the comparison must be performed with reference to the envelope of the signal.

5.5.1 Controlled Model Setpoint Tracking

In the first set of simulations, a step change of the I_q control setpoint from 215 A to 220 A was ordered at $t = 100$ ms. Figs. 5.19 - 5.21 demonstrate the close time-domain fit for the small change in the quadrature current setpoint, for maximum harmonic order of the HSS simulation $h = 49$.

With a larger deviation of the setpoint from the base case at $I_q = 250$ A, the limits of the linearised model are visibly encountered. Figs. 5.22 and 5.23 show the divergence of the dominant closed-loop mode from that of the time-domain simulation, and Fig. 5.24 shows the time series of the δM_d and δM_q control inputs to the linearised model.

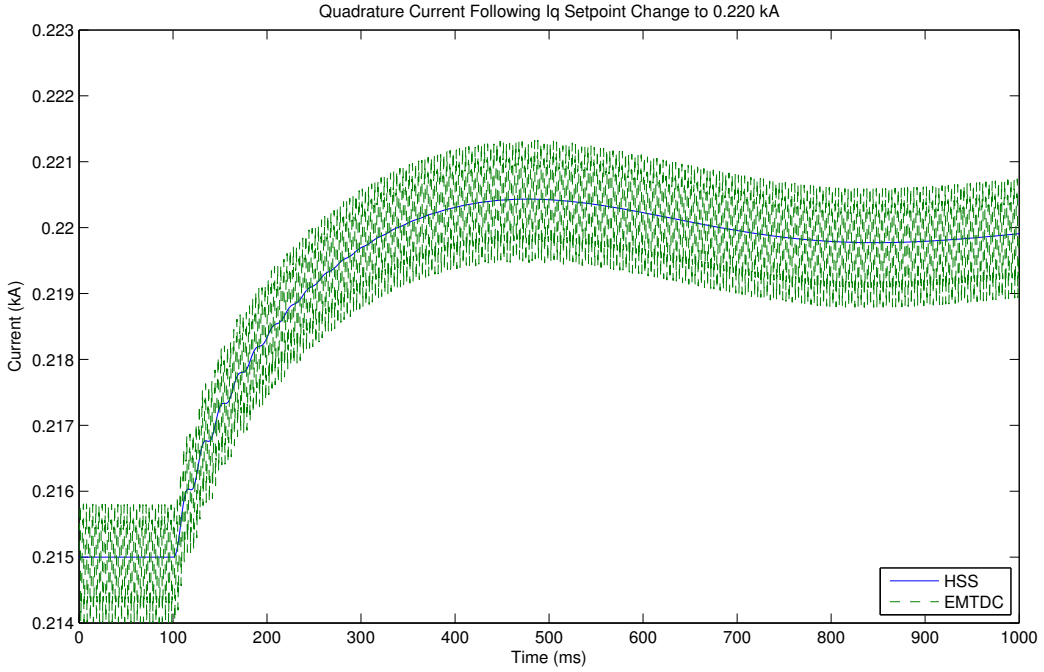

Figure 5.19 Quadrature converter current following a change in the I_q setpoint.

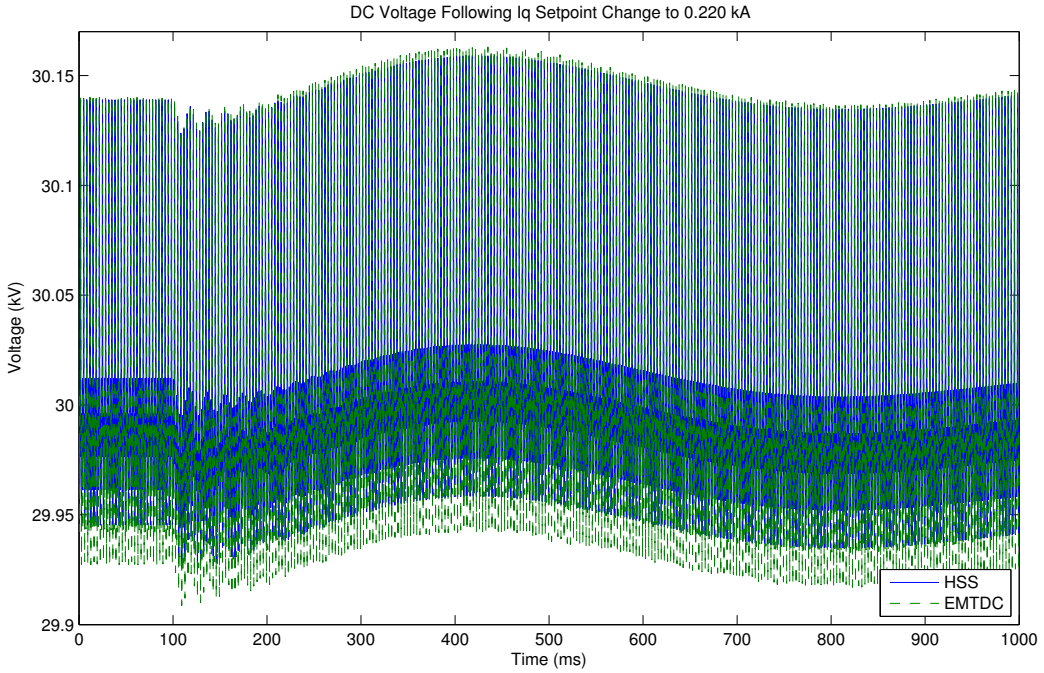

Figure 5.20 DC bus voltage following a change in the I_q setpoint.

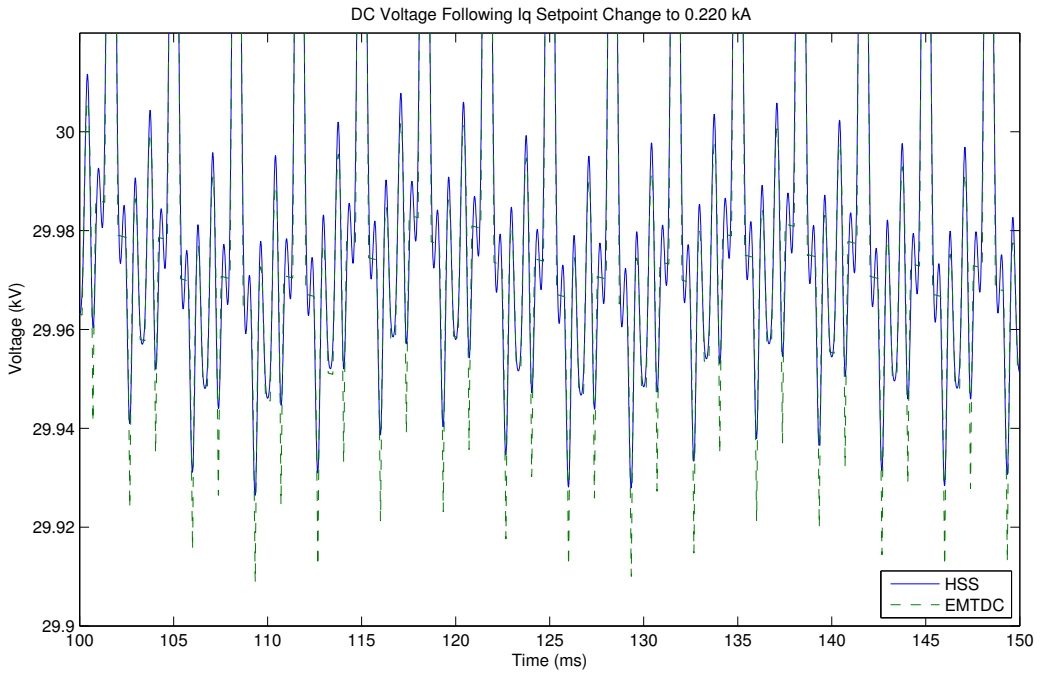

Figure 5.21 DC bus voltage following a change in the I_q setpoint, detailing initial transient response.

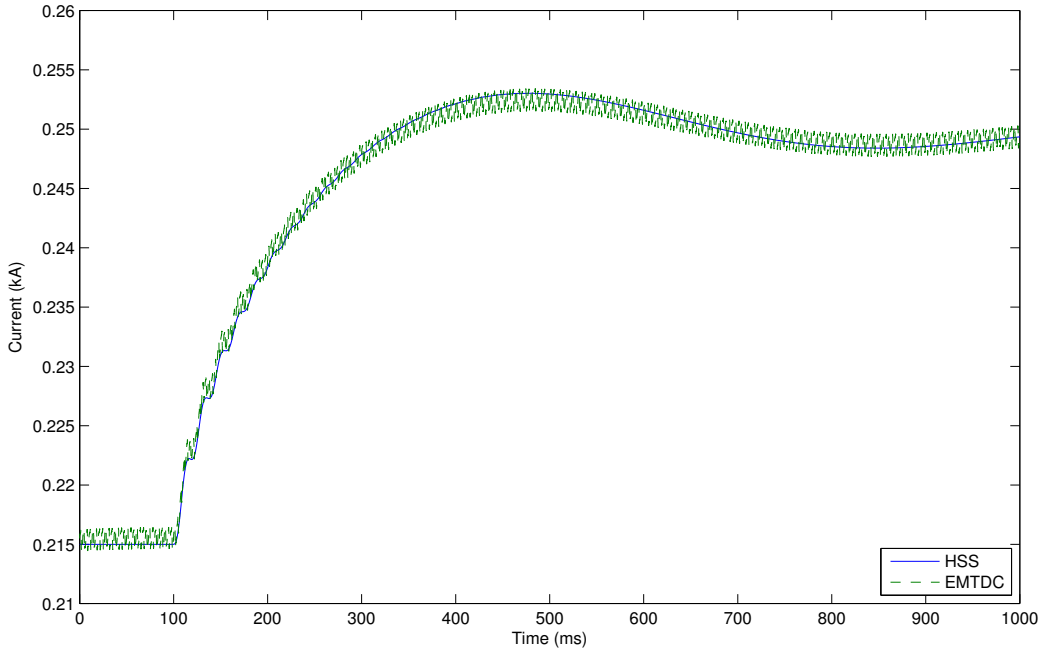

Figure 5.22 Quadrature converter current following a larger change in the I_q setpoint.

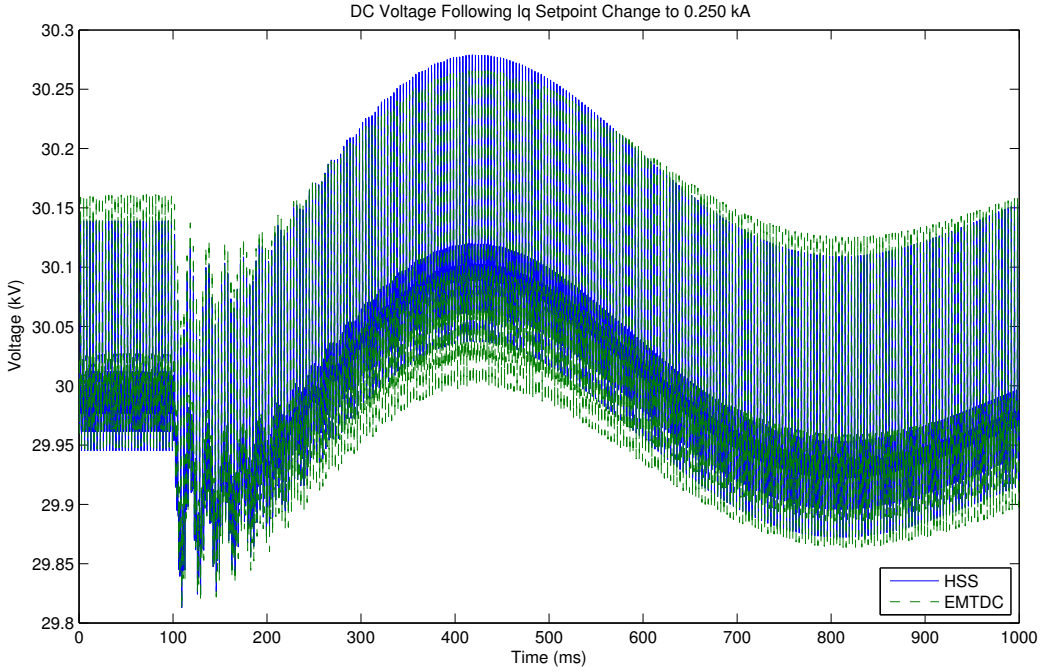

Figure 5.23 DC bus voltage following a larger change in the I_q setpoint.

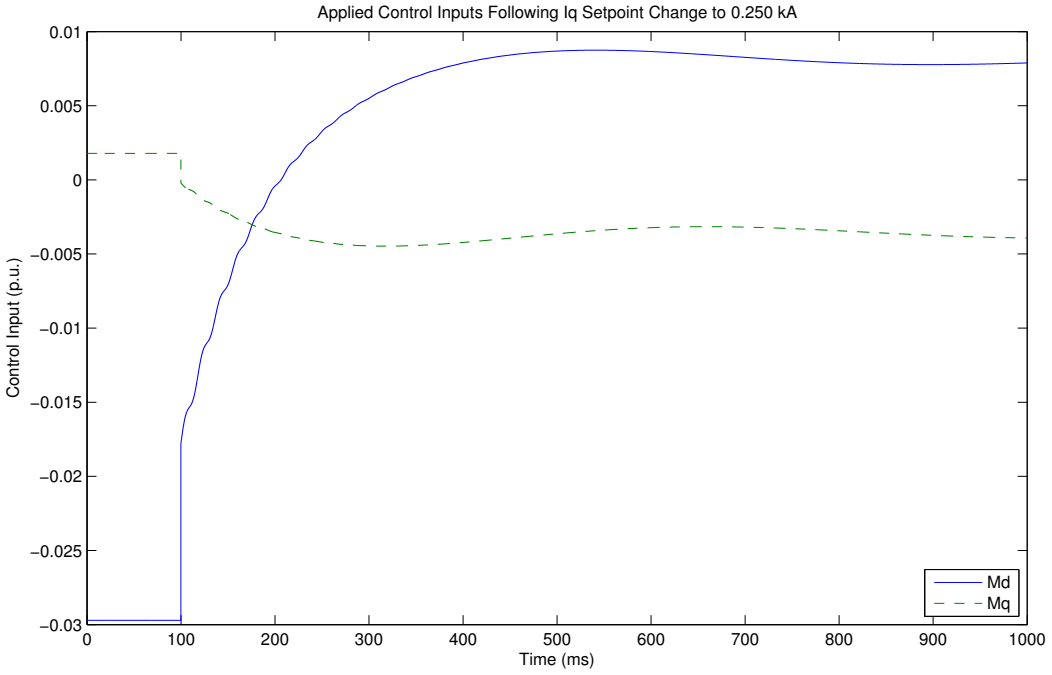

Figure 5.24 Applied control inputs following a larger change in the I_q setpoint.

Table 5.2 Closed-loop test system parameters.

Parameter	Value	Per-unit basis
Base voltage	$V_{base} = 10\,\text{kV}$	
Base MVA	$S_{base} = 2\,\text{MVA}$	
Fundamental frequency	$f_0 = 50\,\text{Hz}$	
Switching frequency	$f_{sw} = 450\,\text{Hz}$	9 p.u.
Base modulation vector	$\vec{M}_{base} = 0.8 - j0.03$	
Source resistance	$R_s = 0.25\,\Omega$	0.005 p.u.
Source inductance	$L_s = 0.01\,\text{H}$	0.0628 p.u.
Converter resistance	$R_c = 1\,\Omega$	0.02 p.u.
Converter inductance	$L_c = 0.04\,\text{H}$	0.251 p.u.
Filter resistance	$R_f = 0.1\,\Omega$	0.002 p.u.
Filter capacitance	$C_f = 5\,\mu\text{F}$	12.7 p.u.
DC-side capacitance	$C_{dc} = 300\,\mu\text{F}$	0.212 p.u.
DC-side resistance	$R_{dc} = 10\,\text{k}\Omega$	2000 p.u.
Converter LC corner frequency	$f_{co} = 355.881\,\text{Hz}$	7.12 p.u.
Quadrature current base setpoint	$I_{q-base} = 215\,\text{A}$ (peak)	1.31 p.u.
DC voltage base setpoint	$V_{dc-base} = 30\,\text{kV}$	
Proportional gain	$K_p = 0.5$	
Integral gain	$K_i = 20$	
Perturbation matrix (rounded)	$\boldsymbol{S} = \begin{bmatrix} -0.2 & -10 \\ -50 & -300 \end{bmatrix}$	
Control gain matrix	$\boldsymbol{K} = \boldsymbol{S}^{-1} = \begin{bmatrix} 0.6818 & -0.0227 \\ -0.1136 & 0.0005 \end{bmatrix}$	

5.5.2 Response to Grid Perturbations

To further test the limits of the linearised model, the response to a drop in grid voltage is simulated, an important response for an actual STATCOM. The control parameters were specified to be more oscillatory, at $K_p = 0.8$, $K_i = 50$. As evidenced in Figs. 5.25-5.28, the 1% grid voltage step kept the model within the same closely linear envelope as the small I_q setpoint changes, but the 5% step showed up a divergence in the dominant oscillatory mode.

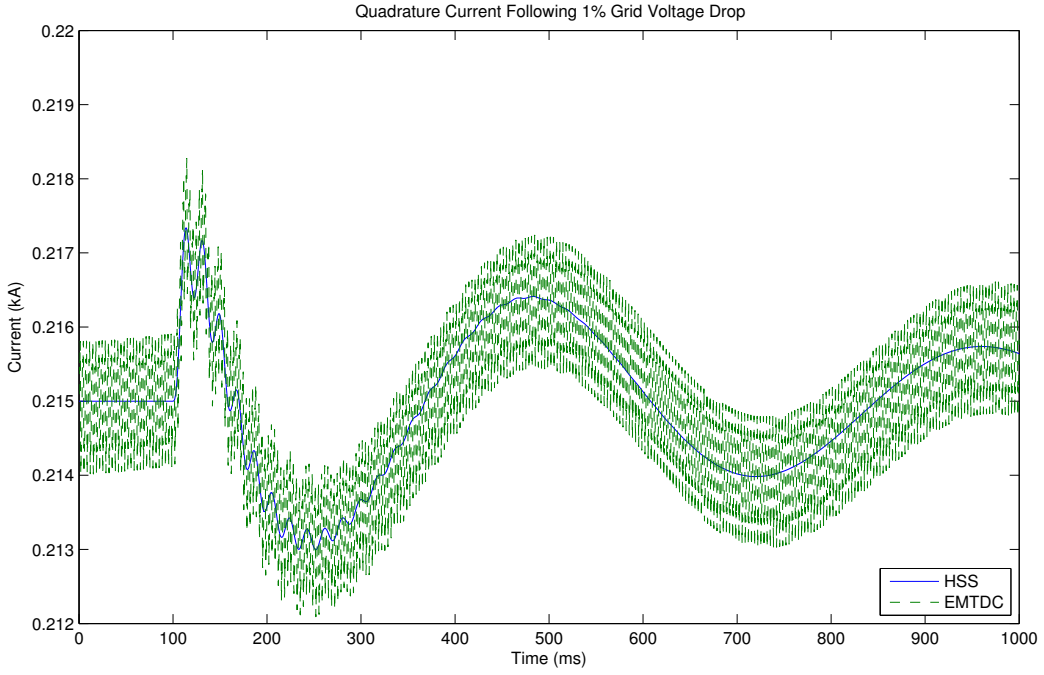

Figure 5.25 Quadrature converter current following a 1% step reduction in the grid voltage.

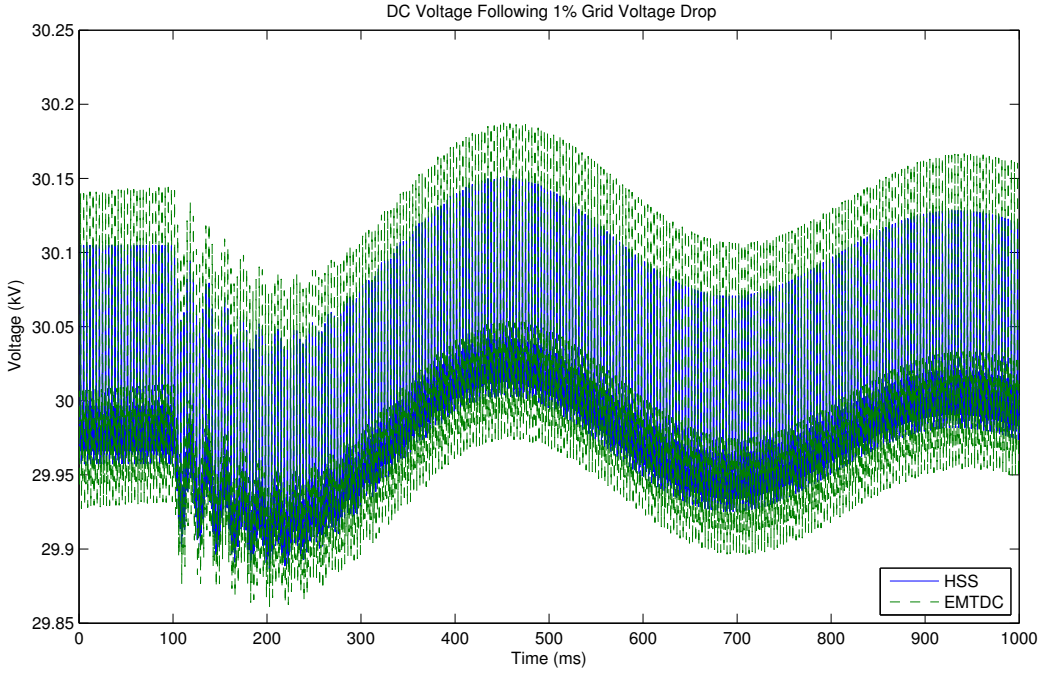

Figure 5.26 DC bus voltage following a 1% step reduction in the grid voltage.

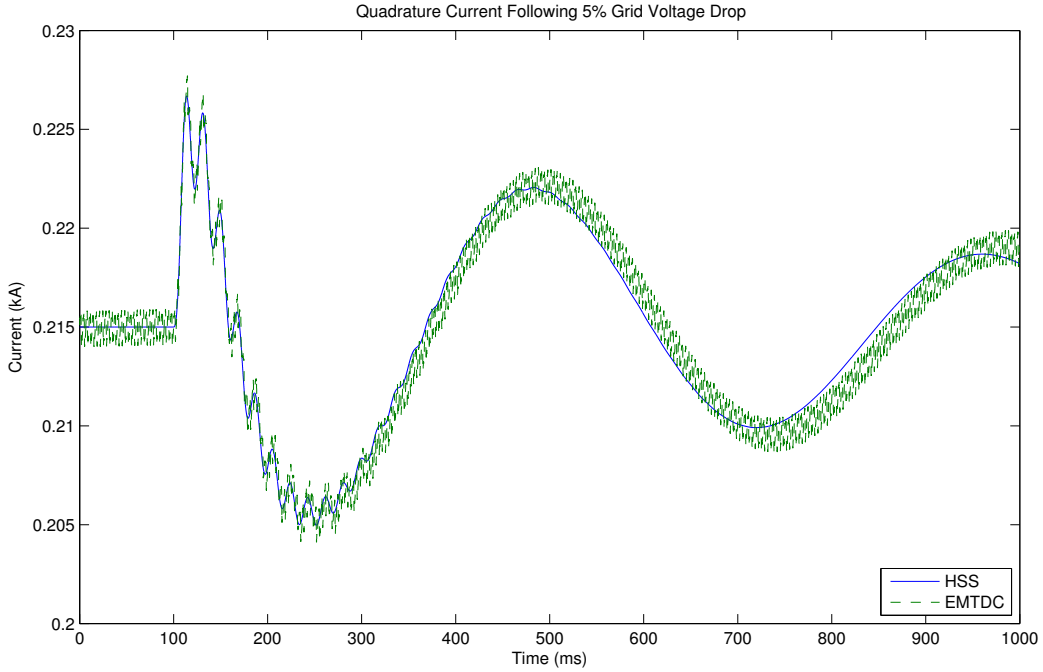

Figure 5.27 Quadrature converter current following a 5% step reduction in the grid voltage.

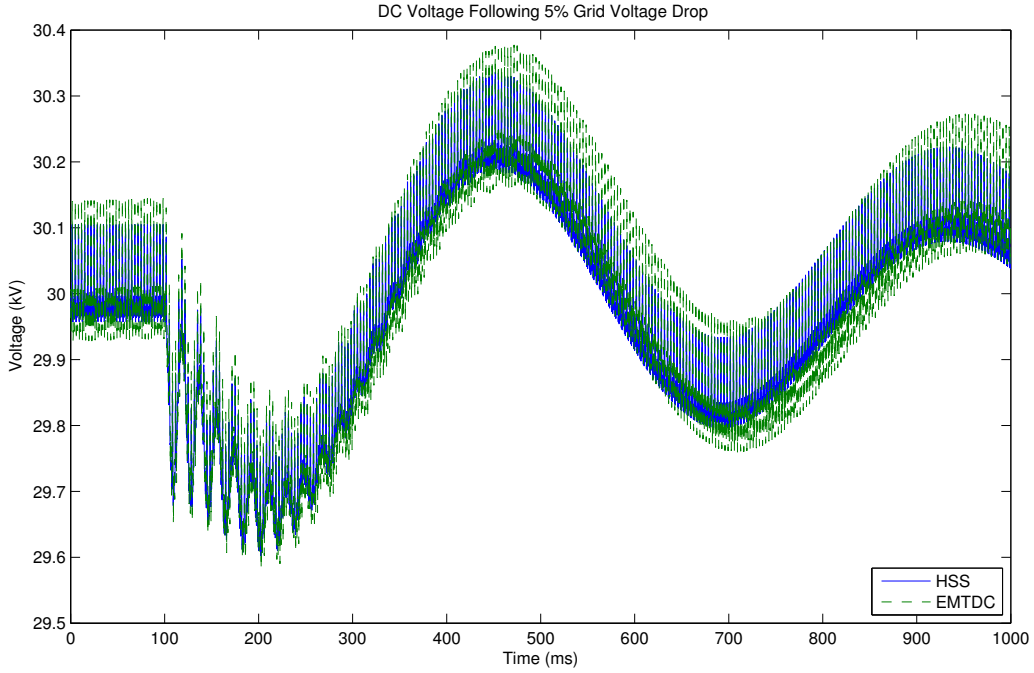

Figure 5.28 DC bus voltage following a 5% step reduction in the grid voltage.

5.5.3 Model Order and Harmonic Interaction

The design of the HSS model allows for the independent variation of the highest modelled harmonic order h in the simulation, with all harmonic state variables and associated coupling terms above this harmonic frequency being neglected. This permits a unique form of experiment, in which the same simulation is evaluated for different harmonic orders to test for the effects of coupling at harmonic frequencies.

The simulation of an I_q setpoint change in Section 5.5.1 was evaluated for $h = 1, 7, 13, 19, 49$, with the limiting case of $h = 1$ being the fundamental frequency only model. The results clustered very tightly into two groups at $h = 1, 7, 13$ and $h = 19, 49$. Figs. 5.29 and 5.30 show, using the state-space outputs of the models, that the dominant mode of the closed-loop response is dependent on harmonic coupling effects at $h = 19$ and below. Fig. 5.31 demonstrates that no further significant change in the response is caused by an increase in the harmonic order from 19 to 49.

Given that the higher-order models are able to accurately match the output of the time-domain simulation in PSCAD as evidenced in Section 5.5.1, it can be concluded that the fundamental frequency model lacks the ability to fully describe the closed-loop dynamics of the converter system with harmonic coupling, although it will be sufficiently close for basic control analysis in isolation. This manner of dependence on harmonic order is expected to be important when evaluating models incorporating multiple converters or other harmonic sources.

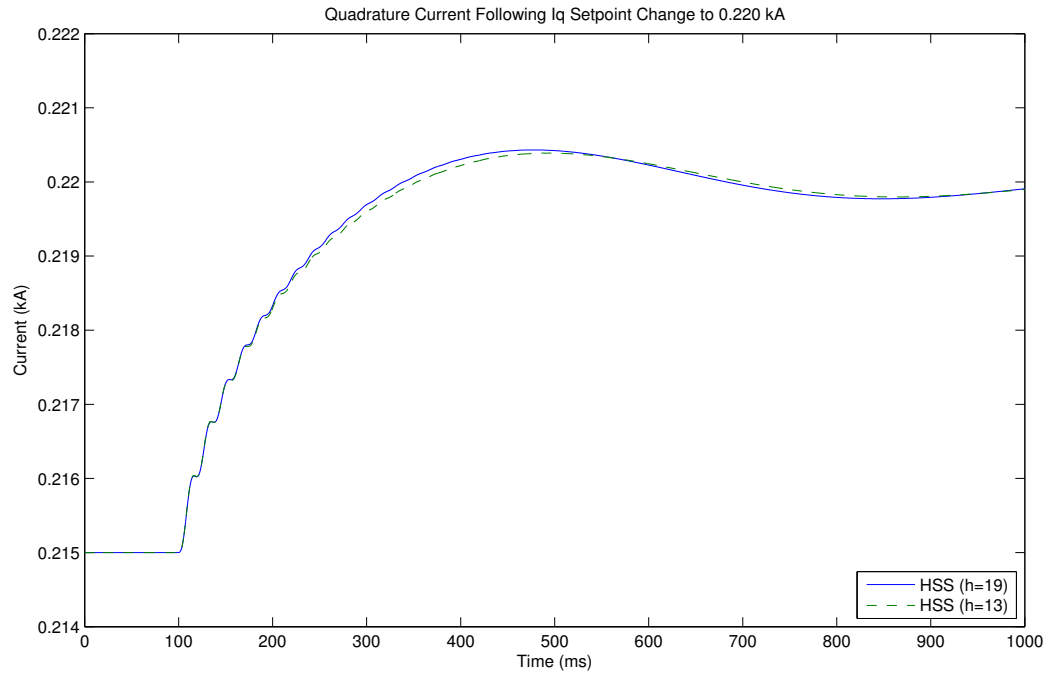

Figure 5.29 Quadrature converter current following a change in the I_q setpoint, showing divergent response for varied maximum harmonic order.

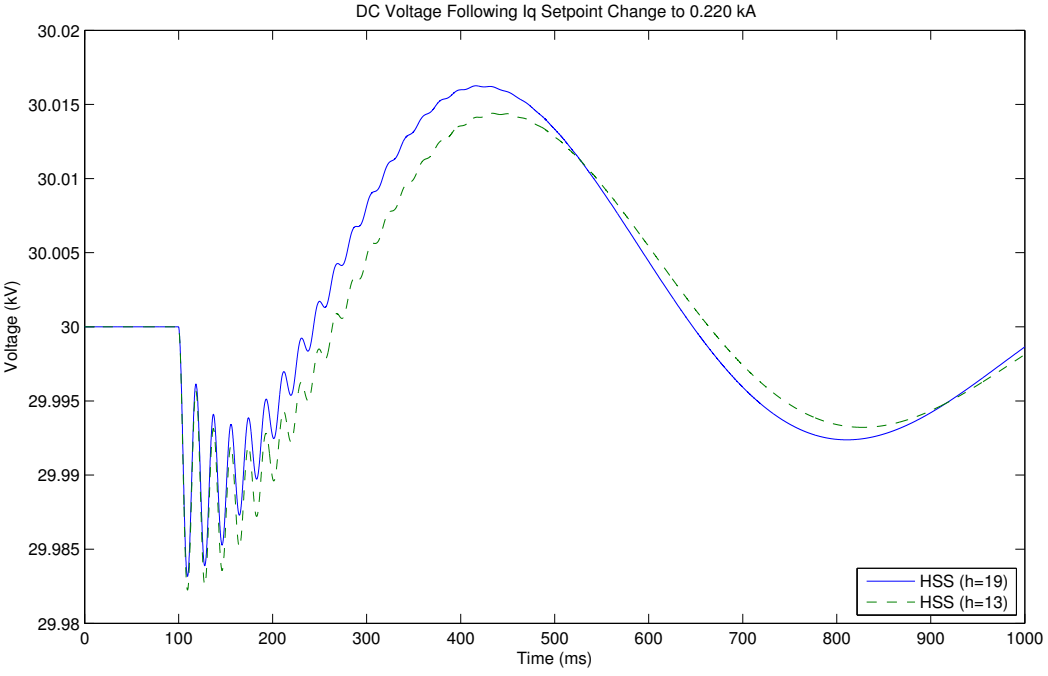

Figure 5.30 DC bus voltage following a change in the I_q setpoint, showing divergent response for varied maximum harmonic order.

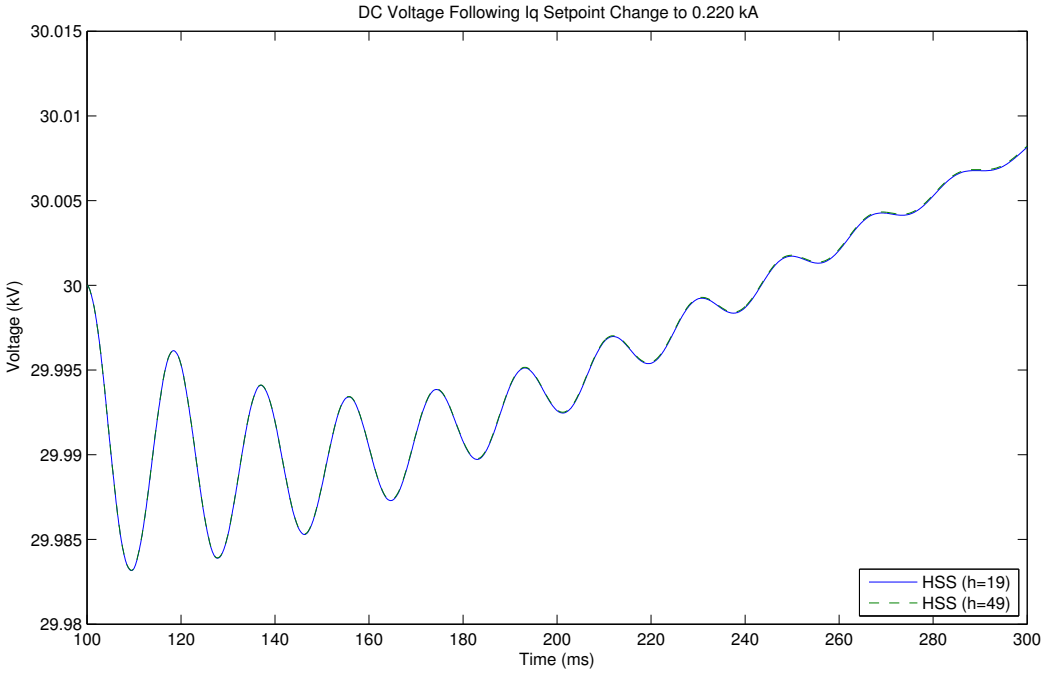

Figure 5.31 DC bus voltage following a change in the I_q setpoint, showing close agreement for further increases in harmonic order beyond h=19.

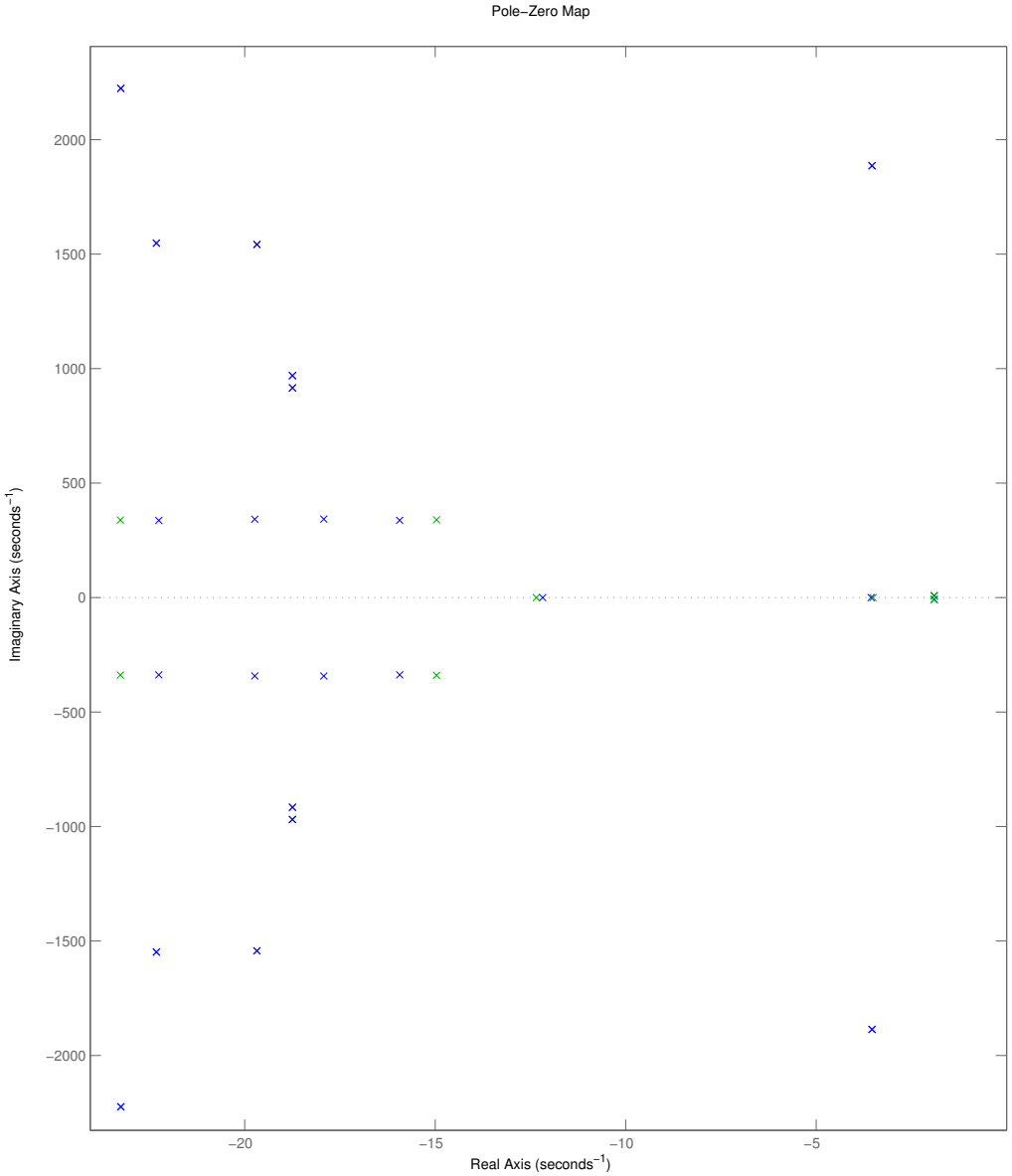

Figure 5.32 Pole-zero map of closed-loop system for h=1 (red), h=19 (blue).

5.5.4 Control Parameter Root Loci

With the basic validity of the closed-loop model established, and the demonstrated link between the identified dominant system poles and the system response, the natural application is the analysis of the control system through the generation of root-loci for variation in the control parameters. These root-loci are unique to the operating point that the closed-loop system was linearised around, and must be approximated by a discrete series of pole-zero plots with varied parameters.

The control system as implemented has two free parameters, the proportional and integral gain constants K_p and K_i, applied to the output of the fixed gain matrix. Figs. 5.36 and 5.37 show the locus for K_p, with the movement of the dominant pole-pair to the left implying a faster settling time as the gain increases, and the other significant group of poles moving right. Figs. 5.38 shows a similar locus for the integral gain, but with the dominant poles becoming both slower and more oscillatory.

The time-domain responses for these parameters are shown in Figs. 5.33 and 5.34, confirming the interpretation of the dominant poles. Fig. 5.35 gives the response of the controller tuned with these root-loci to give a quick settling time to the new setpoint, particularly the current demand, using $K_p = 1.0$, $K_i = 10$, and Fig. 5.39 gives its pole-zero map.

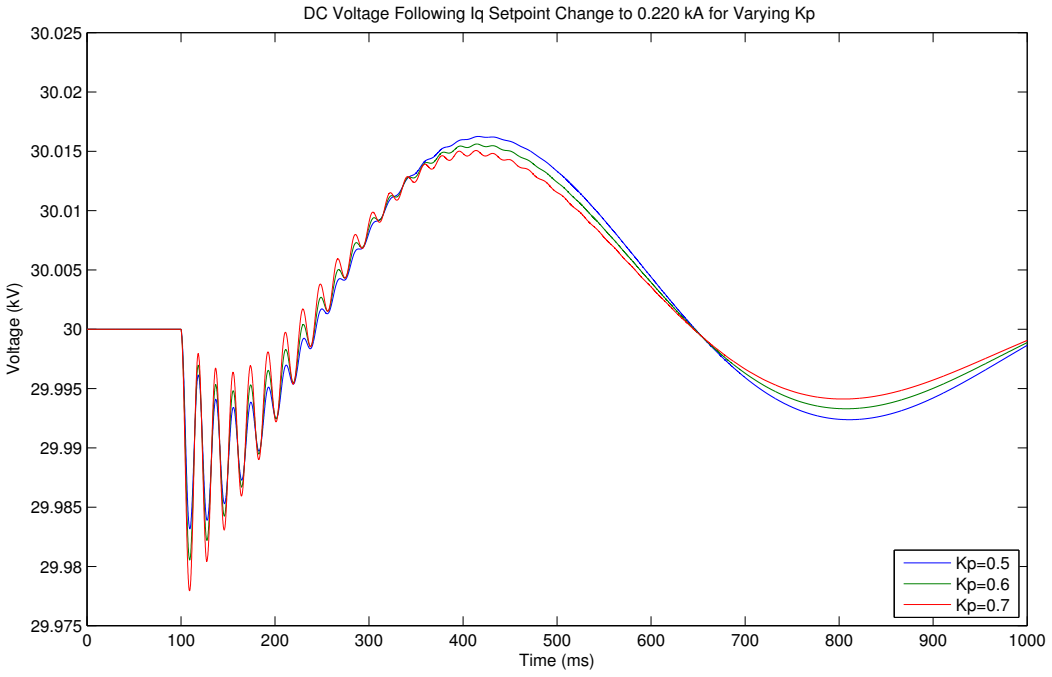

Figure 5.33 DC bus voltage following a change in the I_q setpoint, plotted for different values of K_p.

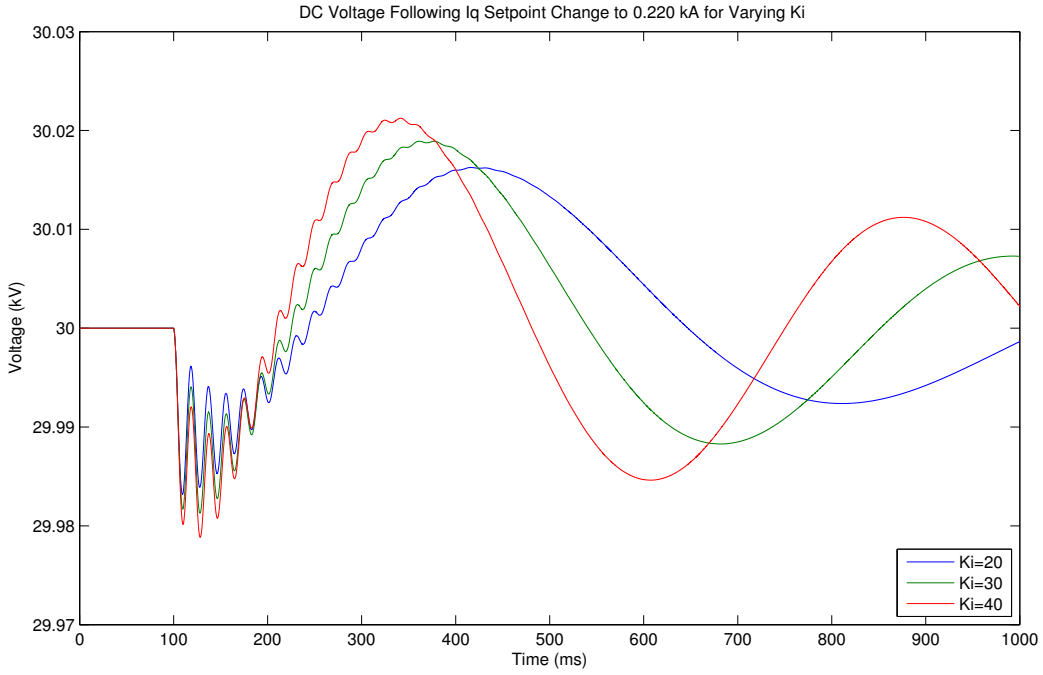

Figure 5.34 DC bus voltage following a change in the I_q setpoint, plotted for different values of K_i.

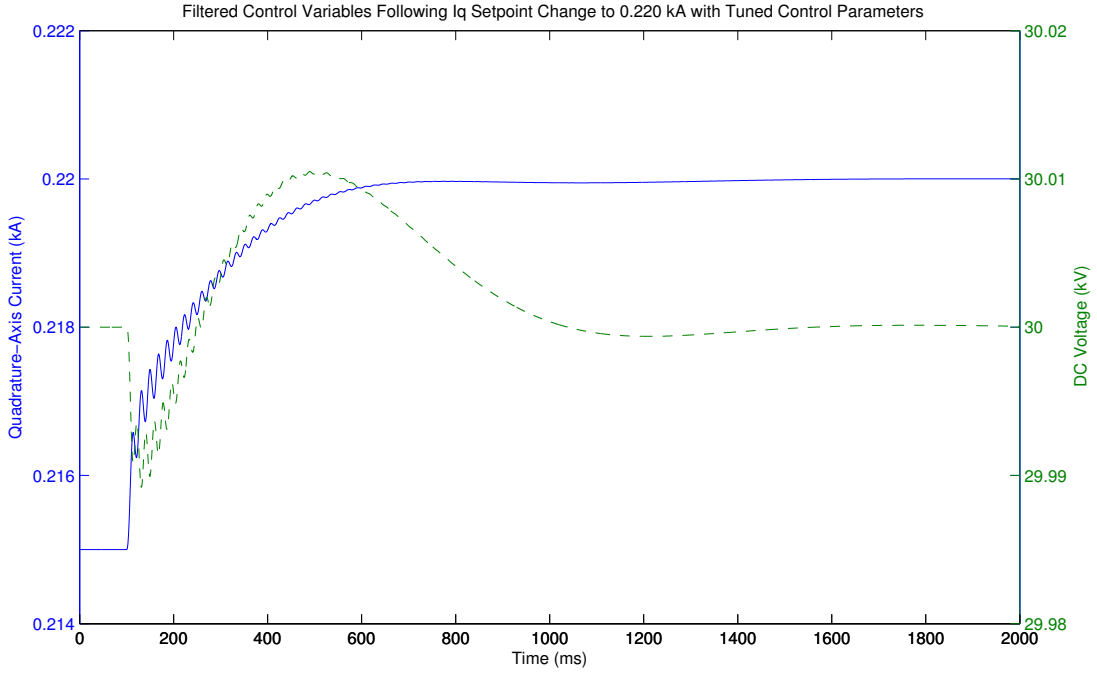

Figure 5.35 DC bus voltage and quadrature current following a change in the I_q setpoint, demonstrating fast settling with a properly tuned controlled.

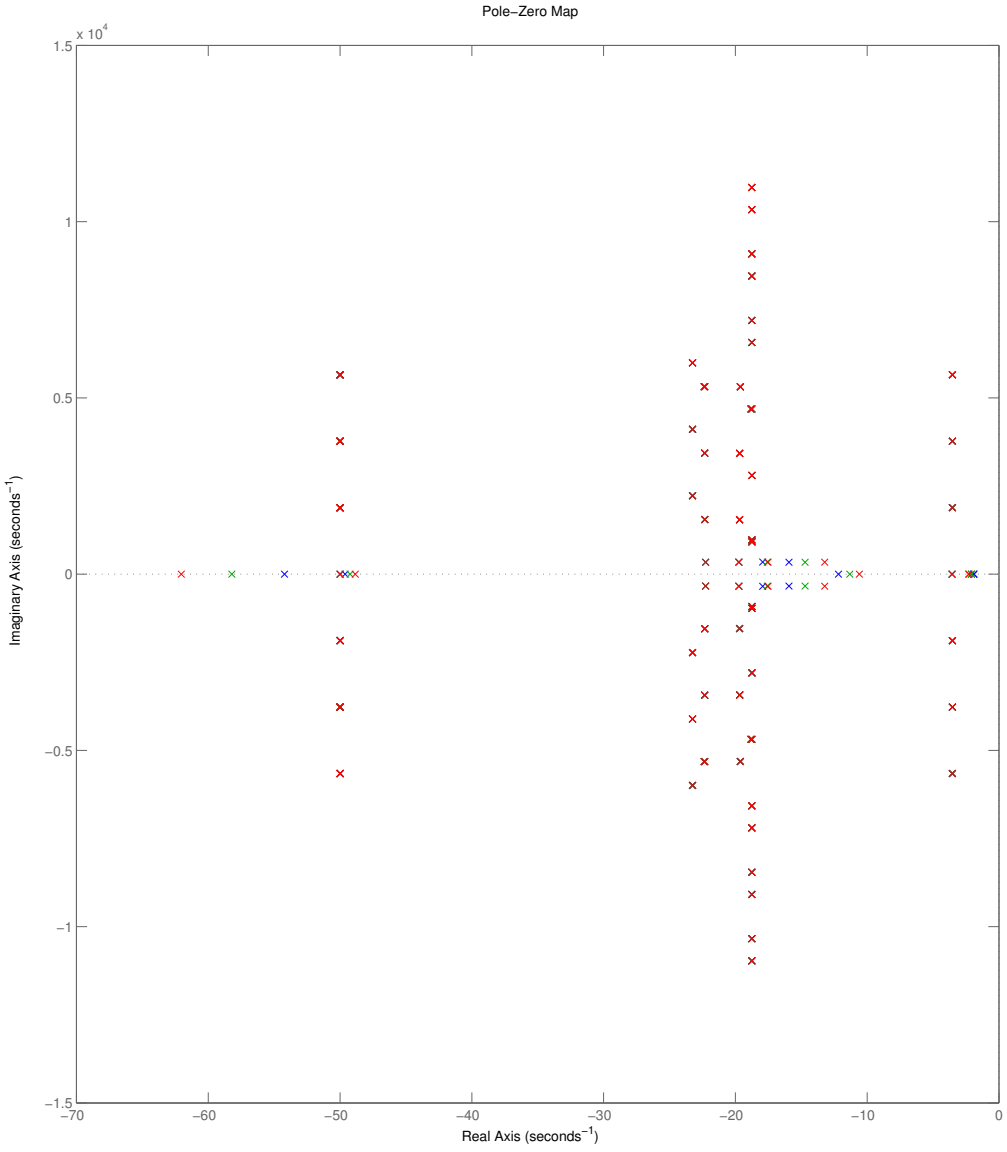

Figure 5.36 Pole-zero map of closed-loop system for $K_p = 0.5$ (blue), $K_p = 0.6$ (green), $K_p = 0.7$ (red).

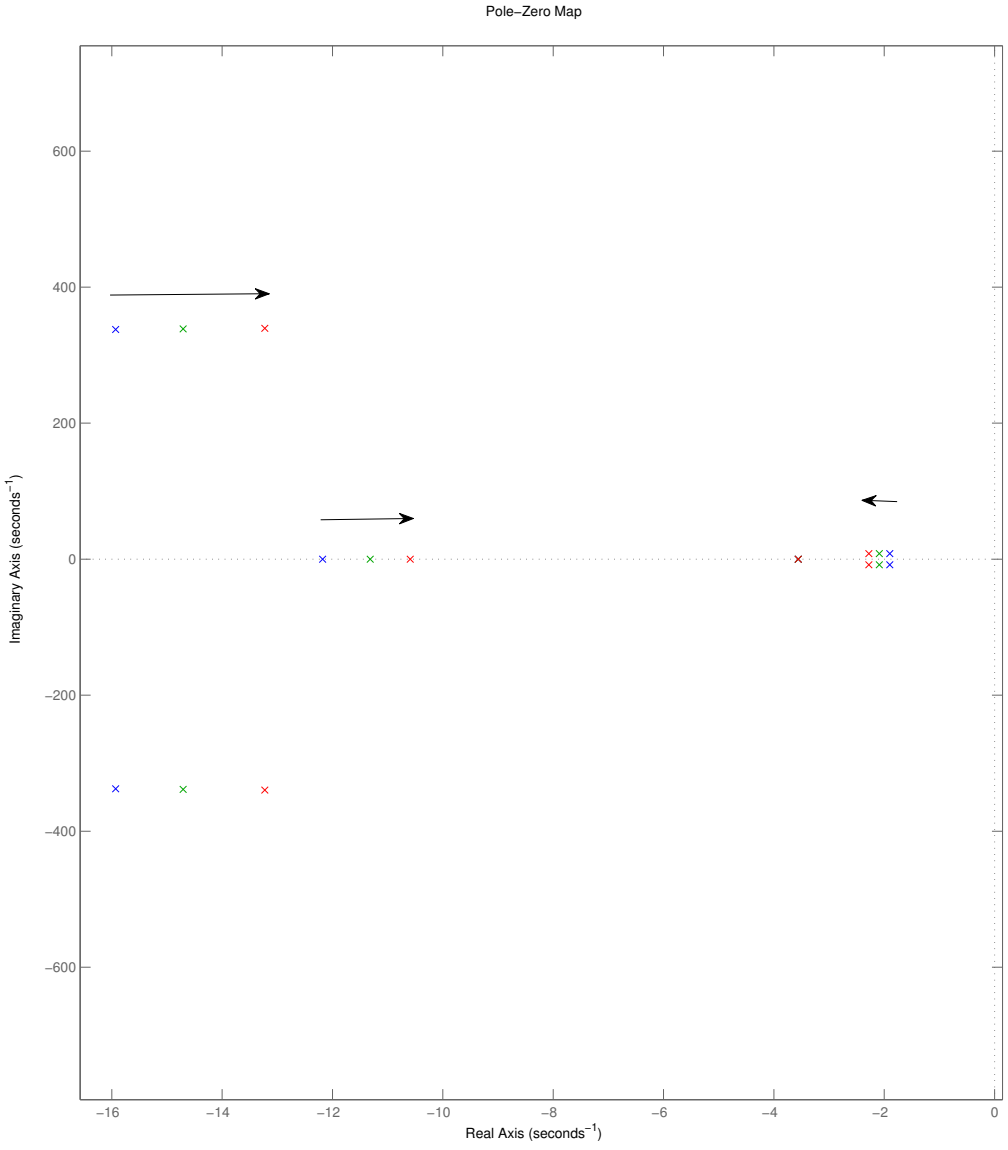

Figure 5.37 Pole-zero map of closed-loop system for $K_p = 0.5$ (blue), $K_p = 0.6$ (green), $K_p = 0.7$ (red), detailing locus of dominant poles.

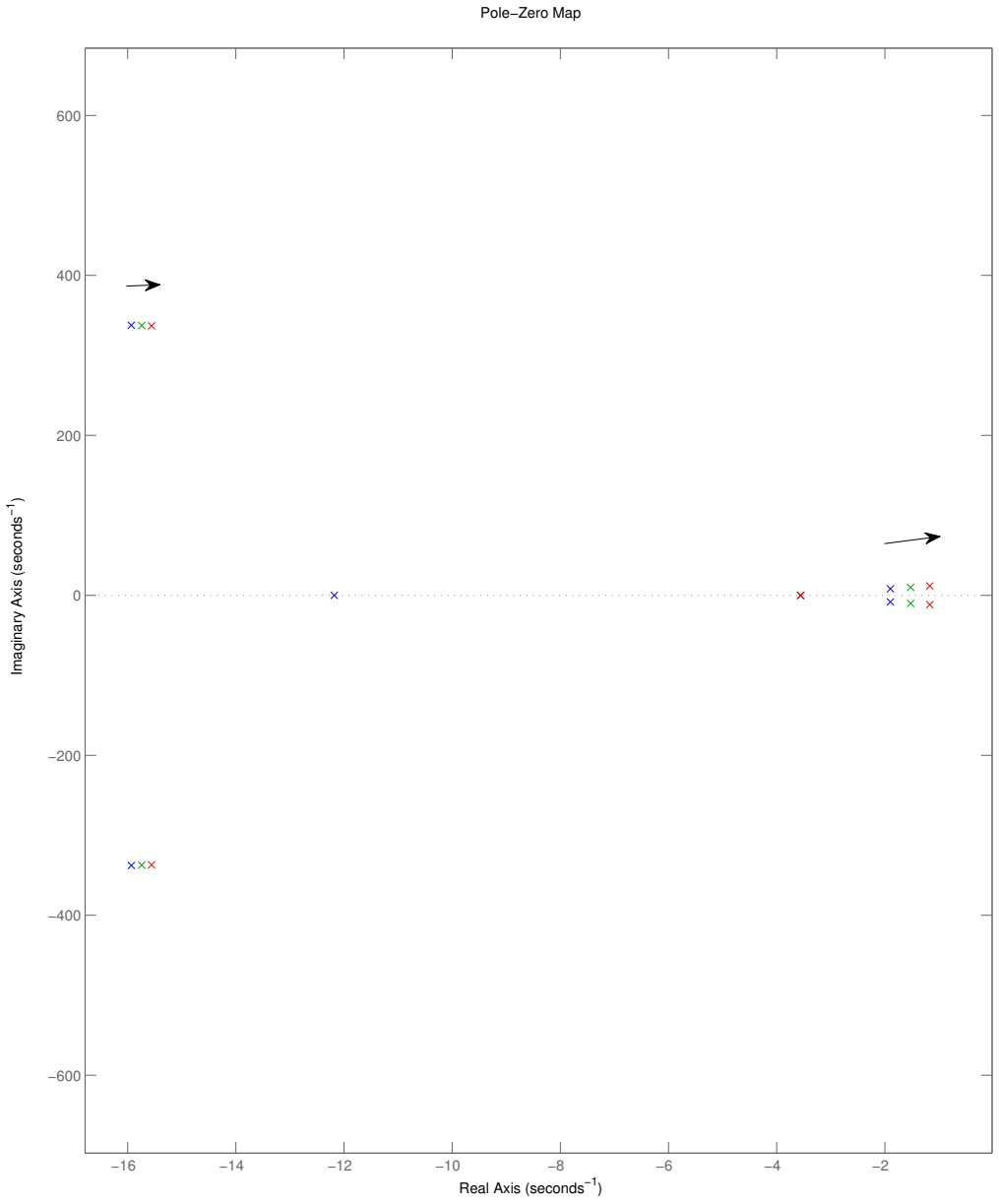

Figure 5.38 Pole-zero map of closed-loop system for $K_i = 20$ (blue), $K_i = 30$ (green), $K_i = 40$ (red), detailing locus of dominant poles.

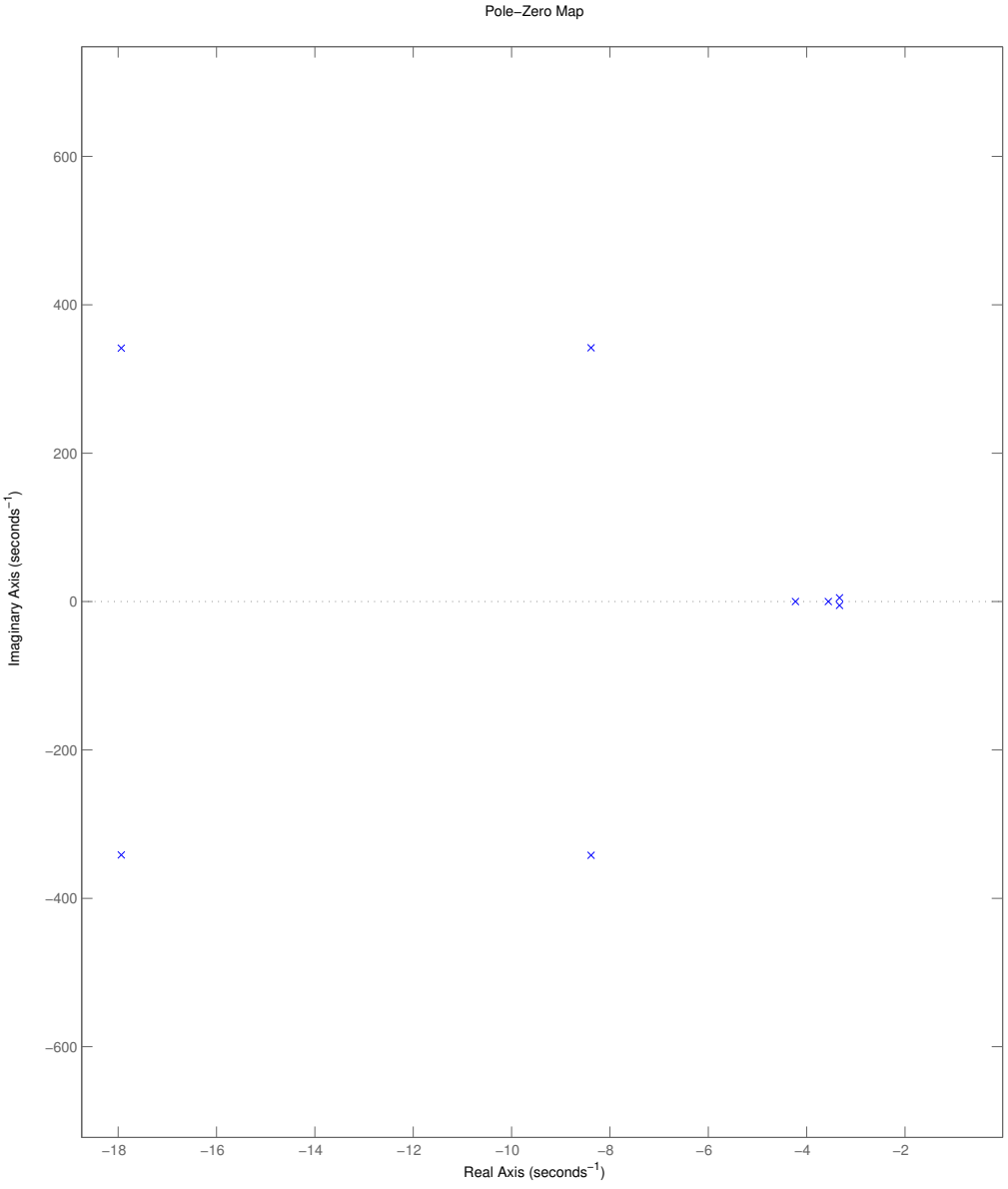

Figure 5.39 Pole-zero map of tuned closed-loop system, detailing dominant poles.

5.5.5 Closed-Loop Response to Grid Imbalance

The closed-loop response to a grid imbalance, in the form of an introduced negative sequence fundamental component, is a fundamental test of the entire modelling framework introduced in this thesis. Using the modulated EMP phasor technique described earlier, a 5% imbalance was introduced to the grid voltage at $t = 100\,\text{ms}$ to the STATCOM system with constant control setpoints and using the tuned control parameters of the previous section. As seen in Figs. 5.40-5.44, the model captures both the envelope of the closed-loop response, and at $h = 49$, the fine time-domain features. In Fig. 5.40, the current measurement can be eventually seen to relax to the pure 100 Hz excitation.

As discussed in Section 5.4.1.2, using the modulation of a balanced phasor to achieve representation of non-characteristic signals necessarily results in the same modulation being transferred through to the control system in the same manner as the linear modulation characteristic of the time-domain dq transform. Using a single harmonic component, in this case the fundamental component of the current harmonic vector, breaks the equivalence of all dynamic EMP signal representations. The result is that to be properly reflected in the control measurements, all such non-characteristic system disturbances must be achieved through modulation of the fundamental frequency component only, in contrast with the uncontrolled model. This is no matter in practise, as any number of non-characteristic signals can be modulated in superposition, this also ensuring an absence of direct dependence on the system harmonic order.

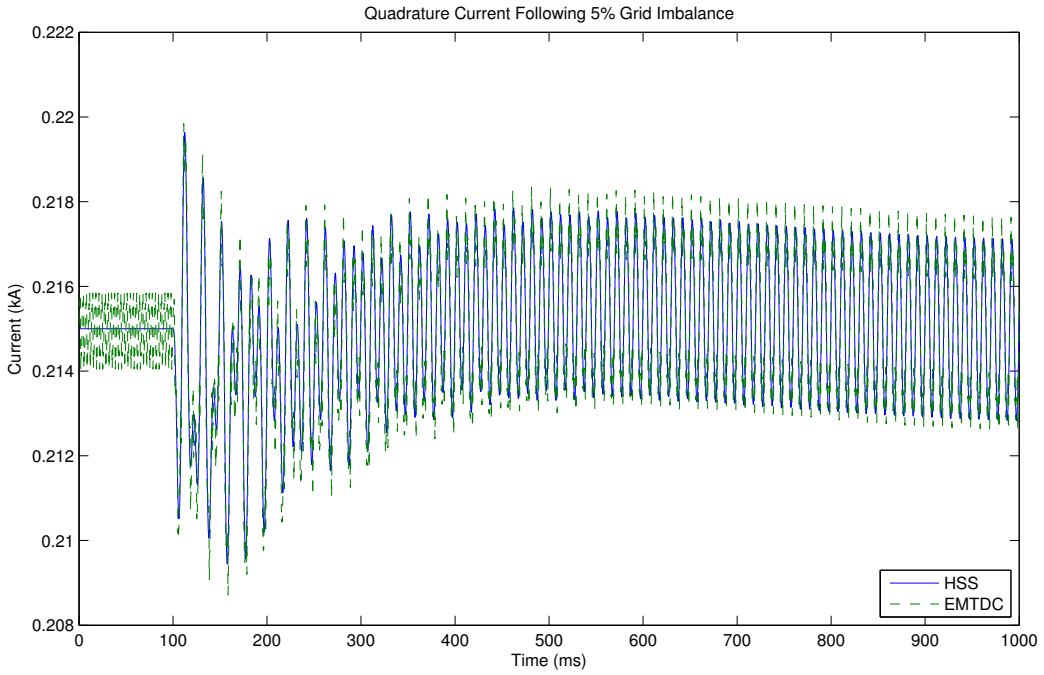

Figure 5.40 Quadrature converter current following the introduction of a 5% imbalance.

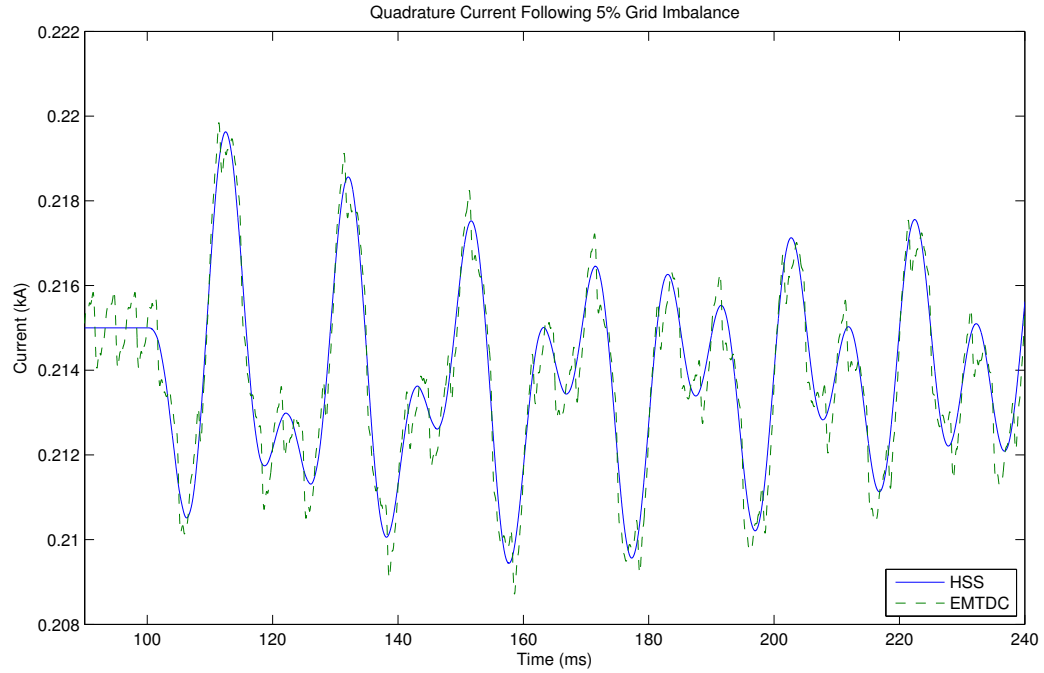

Figure 5.41 Quadrature converter current following following the introduction of a 5% imbalance, detailing initial transient response.

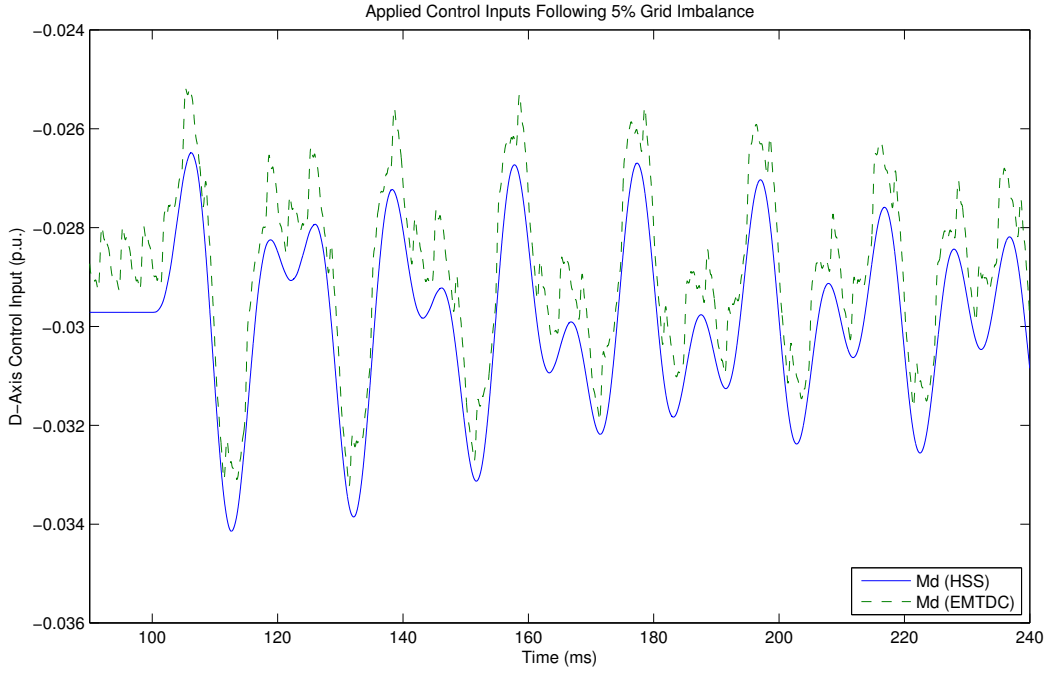

Figure 5.42 D-axis control signal following the introduction of a 5% imbalance, detailing initial transient response.

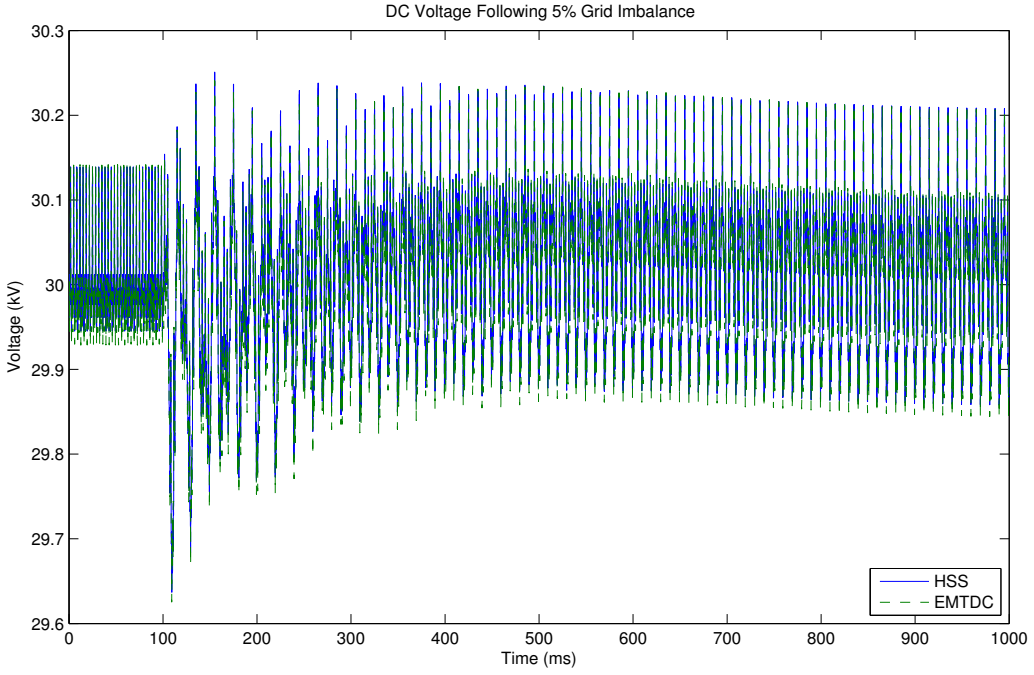

Figure 5.43 DC bus voltage following the introduction of a 5% imbalance.

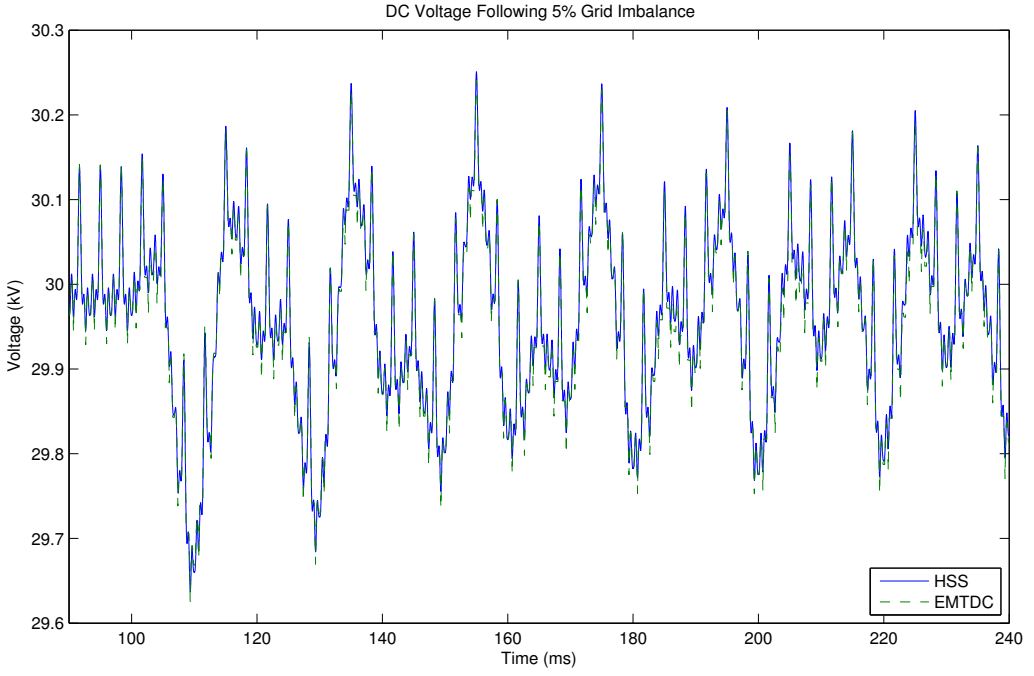

Figure 5.44 DC bus voltage following the introduction of a 5% imbalance, detailing initial transient response.

5.6 CONCLUSIONS

This chapter presented the extension of the fixed-switching HSS VSC model to a closed-loop controlled model using a dual linearisation of the numerical switching function and converter state variables. Simulation results evaluated against PSCAD/EMTDC modelling demonstrate the validity of the linearised model, judged by the ability to accurately capture closed-loop dynamics within a small-signal region of interest that was empirically probed. As demonstrated by the use of generated root-loci to tune the control system, LTI system analysis tools can be meaningfully applied to the linearised HSS model.

One interesting result was the relationship between the modelled harmonic order and the closed-loop response, which revealed a sharp discontinuity at $h = 19$. This demonstrates the flexibility of the fully general HSS modelling approach, which does not require a-priori knowledge of which terms will be significant. The other major result is the validation of the reduced-order modelling framework, proving that unbalanced three-phase closed-loop system dynamics can be effectively captured while preserving major computational efficiency gains.

Chapter 6

CONCLUSIONS AND FUTURE WORK

This final chapter summarises the conclusions drawn from the results obtained, and those formed in the process of developing the model. Directions for further research leading from this work are then discussed.

6.1 CONCLUSIONS

Model Applicability

The ideal application for the developed model is the characterisation of low-frequency harmonic interactions in controlled converters. This is supported by several properties of the model:

- Harmonic flows and couplings can be identified directly in the model output.
- The maximum harmonic order can be easily selected, with no a-priori knowledge of the possible frequency range of interest required.
- The response to closed-loop control can be accurately modelled in a small-signal region of interest around a specified operating point.
- The modular approach to system construction allows for many permutations of VSC system to be easily constructed.
- Fast simulation times permit rapid iteration of design variables and operating points.

The simulations in this thesis use switching frequencies of 450 Hz to 750 Hz ($m_f = 9$ to $m_f = 15$) so as to maximise observed harmonic interaction in a single-converter system. This corresponds to the frequency ranges used in [Möllerstedt and Bernhardsson 2000] (where $f_0 = \frac{50}{3}$Hz, $f_{sw} = 250\,\text{Hz}, m_f = 15$), albeit for a single-phase traction system. This method therefore lends itself to the analysis of VSC systems using GTO/IGCT devices, which operate generally in the sub-1 kHz range.

Modelling Approach

The construction of the converter and associated control system in a global synchronous reference frame provided an ideal basis for the extension of the converter model to include the effects of control variation. The numerical switching function model in this reference frame was ideal for linearisation due to the maximal decoupling between the quadrature control inputs.

The modular system construction method links the electrical and control systems through the identity created by the balanced fundamental frequency reference frame. By breaking the symmetry of the HSS, this fulfils the goal of unifying the electrical and control analyses, allowing direct solution for balanced steady-state inputs including control action, and dynamic simulation for arbitrary inputs including non-characteristic harmonics and other unbalanced components.

State-Space Analysis

State-space analysis methods were found to generalise well to the transformed LTP model of the VSC. Discrete pole-zero root-locus techniques can provide qualitative and quantitative insight into the closed-loop system performance.

Model Limitations

One significant limitation is that the control system must be linear. This requires either the modelled control system to be linear, or a further linearisation to be carried out. Some forms of non-linearities in control systems such as saturation and anti-windup mechanisms are not usually relevant in small-signal studies, some such as multiplicative terms are readily linearised, and others such as variable-structure techniques are not linearisable in this way.

Due to the reduction of the harmonic components of the system to the balanced characteristic harmonic set, the steady-state solution must be balanced; responses to unbalanced inputs may not be solved directly, and unbalanced components may not form the base-case for control linearisation. This is considered to be a feature of the model, as it makes clear the distinction between the balanced steady state and the arbitrary dynamic variation potentially including non-characteristic harmonics or even inter-harmonics. The ac network is restricted to balanced three-phase impedances.

6.2 FUTURE WORK

Paralleled Converter Modelling

With no modification to the developed model, the modular nature of the system construction should allow paralleled converter systems to be studied. This is a rich domain of harmonic interactions which are only obliquely analysable using time-domain models.

Extension to Other Topologies

As discussed, the frequency range of significant harmonic coupling effects lends itself to analysis of high-power converters using IGCT devices. To increase the relevance to practical systems using these devices, the next logical step would be to extend the model to three-level Neutral Point Clamped converters; a valuable topology for IGCT devices [Bhattacharya and Babaei 2011]. This could be readily accomplished using the numerical switching model developed in this thesis, assuming that the neutral-point balancing could be abstracted away as the dead-time compensation is here.

VSC-HVDC Modelling

In combination with the extension to multi-level converters, the HSS converter model could be used to model VSC-HVDC systems, including harmonic interaction on the dc link. Madrigal and Acha used an uncontrolled harmonic domain PWM model to investigate dc-side harmonic resonance phenomena [Madrigal and Acha 2001], which could be expanded upon using a controlled dynamic model. There is also scope for the extension of the HSS model to include inter-harmonic components as in [Ramirez 2011] for the modelling of HVDC systems linking ac networks of varying frequency.

Integration with Existing HSS Models

HSS models for other FACTS devices and power system components exist, such as the TCR model developed in [Orillaza 2011] and the HVDC model in [Hwang and Wood 2012]. Future work could be oriented towards consolidating these models in a unified framework, as these models differ slightly in their approach, particularly when conceptualising the modelling of three-phase systems in the HSS. The challenge will be to consolidate line-commutated switching models in a modular reduced-order framework, which should be assisted by the balanced harmonic signal and network representations described in this thesis.

High-Level System Description and Simulation Environment

If the goal of integration and harmonisation of HSS models described above could be achieved, an ideal next step would be the creation of a generalised simulation framework. The potentially laborious generation of models could be automated, by means of a high-level schema describing the topology and parameters of the system as interconnected blocks, and an associated interpreter to build the state-space system and collate its output. This would be an ambitious step towards a general-purpose HSS simulation environment.

REFERENCES

Alvarez Martin, J.A., Melgoza, J.R. and Rincon Pasaye, J.J. (2011), 'Exact steady state analysis in power converters using Floquet decomposition', In *North American Power Symposium (NAPS), 2011*, IEEE, August, pp. 1–7.

Arrillaga, J. and Watson, N.R. (2008), 'The Harmonic Domain revisited', In *Harmonics and Quality of Power, 2008. ICHQP 2008. 13th International Conference on*, IEEE, pp. 1–9.

Arrillaga, J., Medina, A., Lisboa, Cavia, M.A. and Sanchez, P. (1995), 'The Harmonic Domain. A frame of reference for power system harmonic analysis', *Power Systems, IEEE Transactions on*, Vol. 10, No. 1, February, pp. 433–440.

Bhattacharya, S. and Babaei, S. (2011), 'Series connected IGCT based three-level Neutral Point Clamped voltage source inverter pole for high power converters', In *Energy Conversion Congress and Exposition (ECCE), 2011 IEEE*, IEEE, pp. 4248–4255.

Bracewell, R. (2000), *The Fourier transform and its applications*, McGraw-Hill series in electrical and computer engineering, McGraw Hill.

Chavez, J.D. (2010), 'A modified dynamic harmonic domain distribution line model', In *Power and Energy Society General Meeting, 2010 IEEE*, IEEE, July, pp. 1–7.

Collins, C.D. (2006), *FACTS device modelling in the harmonic domain*, PhD thesis, University of Canterbury, Christchurch, New Zealand.

Deore, S.R., Darji, P.B. and Kulkarni, A.M. (2012), 'Dynamic phasor modeling of Modular Multi-level Converters', In *Industrial and Information Systems (ICIIS), 2012 7th IEEE International Conference on*, IEEE, August, pp. 1–6.

Depenbrock, U. (1993), 'The FBD-method, a generally applicable tool for analyzing power relations', *Power Systems, IEEE Transactions on*, Vol. 8, No. 2, May, pp. 381–387.

Dommel, H.W. (1969), 'Digital Computer Solution of Electromagnetic Transients in Single-and Multiphase Networks', *Power Apparatus and Systems, IEEE Transactions on*, Vol. PAS-88, No. 4, April, pp. 388–399.

Etxeberria-Otadui, I., Viscarret, U., Caballero, M., Rufer, A.C. and Bacha, S. (2007), 'New Optimized PWM VSC Control Structures and Strategies Under Unbalanced Voltage Transients', *Industrial Electronics, IEEE Transactions on*, Vol. 54, No. 5, October, pp. 2902–2914.

Fang, C.C.C. and Abed, E.H. (1999), 'Sampled-data modeling and analysis of closed-loop PWM DC-DC converters', In *Circuits and Systems, 1999. ISCAS '99. Proceedings of the 1999 IEEE International Symposium on*, IEEE, pp. 110–115 vol.5.

Floquet, G. (1883), 'Sur les équations différentielles linéairesa coefficients périodiques', *Ann. Sci. École Norm. Sup*, Vol. 12, pp. 47–88.

Fortescue, C.L. (1918), 'Method of Symmetrical Co-Ordinates Applied to the Solution of Polyphase Networks', *American Institute of Electrical Engineers, Transactions of the*, Vol. XXXVII, No. 2, July, pp. 1027–1140.

Hill, G.W. (1886), 'On the part of the motion of the lunar perigee which is a function of the mean motions of the sun and moon', Vol. 8, No. 1, pp. 1–36.

Holmes, D.G. (1998), 'A general analytical method for determining the theoretical harmonic components of carrier based PWM strategies', In *Industry Applications Conference, 1998. Thirty-Third IAS Annual Meeting. The 1998 IEEE*, IEEE, October, pp. 1207–1214 vol.2.

Holmes, D. and Lipo, T. (2003), *Pulse width modulation for power converters: principles and practice*, IEEE Press series on power engineering, IEEE Press.

Hume, D.J., Wood, A.R. and Osauskas, C.M. (2003), 'Frequency-domain modelling of interharmonics in HVDC systems', *Generation, Transmission and Distribution, IEE Proceedings-*, Vol. 150, No. 1, January, pp. 41–48.

Hwang, M.S. and Wood, A.R. (2012), 'Harmonic State-Space modelling of an HVdc converter', In *Harmonics and Quality of Power (ICHQP), 2012 IEEE 15th International Conference on*, IEEE, June, pp. 573–580.

Kolar, J.W., Ertl, H. and Zach, F.C. (1991), 'Influence of the modulation method on the conduction and switching losses of a PWM converter system', *Industry Applications, IEEE Transactions on*, Vol. 27, No. 6, November, pp. 1063–1075.

Larsen, E.V., Baker, D.H. and McIver, J.C. (1989), 'Low-order harmonic interactions on AC/DC systems', *Power Delivery, IEEE Transactions on*, Vol. 4, No. 1, January, pp. 493–501.

Love, G.N. (2007), *Small Signal Modelling of Power Electronic Converters for the Study of Time-domain Waveforms*, PhD thesis, University of Canterbury, Christchurch, New Zealand.

Madrigal, M. and Acha, E. (2001), 'Harmonic modelling of voltage source converters for HVDC stations', In *AC-DC Power Transmission, 2001. Seventh International Conference on (Conf. Publ. No. 485)*, IET, November, pp. 125–131.

Madrigal, M. and Rico, J.J. (2004), 'Operational Matrices for the Analysis of Periodic Dynamic Systems', *IEEE Transactions on Power Systems*, Vol. 19, No. 3, August, pp. 1693–1695.

Madrigal, M., Acha, E., Mayordomo, J.G., Asensi, R. and Hernandez, A. (2000), 'Single-phase PWM converters array for three-phase reactive power compensation. II. Frequency domain studies', In *Harmonics and Quality of Power, 2000. Proceedings. Ninth International Conference on*, IEEE, pp. 645–651 vol.2.

Mathur, R. and Varma, R. (2002), *Thyristor-Based FACTS Controllers for Electrical Transmission Systems*, IEEE Press series on microelectronic systems, Wiley.

Mohan, N. and Undeland, T. (2007), *Power electronics: converters, applications, and design*, Wiley India.

Möllerstedt, E. and Bernhardsson, B.M. (2000), 'Out of control because of harmonics-an analysis of the harmonic response of an inverter locomotive', *Control Systems, IEEE*, Vol. 20, No. 4, August, pp. 70–81.

Orillaza, J.R.C. (2011), *Harmonic State Space Model of Three Phase Thyristor Controlled Reactor*, PhD thesis, University of Canterbury, Christchurch, New Zealand.

Orillaza, J.R., Hwang, M.S. and Wood, A.R. (2010), 'Switching Instant Variation in Harmonic State-Space modelling of power electronic devices', In *Universities Power Engineering Conference (AUPEC), 2010 20th Australasian*, IEEE, December, pp. 1–5.

Peng, F.Z. and Lai, J.S. (1996), 'Generalized instantaneous reactive power theory for three-phase power systems', *Instrumentation and Measurement, IEEE Transactions on*, Vol. 45, No. 1, February, pp. 293–297.

Pöllänen, R. and Others (2003), 'Converter-flux-based current control of voltage source PWM rectifiers-analysis and implementation', *Acta Universitatis Lappeenrantaensis ISSN 1456-4491*.

Ramirez, A. (2011), 'The Modified Harmonic Domain: Interharmonics', *Power Delivery, IEEE Transactions on*, Vol. 26, No. 1, January, pp. 235–241.

Rao, P., Crow, M.L. and Yang, Z. (2000), 'STATCOM control for power system voltage control applications', *Power Delivery, IEEE Transactions on*, Vol. 15, No. 4, October, pp. 1311–1317.

Rico, J.J., Madrigal, M. and Acha, E. (2003), 'Dynamic harmonic evolution using the extended harmonic domain', *Power Delivery, IEEE Transactions on*, Vol. 18, No. 2, April, pp. 587–594.

Sandberg, H., Möllerstedt, E. and Bernhardsson (2005), 'Frequency-domain analysis of linear time-periodic systems', *Automatic Control, IEEE Transactions on*, Vol. 50, No. 12, December, pp. 1971–1983.

Sao, C.K., Lehn, P.W., Iravani, M.R. and Martínez, J.A. (2002), 'A benchmark system for digital time-domain simulation of a pulse-width-modulated D-STATCOM', *Power Delivery, IEEE Transactions on*, Vol. 17, No. 4, October, pp. 1113–1120.

Stanković, A.M., Mattavelli, P., Caliskan, V.A. and Verghese, G.C. (2000), 'Modeling and analysis of FACTS devices with dynamic phasors', In *Power Engineering Society Winter Meeting, 2000. IEEE*, IEEE, pp. 1440–1446 vol.2.

Vajta, M. (2000), 'Some remarks on padé-approximations', In *Proc. 3rd TEMPUSINTCOM Symp. Intelligent Systems in Control and Measurement*, pp. 53–58.

Watanabe, E.H., Stephan, R.M. and Aredes, M. (1993), 'New concepts of instantaneous active and reactive powers in electrical systems with generic loads', *Power Delivery, IEEE Transactions on*, Vol. 8, No. 2, April, pp. 697–703.

Wereley, N.M. (1991), *Analysis and Control of Linear Periodically Time Varying Systems*, PhD thesis, M.I.T.

Wood, A.R. and Osauskas, C.M. (2004), 'A linear frequency-domain model of a STATCOM', *Power Delivery, IEEE Transactions on*, Vol. 19, No. 3, July, pp. 1410–1418.

Zhou, K. and Wang, D.W. (2002), 'Relationship between space-vector modulation and three-phase carrier-based PWM: a comprehensive analysis', *Industrial Electronics, IEEE Transactions on*, Vol. 49, No. 1, February, pp. 186–196.